Vers une pêche durable : conception d'un système de communication et de localisation acoustique sous-marine basé sur des signaux vobulés

Marwane Rezzouki

université de BORDEAUX

THÈSE PRÉSENTÉE
POUR OBTENIR LE GRADE DE

DOCTEUR DE
L'UNIVERSITÉ DE BORDEAUX

ÉCOLE DOCTORALE : SCIENCES PHYSIQUES ET DE L'INGÉNIEUR

SPÉCIALITÉ : AUTOMATIQUE, PRODUCTIQUE, SIGNAL ET IMAGE

Par **Marwane Rezzouki**

Towards Sustainable Fishing: A Hybrid System for Underwater Acoustic Communication and Localization Based on Chirp Signals

Soutenue le 6/10/2023

Membres du jury :

M. Christophe Laot	Professeur IMT Atlantique	Rapporteur
M. Guillaume Andrieux	Professeur IUT-RT Université de Nantes	Rapporteur
Mm. Christelle Aupetit	Professeur ENSIL-ENSCI	Examinateur
M. Guillaume Terrasson	Enseignant-chercheur ESTIA	Examinateur
M. Guillaume Ferré	Professeur Bordeaux INP	Directeur de thèse

Acknowledgements

I would like to express my sincere gratitude to the following individuals and organizations who have provided support and guidance throughout the realization of this thesis:

First of all, I extend my deepest appreciation to my thesis advisor, Guillaume Ferré, for his unwavering support, insightful feedback, and invaluable expertise. I deeply admire his ability to create an environment where people feel so comfortable to live and work in.

I would like to thank my colleagues and research collaborators at IMS laboratory for their invaluable assistance, stimulating discussions, and willingness to share their knowledge. I would also like to acknowledge the support and resources provided by CIDPMEM and Steinberg Protocol. Their infrastructure, facilities, and access to research materials have been instrumental in completing this thesis.

Finally, I extend my appreciation to my family and friends for their unwavering support, encouragement, and understanding throughout this long journey. Their love, motivation, and belief in my abilities have been the driving force behind my accomplishments.

Title — Towards Sustainable Fishing: A Hybrid System for Underwater Acoustic Communication and Localization Based on Chirp Signals

Abstract — Over the last decades, underwater acoustic communication and localization systems have received much interest in diverse applications such as conducting ocean research, exploring natural resources, connecting autonomous underwater vehicles, and navigation. However, using acoustic waves that propagate at a low speed, approximately 1500 m/s, limits the bandwidth of communication. Besides, the underwater acoustic channel (UWA) is considered one of the most difficult mediums to use because of the severe transmission loss, multipath, high Doppler spread and shift, and important time and spatial variability. As a result, ensuring data link communication or localization in such channels requires the deployment of transmitters with high power, which could acoustically pollute the environment and participate in the migration of species. In this context, the purpose of this thesis is to enable a more sustainable and responsible fishing practice. We focused on addressing the issue of lost fishing nets in the ocean. Based on the waveform of the emitted signals, which is linear frequency modulation (chirp), we propose a hybrid acoustic system for communication and localization underwater. This system offers fishers the ability to enhance their fishing activities by establishing a reliable data link and facilitating the tracking of the fishing nets. This way, fishers will be able to find their nets if they get lost and avoid the creation of waste in the ocean.

The proposed system is based on a technique called differential chirp spread spectrum (DCSS) with additional processes at the receiver to overcome the challenging characteristics of the UWA channel. The DCSS modulation offers the ability to deploy a less disruptive network for marine animals since it is possible to demodulate received signals at a low level of signal-to-noise ratio (SNR). Moreover, multiple synchronized hydrophones are used at the receiver to calculate the time differential of arrival (TDOA) and then estimate the localization of the acoustic sources.

Keywords — Sustainable fishing, UWA channel, DCSS communication, TDOA-based positioning.

Titre — Vers une pêche durable : conception d'un système de communication et de localisation acoustique sous-marine basé sur des signaux vobulés.

Résumé — Au cours des dernières décennies, les systèmes de communication et localisation acoustiques sous-marins ont suscité un grand intérêt dans diverses applications telles que la recherche océanique, l'exploration des ressources naturelles, la connexion de véhicules autonomes sous-marins et la navigation. Cependant, l'utilisation d'ondes acoustiques qui se propagent à une faible vitesse, environ 1500 m/s, limite la bande de communication. En outre, le canal acoustique sous-marin (ASM) est considéré comme l'un des milieus les plus difficiles à utiliser en raison de l'importante perte de transmission, l'effet multi-trajets, l'effet Doppler et la variabilité temporelle et spatiale. Par conséquent, assurer une communication dans ces canaux nécessite le déploiement des émetteurs avec une grande puissance de transmission ce qui pourrait polluer acoustiquement l'environnement et participer à la migration des espèces marins. Dans ce contexte, l'objectif de cette thèse est de proposer des solutions techniques pour rendre la pêche durable et responsable. Plus précisement, nous nous sommes concentrés sur la problèmatique des filets de pêche perdus dans l'océan. En se basant sur la forme d'onde des signaux émis, qui est une modulation linéaire de fréquence, nous proposons un système acoustique hybride permettant la communication et la localisation des filets de pêche. Ce système offre aux pêcheurs la possibilité de bien mener leurs activités de pêche en établissant une communication fiable et en facilitant le suivi des filets de pêche. De plus, ce système permettrait également aux pêcheurs de retrouver leurs filets de pêche en cas de perte et d'éviter la création de déchets dans l'océan.

Le système proposé est basé sur une technique appelée "differential chirp spread spectrum" (DCSS) avec des traitements supplémentaires au niveau du récepteur pour surmonter les caractéristiques difficiles du canal ASM. La modulation DCSS permet de déployer un réseau moins perturbant pour les animaux marins, puisqu'il est possible de démoduler les signaux reçus à un niveau faible de rapport signal-bruit. En outre, multiples hydrophones synchronisés sont utilisés au niveau du récepteur pour calculer la différence de temps d'arrivée et estimer ensuite la localisation des sources acoustiques.

Mots clés — pêche durable, canal ASM, communication DCSS, positionnement basé sur TDOA.

Résumé des travaux de la thèse

Connus sous le nom de filets fantômes, les filets de pêche perdus, abandonnés ou jetés dans l'océan ont suscité une attention internationale croissante au cours des dernières décennies. Plusieurs causes sont responsables à la création des filets fantômes. Des facteurs tels que les conditions météorologiques extrêmes, des enchevêtrements dans les engins de pêche ou des collisions avec des structures sous-marines ou des navires peuvent entraîner le détachement ou l'abandon de filets de pêche dans l'océan. De plus, le manque de maintenance et d'entretien régulier de l'équipement peut également entraîner des filets endommagés dans l'océan.

Le phénomène des filets fantômes a des conséquences environnementales et économiques catastrophiques. En effet, un filet de pêche est un outil de travail nécessaire et onéreux pour les pêcheurs. Lorsqu'il est perdu en mer, ces derniers sont souvent contraints de retourner sur les lieux de pêche et d'effectuer des recherches laborieuses pour retrouver le filet perdu. Cette méthode de recherche n'est pas pratique et chronophage, car les courants marins peuvent ramener les filets perdus loin de leur emplacement initial.

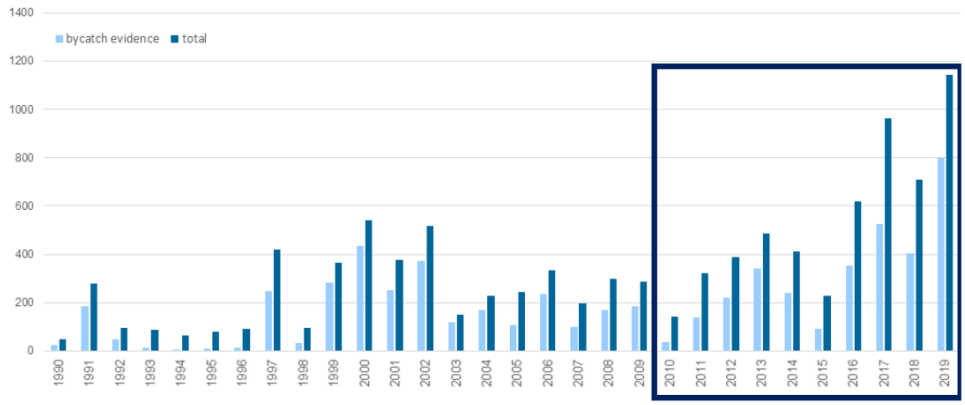

Figure 1: Échouage de cétacés sur la côte atlantique d'après le rapport de 2020 [1]

De plus, les filets fantômes font partie des principaux contributeurs à la pollution des océans et constituent une menace pour les biotopes [2, 3]. Les filets fantômes capturent tout ce qui se trouve sur leur chemin, y compris les poissons et d'autres espèces animales telles que les

dauphins et les tortues [4]. En conséquence, les animaux marins peuvent souffrir de blessures, de stress ou de mortalité en raison de l'enchevêtrement ou de l'asphyxie. Le problème des prises accidentelles peut perturber les écosystèmes et entraîner une diminution des populations d'espèces vulnérables ou en voie de disparition. Selon le Réseau National Échouages, la capture dans les filets de pêche reste la principale cause de mortalité observée chez les dauphins communs lors de plusieurs échouages en hiver depuis les années 1990 dans l'océan Atlantique (voir Figure 1).

Réduire l'impact des filets fantômes est crucial pour une pêche durable et la conservation de la biodiversité marine. Pour résoudre ce problème, de nombreuses initiatives ont été lancées ces dernières années. Par exemple, des dispositifs acoustiques, tels que des répulsifs sonores (pingers) ou des dispositifs acoustiques dissuasifs, sont souvent utilisés pour émettre des signaux qui dissuadent certaines espèces marines de s'approcher des filets de pêche, réduisant ainsi le risque de prises accidentelle [5, 6, 7]. Cependant, plusieurs études ont démontré que de tels dispositifs ne sont pas efficaces sur toutes les espèces. De plus, les animaux peuvent s'habituer aux signaux émis lors d'un déploiement à long terme [8, 9].

Au niveau national, plusieurs projets ont été lancés pour aborder cette problématique. Notamment, le programme LICADO est l'une des recherches en cours de réalisation [10]. Cette initiative est financée dans le cadre du Fonds européen pour les affaires maritimes et la pêche (FEAMP) dans le but de limiter les prises accidentelles des dauphins communs dans le golfe de Gascogne. Sur le plan technique, l'objectif est de développer de nouveaux systèmes acoustiques répulsifs plus fiables et efficaces. De plus, une réflexion sur les pratiques d'évitement et les stratégies de commerce des filets est prévue dans ce projet.

Les contributions de ce manuscrit ont été réalisées dans le cadre du projet Deep-SMS (Smart Monitoring System). Ce projet a été initié pour proposer des solutions techniques permettant de rendre la pêche au filet dit calé innovante, résolument durable et compétitive. Techniquement, le projet consiste à développer un système permettant de localiser un dispositif émetteur attaché à un filet de pêche à partir dune antenne de réception embarquée sur le navire de pêche. Ce système est conditionné par la forme donde des signaux émis. Celui-ci doit permettre simultanément :

- La localisation à au moins 1 km dun filet de 10 km de long à une profondeur maximale de 500 mètres.
- La prise de données marines in-situ attenantes aux conditions de pêche (température de leau dans la zone de pêche, houle, etc.), afin notamment de mieux comprendre les déplacements des espèces pêchées.

Afin d'atteindre cet objectif, nous proposons un système hybride qui combine la localisation et la communication des filets de pêche sous l'eau. Comme indiqué dans la Figure 2, le principe

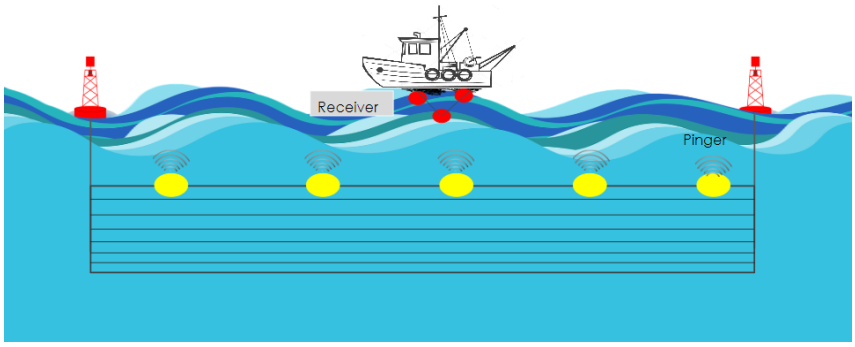

Figure 2: Architecture du système proposé

de fonctionnement est le suivant : un filet de pêche équipé par des émetteurs acoustiques qui envoient des signaux contenant de l'information au navire. Ce dernier est équipé par une antenne acoustique composée de plusieurs récepteurs (hydrophones) pour écouter les signaux et les traités avec une carte électronique dédiée. Ce système permettrait aux pêcheurs de retrouver leurs filets de pêche en cas de perte et d'éviter la création de déchets dans l'océan.

Contributions et plan de la thèse

Les contributions de cette thèse sont les suivantes :

1. Fournir une compréhension du canal acoustique sous-marin (ASM) : propriétés physiques, caractéristiques, modèles existants et méthodologie de caractérisation.

2. Étudier l'impact du canal ASM sur la modulation à étalement de spectre -chirp spread spuctrum- (CSS). Plus précisément, l'effet de multipath et l'effet Doppler.

3. Présenter la technique "differential chirp spread spectrum" (DCSS) pour la communication acoustique sous-marine en tant qu'amélioration de la technique CSS. Des traitements supplémentaires sont introduits dans le schéma CSS conventionnel, tels que le codage différentiel, le traitement Doppler et l'égalisation, pour minimiser l'impact des canaux ASM.

4. Introduire le matériel développé pour réaliser des expérimentations dans des environnements acoustiques sous-marins. Une étude de caractérisation est réalisée pour déterminer la portée maximale en utilisant la communication DCSS.

5. Assurer la localisation à l'aide des signaux DCSS. En termes de matériel, une antenne composée de cinq récepteurs est déployée pour mesurer la différence de temps d'arrivée (TDOA). Nous exploitons le récepteur DCSS pour calculer le début des trames et ensuite

la TDOA entre les récepteurs. Enfin, à travers la localisation basée sur la TDOA, telle que les moindres carrés, nous estimons la position de l'émetteur.

6. Proposer différentes méthodes de calcul de la TDOA à l'aide des signaux DCSS et fournir une comparaison des performances.

En plus de l'introduction générale et de la conclusion, le plan de la thèse est structuré en trois chapitres principaux, comme suit :

Chapitre 1 : Dans ce chapitre, nous proposons une compréhension du canal ASM. Nous commençons par introduire les caractéristiques du canal ASM, notamment l'atténuation, le bruit de milieu, l'effet Doppler et l'effet de multipath. Ensuite, nous nous concentrons sur la modélisation du canal en utilisant des approches déterministes et statistiques. De plus, nous citons les simulateurs largement utilisés pour les canaux ASM et designons les modèles que nous avons utilisés dans ce travail. Enfin, nous présentons la méthodologie de caractérisation du canal ASM.

Chapitre 2 : Dans ce chapitre, nous établissons un budget de liaison acoustique pour la communication acoustique sous-marine passive. Ensuite, nous abordons les techniques les plus utilisées pour la communication acoustique sous-marine à faible rapport signal sur bruit (SNR). Ces techniques ont un intérêt environnemental à cause de leur capacité à utiliser des systèmes de transmission à faible puissance. Ensuite, nous détaillons le schéma de communication proposé DCSS, qui pourrait potentiellement protéger les animaux marins de la pollution acoustique. De plus, nous présentons le système qui a été spécialement développé pour mener des expérimentations dans des environnements acoustiques sous-marins. Ensuite, nous étudions ses performances pour déterminer sa portée maximale. Finalement, nous présentons et discutons les résultats expérimentaux de la technique DCSS obtenus à partir des tests réalisés à l'océan et dans un lac.

Chapter 3 : Dans ce chapitre, nous nous concentrons sur la partie de localisation du système proposé. Tout d'abord, nous introduisons le principe de la localisation basée sur la TDOA. Ensuite, nous présentons les méthodes existantes pour calculer la position basée sur la TDOA en cas de mesures bruitées. Après cela, nous présentons la méthode de calcul de la TDOA en utilisant le récepteur DCSS. Afin de minimiser l'erreur de calcul de la TDOA, nous proposons différentes méthodes de calcul en utilisant des signaux chirp et effectuons une comparaison des performances dans les canaux ASM. Enfin, nous présentons et discutons les résultats du système proposé dans un scénario de localisation de source en utilisant la modélisation du canal basée sur le simulateur Bellhop.

Contents

Introduction

Known as ghost nets, lost, abandoned, or discarded fishing nets in the ocean have received increasing international attention in the past decades. Several causes are responsible for the creation of ghost nets. Factors such as severe weather conditions, gear entanglement, or collisions with underwater structures or vessels can lead to the detachment or abandonment of fishing nets in the ocean. Moreover, the lack of proper equipment management and maintenance protocols could result in damaged or entangled nets that are left behind in the ocean.

The ghost nets phenomenon has a significant impact on the ocean ecosystem as well as fishing activity. Indeed, this issue has economic and social implications for fishers and fishing communities. When the nets get lost, fishers usually return to the fishing area to search for their profits to reduce the damage. This method is incredibly time-consuming, and it is not practical since the water currents can drift the lost nets away.

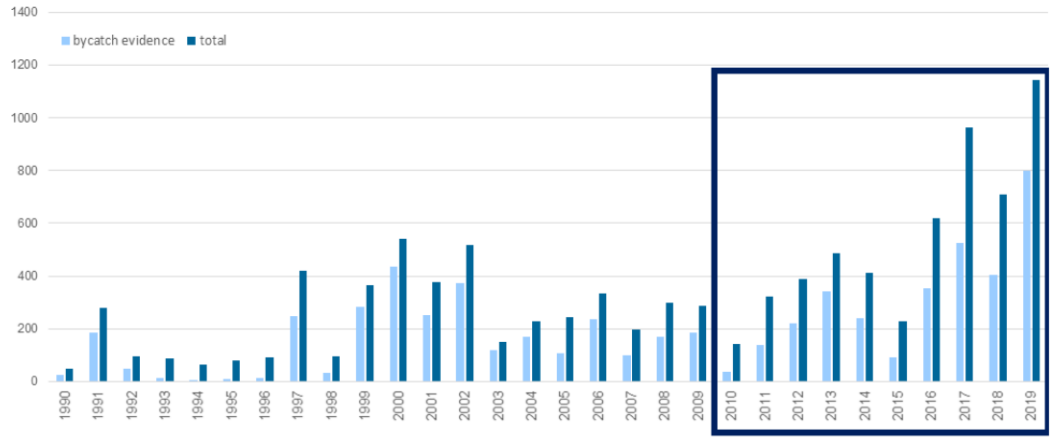

Figure 3: Stranding of cetaceans on the Atlantic coast from 2020 report

Moreover, ghost nets are among the major contributors to ocean pollution and a serious threat to marine life [2, 3]. The ghost nets trap everything in their path, including fish and other species of animals like dolphins and turtles [4]. As a result, marine animals may suffer injuries, stress, or mortality due to entanglement, suffocation, or being brought to the surface.

The bycatch problem can disrupt ecosystems and lead to declines in vulnerable or endangered species populations. According to the French Stranding Network, the capture in fishing gear remains the main cause of mortality observed in common dolphins during multiple stranding events in winter since the 1990s in the Atlantic Ocean (see Figure 3) [1].

Reducing the impact of ghost nets is crucial for sustainable fishing and the conservation of marine biodiversity. To address this issue, numerous initiatives have been launched in recent years. For example, acoustic devices, such as pingers or acoustic deterrent devices, are often used to emit signals that deter certain marine species from approaching fishing nets, reducing the risk of bycatch [5, 6, 7]. However, several works have demonstrated that such devices are not effective on all species. Besides, animals may habituate to the emitted signals in long-term deployment [8, 9].

At the national level, several projects have been launched to address this issue. Namely, the LICADO program is one of the ongoing research [10]. This initiative is financed as part of the European Maritime Affairs and Fisheries Fund (FEAMP) in order to limit the incidental catches of common dolphins in the Bay of Biscay. Technically, the purpose is to develop new acoustic-repellent systems that are more reliable and effective. Moreover, a reflection on avoidance practices and strategies for net handling is fixed.

The contributions of this manuscript have been done in the framework of the Deep-SMS (Smart Monitoring System) project. This project was initiated to provide technical solutions to promote sustainable fishing. Technically speaking, the project revolves around the creation of a system capable of pinpointing a transmitting device that is attached to a fishing net using a receiver installed aboard the fishing vessel. The effectiveness of this system relies on the specific waveform of the transmitted signals underwater. Two functionalities are expected from this work, which can be summarized as follows:

- The location of a fishing net (10 km long) at a maximum depth of 500 meters, at least 1 km from the vessel.
- Collect marine data related to fishing conditions (water temperature in the fishing zone, swell, etc.). This information would help in tracking the fishing zones.

In order to accomplish this goal, we put forward a hybrid system that combines localization and communication of fishing nets underwater. As shown in Figure 4, the concept of this system can be described as follows: the fishing net is outfitted with acoustic transmitters that emit signals carrying the information to the fishing vessel. The vessel, in turn, is equipped with an acoustic antenna consisting of multiple receivers (hydrophones) that record and process these signals using a dedicated electronic board to retrieve carried data and localize the transmitter that sends the information. This system would help fishers track their fishing nets if they got lost and avoid the creation of waste in the ocean.

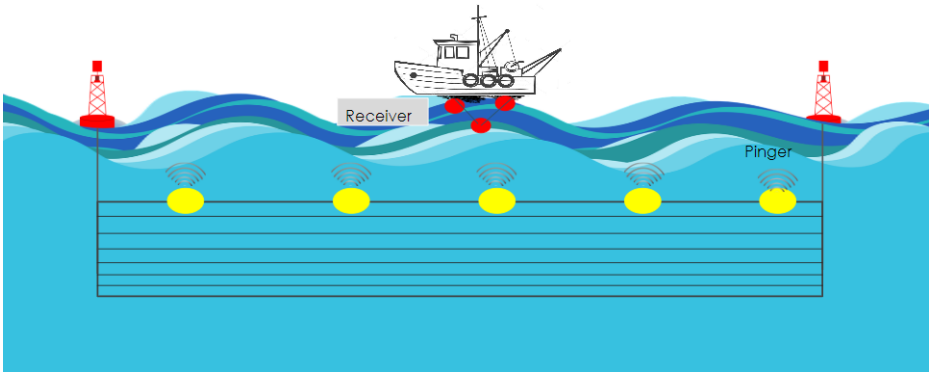

Figure 4: Architecture of the proposed system

Thesis contributions and outline

The thesis contributions are the following:

1. Provide an understanding of an underwater acoustic channel (UWA): physical proprieties, characteristics, existing models, and the methodology of characterization.

2. Study the impact of the UWA channel on chirp spread spectrum (CSS) modulation. More precisely, the multipath effect and the Doppler effect.

3. Present differential chirp spread spectrum (DCSS) technique for underwater acoustic communication as an enhancement of CSS technique. Addition processes are introduced to the conventional CSS scheme, such as differential encoding, Doppler processing, and equalization, to mitigate the intense characteristics of UWA channels.

4. Introduce the hardware to carry out experiments in underwater acoustic environments. A characterization study is provided to determine the maximum achievable range using DCSS communication.

5. Ensure localization using DCSS signals. In terms of hardware, an antenna composed of five receivers is deployed to measure the time difference of arrival (TDOA). We exploit the DCSS receiver to calculate the start time of frames and then TDOA between receivers. Finally, through TDOA-based positioning, such as least squares, we estimate the transmitter position.

6. Propose different methods of TDOA calculation using DCSS signals and provide a performance comparison.

In addition to the general introduction and conclusion, the dissertation outline is structured in three main chapters as follows:

Chapter 1: In this chapter, we provide a comprehension of the UWA channel. We begin by discussing the characteristics and challenges of the UWA channel, including attenuation, environment noise, Doppler effect, and multipath effect. Then, we focus on channel modeling using deterministic and statistical approaches. Besides, we highlight the widely used simulators for UWA channels and design the models we used in this work. Lastly, we demonstrate the methodology of UWA channel characterization using probe signals.

Chapter 2: In this chapter, we establish an acoustic link budget for passive communication. Then, we provide an overview of the most commonly used techniques for underwater acoustic communication at low signal-to-noise ratio (SNR) levels, which are environmentally friendly due to their ability to use low-power transmitting systems. Next, we delve into the proposed communication scheme, the differential chirp spread spectrum technique, which could potentially protect marine animals from acoustic pollution. Moreover, we present the system that has been developed specifically for conducting experiments in underwater acoustic environments. After that, we study its performance to determine its maximum achievable distance. Finally, the experimental results of the DCSS technique obtained from trials conducted in both lake and ocean settings are presented and discussed.

Chapter 3: In this chapter, we focus on the localization part of the proposed system. Initially, we provide an overview of localization based on the time differential of arrival (TDOA). Then, we introduce the existing methods to compute the TDOA-based positioning technique in case of noised measurements. After that, we present the method of TDOA calculation using the DCSS receiver. In order to minimize the error of TDOA calculation, we present various methods of computation using chirp signals and provide a performance comparison in UWA channels. Finally, we present and discuss the result of the proposed system in a scenario of source localization using Bellhop-Based channel modeling for network simulation.

CHAPTER 1

Underwater acoustic channel

The purpose of this chapter is to provide an understanding of the UWA channel. Firstly, we introduce the main characteristics and difficulties of an UWA channel (i.e., attenuation, environment noise, Doppler effect, and multipath effect). Then, we focus on channel modeling using deterministic and statistical approaches. After that, we present some of the existing simulators for UWA channels. Finally, we explain the methodology to characterize the UWA channel through probe signals.

1.1 Characteristics of underwater acoustic channel

This section is dedicated to the main characteristics of the UWA channel. Indeed, due to water's physical properties, such as permittivity and electrical conductivity, acoustic waves are widely used for communication or localization purposes, especially in long ranges compared to electromagnetic waves. Moreover, optical waves are another means to make communication, particularly in short ranges, but the ambient light and the scattering of the top and the sea floor could strongly impact them. However, the UWA channel is far from ideal because of multiple constraints such as multipath scattering, long delay spread, and high Doppler spreading and shifting. Besides, the UWA channel is characterized by severe transmission loss and strong spatial and temporal variability.

1.1.1 Sound speed variations

The acoustic wave propagates underwater at a speed around 1500 m/s. This value is not constant over time, it depends on other parameters such as temperature, salinity, and pressure. The

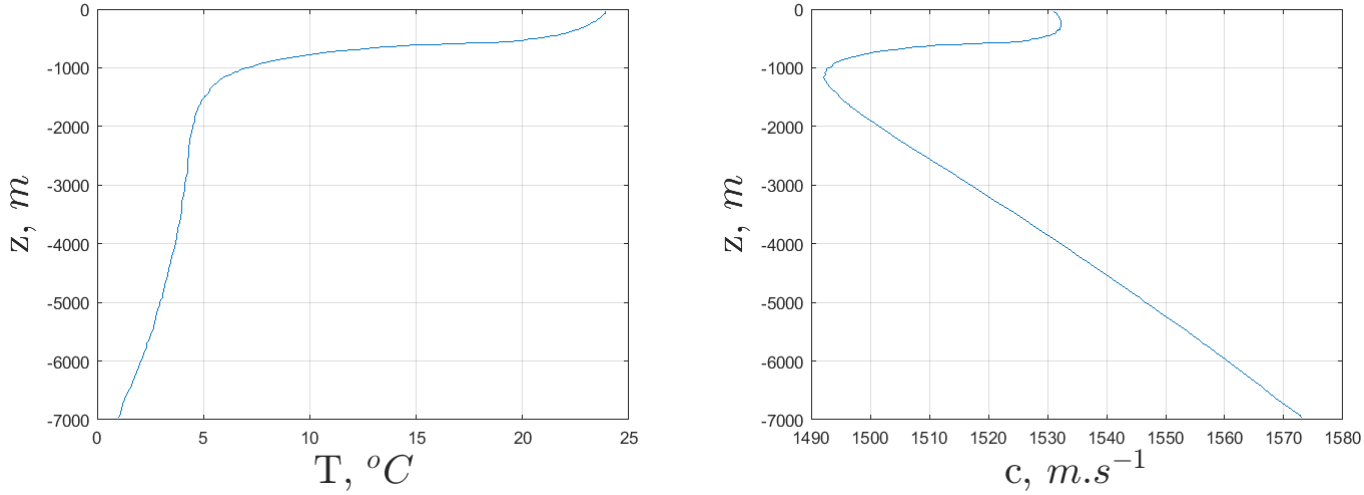

(a) Temperature profile in deep waters

(b) Deep water celerity profile

Figure 1.1: Bathycelerimetric profiles in deep water

empirical formula proposed by Clay and Medwin [11], simplifies the expression of the sound underwater to the following equation:

$$c = 1449,2 + 4,6\,T - 0,055\,T^2 + 0.00029\,T^3 + (1,34 - 0,010\,T)(S - 35) + 0,016\,z \quad (1.1)$$

where c is the speed of the sound in m/s, T is the temperature in degrees Celsius, S is the salinity in ppt (kg salt per kg water in parts per thousand), and z is the depth in meters. According to the equation (1.1), the sound increases with each of these parameters. In regions close to the surface, the temperature and pressure are almost constant. Consequently, the speed of the sound varies slightly. whereas, as the depth increases the temperature decreases directly, involving a decrease in the speed (see Figure 1.1). In general, the speed varies in an interval of 1450 m/s and 1500 m/s which is sufficient to impact the path of the acoustic wave in the medium.

1.1.2 Propagation of acoustic wave and rays theory

The propagation of acoustic waves can be seen as a mechanical perturbation that travels through a fluid. The physical parameter used to describe the propagating disturbance is identified as acoustic pressure [12]. The following equation defines the propagation of the acoustic wave in a homogeneous medium:

$$\frac{\partial^2 p}{\partial x^2} + \frac{\partial^2 p}{\partial y^2} + \frac{\partial^2 p}{\partial z^2} = \frac{1}{c^2(x,y,z)} \frac{\partial^2 p}{\partial t^2} \quad (1.2)$$

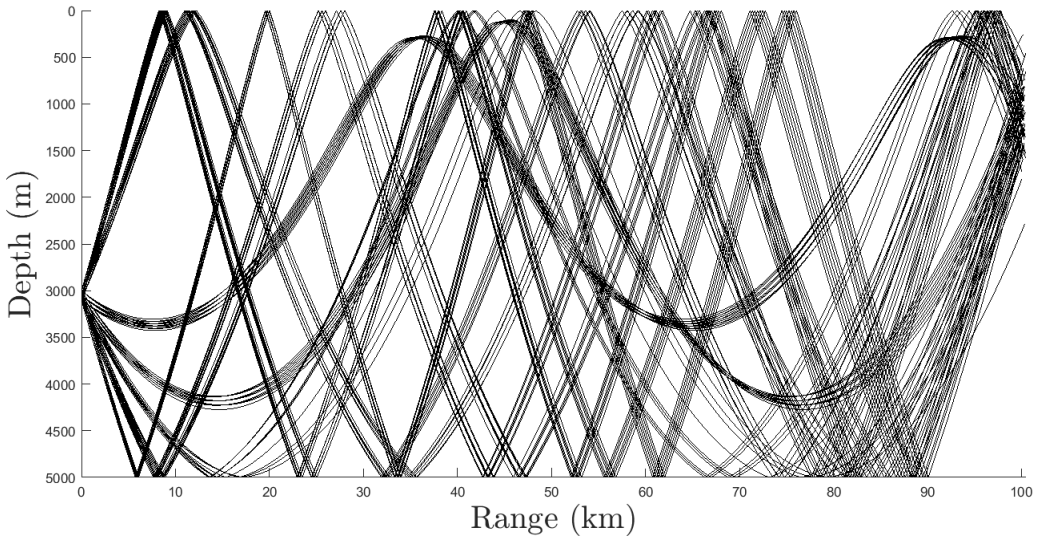

Figure 1.2: Rays tracing example (Bellhop)

where p is the acoustic pressure that depends on time and position, and c is the sound velocity. The models proposed to simulate the propagation of the acoustic wave underwater solve the equation (1.2). In light of the most commonly used methods for propagation modeling, there is ray theory [13, 14], normal mode [15, 16], parabolic equation [17, 18], wave-number integration [19, 20], energy flux [21, 22]. A study of the choice of the most suitable underwater acoustic model is made by [23] while considering the setup of transmitting and receiving elements (range, and depth) and also the frequency band.

The ray tracing technique is considered the most intuitive model for underwater acoustic waves in high frequencies. Indeed, this theory models the acoustic wave as a set of rays that are normal to wavefronts of constant phase. According to Snells law, a ray follows straight lines from the source in a medium with a constant speed. Whereas, in a medium, with a variant speed, the rays follow curved paths. Once the rays are computed, the acoustic field levels are calculated by summing the rays near the receiver. The rays are often extended in size by using the Gaussian beam approximation. Ray interaction with the seafloor is achieved using a reflection coefficient without penetration into the seafloor. As an example, Figure 1.2 shows the propagation of an acoustic wave in the ocean environment using Bellhop software for ray tracing.

1.1.3 Transmission Loss

When the acoustic wave propagates underwater, it loses its energy because of different phenomena (See Figure 1.3). We note two deterministic phenomena that have a major proportion in the calculation of losses: geometric divergence and absorption. A variety of empirical models exist to describe the transmission losses introduced in [24].

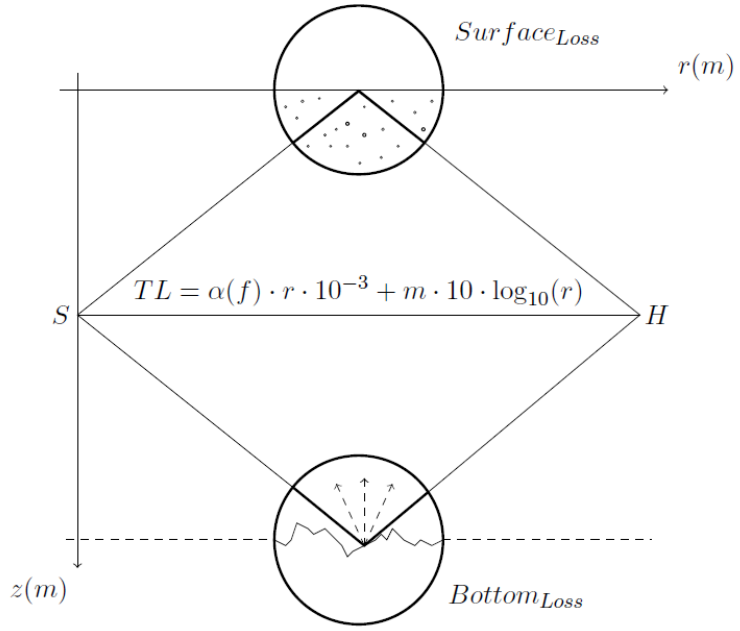

Figure 1.3: Losses of the acoustic wave underwater between point S and point H

1.1.3.1 Geometric Loss

In an unconstrained environment, the acoustic wave emitted by a source with a certain power spreads on spherical support. This power is then distributed on the surface of this sphere. As the wave propagates, the radius of the sphere increases. The initial power is then distributed over a larger surface, followed by a decrease in power. The geometric divergence of an acoustic wave is expressed as follows:

$$TL_{geometric} = m\ 10\ log_{10}(r) \tag{1.3}$$

where r is the propagation distance in meters and m is the index of the propagation of the acoustic wave. Typically, an emission in shallow waters is associated with cylindrical propagation ($m = 1$), and an emission in deep water is associated with spherical propagation ($m = 2$).

1.1.3.2 Absorption Loss

The acoustic wave is also subject to attenuation by underwater absorption. These losses are the consequence of the nature of water. Indeed, viscous absorption and ionic relaxation occur underwater because of the presence of boric acid and magnesium sulfate salts in water [25]. These losses are expressed as follows:

$$TL_{absorption} = \alpha(f)\ \frac{r}{1000} \tag{1.4}$$

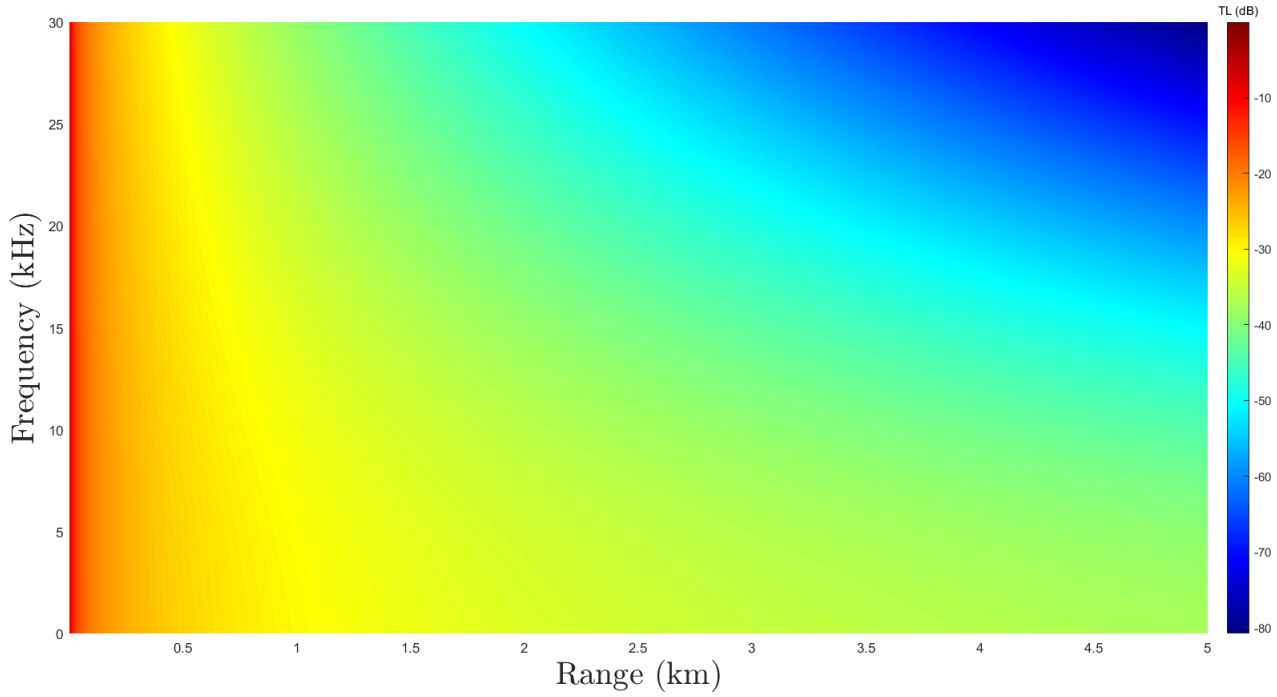

Figure 1.4: Transmission Loss in dB using Thorp model

with $\alpha(f)$ is the absorption coefficient in dB/km and r is the distance of propagation in meters. Several formulas exist to calculate the absorption coefficient α. As an example, François-Garrison [24] proposed an empirical formula that takes into account the relaxation frequency of boric acid, the relaxation frequency of magnesium, and the effect of temperature and depth. The commonly used formula depends only on the frequency proposed by Thorp [26]. For frequencies higher than a few hundred Hz it simplifies the absorption coefficient into:

$$\alpha(f) = 0,11\ \frac{f^2}{1+f^2} + 44\ \frac{f^2}{4100+f^2} + 2.75\ 10^{-1} f^2 + 0,003 \tag{1.5}$$

with f is the frequency expressed in kHz. According to equation (1.5) the coefficient increases with frequency. Therefore, at high frequencies, the attenuation becomes more significant which limits the available bandwidth.

Finally, considering both types of losses of an acoustic wave underwater, the overall expression of the transmission loss (TL) can be expressed as:

$$TL(r,f) = m\ 10\ log_{10}(r) + \alpha(f)\ \frac{r}{1000} \tag{1.6}$$

Figure 1.4 shows the level of transmission loss using the Thorp model at a given distance and carrier frequency. As we can see, the transmission loss is low at short range and becomes

more significant at long range and more particularly at high frequencies.

1.1.3.3 Reflection loss

In addition to geometric and absorption losses, there is the reflection loss of the acoustic wave underwater caused by the surface and the seafloor. These losses are considered quite complex to model because of the difficult relief of the medium. When the acoustic wave propagates towards the surface, it is totally reflected and it is dephased by π [27]. However, the layer of bubbles on the surface caused by the wave crash can have an important impact on the propagation of the wave, because of its persistence. The expression used to model the reflection of the acoustic wave on the surface given by [28] is:

$$Surface_{Loss} = \begin{cases} \frac{1}{sin(\theta)}\ 1.26\ 10^{-3}\ v^{1.57} f^{0.85} & if\ v \geq 6 \\ \frac{1}{sin(\theta)}\ 1.26\ 10^{-3}\ v^{1.57} f^{0.85}\ e^{1.2(v-6)} & otherwise \end{cases} \tag{1.7}$$

with f is the frequency, v is the wind speed wind in m/s and θ is the incidence angle of the acoustic wave.

Likewise, when an acoustic wave reaches the bottom, it is totally reflected if the angle of incidence is lower than the angle of grazing [27]. Above this angle of grazing, a part of the wave is reflected in the specular direction (the angle of reflection is equal to the angle of incidence), and the other part is diffused in all directions. Considering the bottom bounce configuration, the velocities c_1 and c_2 of the acoustic wave at the water layer and sea floor layer, then the angle of grazing can be defined as:

$$\theta_c = arccos(\frac{c_1}{c_2}) \tag{1.8}$$

The losses related to the partial reflection at the bottom are expressed as follows [24]:

$$Bottom_{Loss} = 10\ log_{10} \left(\left[\frac{m\ sin\ \theta_1 - (n^2 - cos^2\ \theta_1)^{1/2}}{m\ sin\ \theta_1 + (n^2 - cos^2\ \theta_1)^{1/2}} \right]^2 \right) \tag{1.9}$$

where $m = \frac{\rho_2}{\rho_1}$ and $n = \frac{c_1}{c_2}$, c_1 and c_2 are the velocities of the water and the bottom respectively, ρ_1 and ρ_2 the associated densities. To take into account the relief of the bottom and the irregularities of the interfaces, [29] introduced the Rayleigh parameter that characterizes the roughness as follows:

$$\Gamma = \frac{4\pi f \delta}{c_1} cos(\theta_c) \tag{1.10}$$

δ is here the standard deviation of the height irregularities. As an example, for a sandy

bottom, δ = 6 cm. Thus, the loss expression at the bottom according to [30] is:

$$Bottom_{Loss} = 10\ log\left(\left[\frac{m\ sin\ \theta_1 - (n^2 - cos^2\ \theta_1)^{1/2}}{m\ sin\ \theta_1 + (n^2 - cos^2\ \theta_1)^{1/2}}\ e^{-\frac{\Gamma^2}{2}}\right]^2\right) \tag{1.11}$$

Therefore, the overall expression of the transmission loss can be defined as a summation of equations (1.6), (1.7) and (1.11). For simplicity, only the expression in (1.6) is usually used in the literature for modeling the transmission loss.

1.1.4 Environment noise

The ambient noise represents the background noise in the medium which can be natural or man-made. The main sources model of ambient noise is turbulence, shipping, waves, and thermal noise. Each source can be modeled by a Gaussian power spectral density (PSD) distribution given by [31] as:

$$N(f) = N_t(f) + N_s(f) + N_w(f) + N_{th}(f) \tag{1.12}$$

- Turbulence Noise is mostly present in low frequencies (f<10 kHz).

$$10\ log_{10}(N_t(f)) = 17 - 30\ log_{10}(f) \tag{1.13}$$

- Shipping traffic produces noise from 10 Hz to 100 Hz.

$$10\ log_{10}(N_s(f)) = 40 - 20(s_a - 0.5) + 26\ log10(f) - 60\ log_{10}(f + 0.03) \tag{1.14}$$

  where s_a design the activity factor (0 low activity, 1 high activity)

- Surface motion and wind-driven waves generate noise in the frequency region of 100 Hz to 100 kHz.

$$10\ log_{10}(N_w(f)) = 50 + 7.5\ v^{1/2} + 20\ log_{10}(f) - 40\ log_{10}(f + 0.4) \tag{1.15}$$

- Thermal noise is dominant in high frequencies (f>100 kHz).

$$10\ log_{10}(N_{th}(f)) = -15 + 20\ log_{10}(f) \tag{1.16}$$

Figure 1.5 shows the power spectral density plots for different vessel traffic intensity values s_a and different wind speeds v. We observe that at frequencies between 10kHz and 100kHz, the contribution of maritime traffic has no influence, and only the wind speed impacts the noise's power.

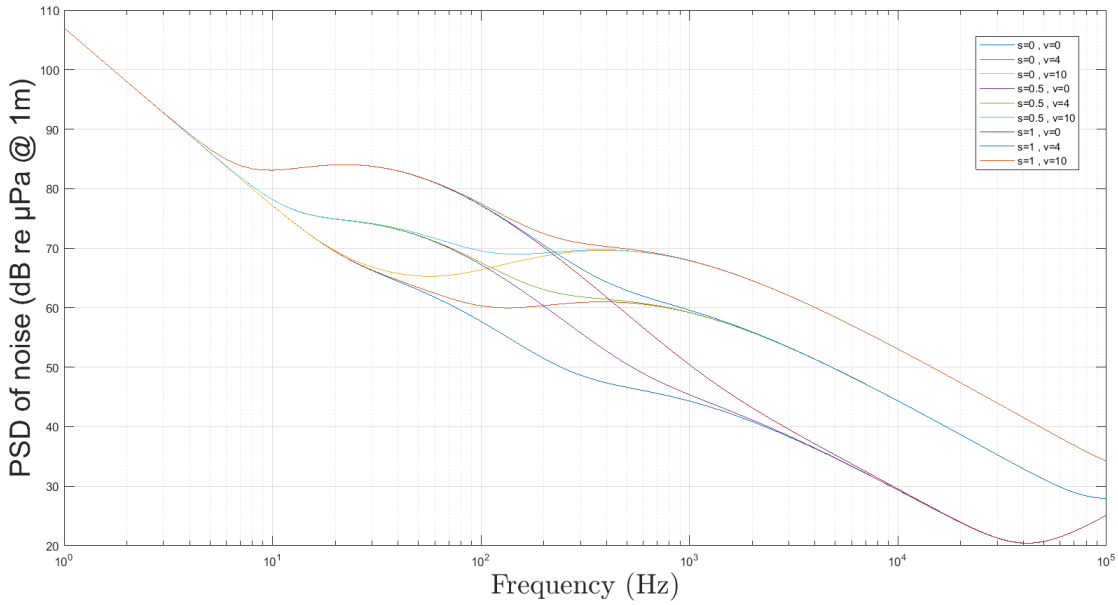

Figure 1.5: Noise PSD plots for different vessel traffic intensity values s_a and different wind speeds v

1.1.5 Multipath effect

As we have seen previously in the section 1.1.2, the acoustic wave propagates underwater in different directions. Due to the reflections at the bottom and surface, the received signal will result from several distinct paths traveled by the emitted wave. These paths have their own delay, phase shift, and attenuation. This phenomenon is known as the multipath effect and is one of the most challenging characteristics of UWA channels.

Because of the low speed of the acoustic wave underwater, the delays are quite different for each path. In vertical channels, the order of delay is very low. Whereas in horizontal configurations, the multipath spreads lead to significant time dispersion. The order of the channel delay spread is around 10 ms and can reach 50 ms according to [32]. Consequently, for a fixed set of communication, the multipath effect can lead to an important inter-symbol interference (ISI). The mathematical expression describing the multipath effect in the UWA channel will be introduced in the section 1.2.

1.1.6 Doppler effect

Due to the low propagation speed of acoustic waves underwater, the observed signal at the receiver could undergo a significant Doppler effect in the medium. This effect is mostly caused by the relative motion of the transmitting and receiving elements. Besides, it can also be produced as a contribution of the medium. More precisely, the reflection of the acoustic wave with the

surface, or the contact with air bubbles or with a marine organism (crustaceans for example) leads to a diffusion and consequently to the Doppler effect. Unlike electromagnetic waves in terrestrial environments, the Doppler effect is modeled as a frequency shifting because of the high speed of the wave, approximately 3×10^8 m/s. In underwater acoustic environments, the Doppler effect is interpreted as frequency shifting and extension or compression of the signal in the time domain, also known as Doppler spreading.

Let $s(t)$ denote the transmitted signal; then the Doppler effect applied to $s(t)$ can be modeled in the time domain as:

$$r(t) = s((1 + \Delta)t) \tag{1.17}$$

where $r(t)$ is the transformed signal by the Doppler effect, $\Delta = \frac{v_r}{c}$ is the Doppler factor defined as the ratio of the relative speed between transmitter and receiver v_r, and the speed of sound underwater c. It should be noted that in UWA channels, the transmitted signal could be delayed and attenuated because of the multipath effect. As a result, the received signal will be stretched or compressed in time by multiple Doppler factors. The following section introduces the overall formula used to describe both phenomena.

1.2 Underwater acoustic channel modeling

In this section, we focus on the channel impulse response of UWA channels. Firstly, we introduce the conventional formula used to model the UWA channel while considering the aforementioned characteristics of the medium. Then, we present the statistical models for UWA channels widely used for wireless communications.

1.2.1 Channel impulse response

The transformation caused by the UWA channel to a transmitted signal $s(t)$ is described by the channel impulse response (CIR) $h(t, \tau)$ that satisfies the following equation:

$$r(t) = h \otimes s(t) + w(t) = \int_{-\infty}^{\infty} h(\tau, t)s(t - \tau)d\tau + w(t) \tag{1.18}$$

where $\otimes$ represents the convolution operation and $r(t)$ is the received signal. Practically, the received signal contains noise $w(t)$. This noise is made by the electronic components. It is white, Gaussian, with zero mean. Its power is proportional to the sampling frequency of the signal, the temperature, and the Boltzmann constant. The UWA channel is modeled as a random channel. This description is more robust in the sense that transmission systems should be able to operate in a multitude of different propagation environments.

1.2.2 Assumption of WSSUS

While using the statistical models to describe the channel impulse response, the wide sense stationnary uncorrelated scattering (WSSUS) is often invoked. A channel is called wide-sense stationnary if its stochastic properties of order 1 and 2 are time-invariant (1.19).

$$\begin{cases} \mathbb{E}\{h(t_1,\tau)\} = \mathbb{E}\{h(t_2,\tau)\} \\ \mathbb{E}\{h(t_1,\tau)h(t_2,\tau)^*\} = \mathbb{E}\{h(t,\tau)h(t+t_2-t_1,\tau)^*\} \end{cases} \tag{1.19}$$

Moreover, the uncorrelated scattering (US) assumption involves no correlation between the fading coming from different signal scatters. Hence, the impulse response $h(t,\tau)$ is uncorrelated in τ domain. Consequently, considering both assumptions the auto-correlation function of the impulse response $R_h(t,t+\Delta t,\tau,\tau+\Delta\tau)$ is simplified from a four-dimension function into two dimensions-function $R_h(\Delta t,\Delta\tau)$.

Numerous works consider that the UWA channel is under the assumption of WSSUS [33, 34]. In practice, these conditions are not always verified according to [31, 35, 36]. However, within a limited time window and bandwidth, these assumptions can be considered more reasonable, so we discuss a quasi-WSSUS model.

1.2.3 Approximation of time-varying multipath channel

The underwater acoustic channel, particularly in shallow waters, is considered a time-varying multipath channel because of the reflections of the acoustic wave at the surface and the seafloor. In addition, it is also subject to the Doppler effect because of the motions and the moving transmitting and receiving elements. The expression of the impulse response mostly used to describe both phenomena for narrow band signals is, therefore, the following [37, 38]:

$$h(\tau,t) = \sum_p h_p(t)\delta(t-\tau_p(t)) \tag{1.20}$$

where $h_p(t)$ and $\tau_p(t)$ refer to the complex gain and the relative delay of path p, respectively. As the Doppler effect accrued at each path delay, the expression of $\tau_p(t)$ becomes:

$$\tau_p(t) = \tilde{\tau_p} - \int_0^t \frac{v_r(u)}{c}du \tag{1.21}$$

where $\tilde{\tau_p}$ represents the nominal time-delay of p^{th} path, and $v_r(t)$ is the relative speed between the transmitter and receiver in which the surface motion and the vehicular motion are included. For a fixed frame of data, the amplitudes are assumed constant within one data block $h_p(t) \approx h_p$, and the number of paths is limited to N_p paths. As a result, the channel impulse response

becomes:

$$h(t,\tau) = \sum_{p=1}^{N_p} h_p \delta(t - \tau_p(t)) \tag{1.22}$$

(1.22) is mostly used in deterministic channel modeling. As an example, the Bellhop ray tracing model is widely used for UWA channels [14]. It uses the sound speed profile at a given location to trace the path of different rays. Based on this output, it estimates the time travel τ_p (without the Doppler effect) and the amplitudes h_p. Besides, considering the bandwidth and the frequency of the transmitted signal, the model allows the calculation of the transmission loss.

1.2.4 Statistical models of underwater acoustic channel

Over the last decades, underwater acoustic channel modeling using statistical models has received much interest in the research community since conducting experiments and collecting real data is not always affordable. In this section, we introduce an overview of the existing statistical approaches to assess the characteristics of UWA channels.

1.2.4.1 Channel fading models

Several works studied the UWA channels stochastically using the analyses of experimental acoustic data collected in a particular location. As there is no conclusion about the most suitable distribution to the amplitude and the phase fluctuations of the channel, several distributions have been tested in the literature, and most of them are used in radio frequency communication scenarios. The main used distributions in the literature are listed in Table 1.1. The goodness of fit is usually carried out using different metrics of comparison such as Kullback-Leiber (KL) divergence criteria [39], the Bhattacharyya distance [40], Jensen-Shannon (JS) divergence [41], or Komlmogorov-Smirnov (KS) static [42].

Table 1.1: The probability density function of different distributions

Distribution	Probability density function
Rayleigh	$f(x;\sigma) = \frac{x}{\sigma^2} e^{-\frac{x^2}{2\sigma^2}}$, $x \geq 0$, with $\sigma^2 = \mathbb{E}(x)/2$, $\sigma \geq 0$
Nakagami	$f(x;m,\Omega) = \frac{2m^m}{\Gamma(m)\Omega^m} x^{2m-1} e^{-\frac{m}{\Omega}x^2}$, with $\Gamma(m) = \frac{x^{2m}}{\sigma^m}$ and $\Omega = \frac{x^2}{m}$
Rician	$f(x\|\nu,\sigma) = \frac{x}{\sigma^2} e^{\frac{-(x^2+\nu^2)}{2\sigma^2}} I_0(\frac{x\nu}{\sigma^2})$, with $I_0(z)$ is modified Bessel function of first kind
K-distribution	$f(x;\mu,\alpha,\beta) = \frac{2}{\Gamma(\alpha)\Gamma(\beta)} (\frac{\alpha\beta}{\mu})^{\frac{\alpha+\beta}{2}} K_{\alpha-\beta}(2\sqrt{\frac{\alpha\beta x}{\mu}})$ with $K(z)$ is a modified Bessel function of the second kind

Gamma distribution	$f(x;\alpha,\lambda) = \frac{\lambda^\alpha x^{\alpha-1} e^{-\lambda}}{\Gamma(\alpha)}$ $x > 0$, with $\alpha > 0$ and $\lambda > 0$
Beta distribution	$f(x;\alpha,\beta) = \frac{\Gamma(\alpha+\beta)}{\Gamma(\alpha)\Gamma(\beta)} x^{\alpha-1}(1-x)^{\beta-1}$

A summary of channel fading modeling based on different environments is shown in Table 1.2. The study consists of estimating the channel impulse response and the probability density function (PDF) of channel fading. After that, a criterion of the goodness of fit is applied to the measured channel PDF and to the theoretical PDFs to design the best fit.

Table 1.2: Example of works modeling UWA channel from experiment data

Ref	Channel	Probe signal	Tested distribution	Criterion	Best fit
[43]	Narragansett Bay (Race 08)	BPSK	- Rayleigh	-	Rayleigh
[44]	Pacific Ocean (KAM'08)	Turyn sequence	- Log-normal - Rician - Nakagami	-	Rician
[45]	Hudson River	Linear frequency modulation (LFM)	- Beta - Gamma - Rayleigh - Log-normal - Nakagami - Rician	Kullback-Leibler Bhattacharyya distance	- Rician at a distance of 200m. - Nakagami at a distance of 505 m.
[46]	Naragansett Bay, Rhode Island	-	- Rayleigh - Gamma - K-distribution	Kolmogorov-Smirnov	K-distribution
[47]	- Swimming pool - Water tank - Lake Erie - Lake LaSalle	Chirp signals DS-CDMA	- Rayleigh - Weibull - Rician - Beta - Nakagami	Kullback-Leibler	- Weibull and Rician for the tank, pool, and lake LaSalle. - Beta for lake Erie.
[48]	Mediterranean sea in La Algameca Chica (UCEX)	-	- $k-\mu$ Shadowed distribution. - Rician	Defined in [48] based on Kolmogorov-Smirnov	$k-\mu$ Shadowed distribution.

As depicted in Table 1.2, the result shows that the UWA channel doesn't necessarily follow Rayleigh or Rician distributions. This variety is due to experiment-specific properties such as the setup of the experiment and the probing signals. In addition, the time intervals during which the channel is observed are essential elements to consider. Other works distinguish between

long-term and short-term statistics to conclude about the channel fluctuations. For example, [49] showed that the long-term amplitude fading statistics follow a log-normal distribution, whereas the short-term amplitude fading statistics follow a Rayleigh distribution. Based on these results, they conclude that the joint long-term and short-term distributions yield a distribution close to the K distribution.

1.2.4.2 Statistical UWA channel modeling using small-scale and large-scale phenomena

As mentioned in the previous section, no standard static model satisfies the variability of UWA channels. A new consideration of enhancing the channel modeling is proposed in [50] by studying its characteristics in two scales: small-scale and large-scale effects. The distinction between small and large scale is referred to the order of the wavelengths. The small-scale effects design the scattering and motion-induced Doppler shifting that leads to the high variability of the channel. Large effects describe the location uncertainty that impacts the received power at a given location. The proposed time-varying channel transfer function is defined as:

$$H(f,t) = \bar{H_0} \sum_p h_p \tilde{\gamma_p}(f,t) e^{-j2\pi f \tau_p} \tag{1.23}$$

with,

$$\tilde{\gamma_p}(f,t) = \gamma_p(f,t) e^{j2\pi a_p f t} \tag{1.24}$$

and,

$$\gamma_p(f,t) = \frac{1}{h_p} \sum_{i \geq 0} h_{p,i} e^{-j2\pi f \delta_{\tau_{p,i}}} \tag{1.25}$$

where $\gamma_p(f,t)$ represents the small-scale coefficient composed of the intrapath gains $h_{p,i}$ and intrapath delays $\delta_{\tau_{p,i}}$ which are generated as random parameters to model random placement of scattering points within a scattering field. The coefficient $e^{j2\pi a_p f t}$ characterizes the Doppler effect at each path p. The path delays τ_p is calculated using the propagation paths of length l_p and the speed of sound in water c using the following formula:

$$\tau_p = l_p/c - l_0/c \tag{1.26}$$

The term $l_p = \bar{l_p} + \Delta l_p$ represents the propagation paths of nominal length $\bar{l_p}$ and the coefficient Δl_p modeling the location uncertainty (variation). The path gain h_p is approximated using the length l_p by:

$$h_p = \bar{h_p} \frac{1}{\sqrt{(1 + \frac{\Delta l_p}{\bar{l_p}})^k a_0^{\Delta l_p}}} \tag{1.27}$$

with,

$$\bar{h_p} = \frac{\Gamma_p}{\sqrt{(\frac{\bar{l_p}}{l_0})^k a_0^{\bar{l_p}-\bar{l_0}}}} \tag{1.28}$$

The constant a_0 is the absorption coefficient that can be chosen at any frequency within the defined bandwidth here it is approximated to 1. Γ_p is the cumulative reflection coefficient encountered over n_{sp} surface and n_{bp} bottom reflections along the p^{th} path. Under the assumption of $\Delta l_p \ll \bar{l_p}$ and $k \ll \bar{l_p}$ the expression of h_p is simplified to the following expression:

$$h_p \approx \bar{h_p} e^{-\varepsilon_p \Delta l_p/2} \tag{1.29}$$

with $\varepsilon_p = a_0 - 1 + \frac{k}{\bar{l_p}}$. Considering the location variation the parameters h_p and τ_p design the large-scale parameters. Given that the path variation can be modeled as Gaussian, the path gain is generated using log-normal distribution.

This model has been performed using experimental data with different varieties of mobility. The probing signals used were pseudo-noise (PN) sequences and binary phase-shift keying (BPSK). The setup of experimental channels is listed in Table 1.3.

Table 1.3: The setup of experiments

Experiment	B (kHz)	rate (kb/s)	range (km)	d_{T_x} (m)	d_{R_x} (m)	d_{water} (m)
SPACE	8-17	6.5	0.06-1	4	2	10
MACE	10.5-15.5	5	0.5-4	45	60	100
KAM	8.5-17.5	6.5	3	58	59	103
PS	8-12	-	0.2-1	3	130	130

The obtained result demonstrated that the probability distributions and correlation functions of small and large-scale parameters have a good match with the theoretical models.

1.2.4.3 Geometric-Based channel model for underwater acoustic channel

In addition to the previous models of underwater acoustic channels, another approach is proposed to model the UWA channel geometrically. Indeed, it consists of modeling the multipath scattering environments between the transmitter and the receiver underwater, while assuming that the scatters are randomly distributed on the surface and the bottom [51, 52, 53].

To understand the principle of modeling we focus on work introduced in [53]. As shown in Figure 1.6, this model studies the propagation of scattering between a transmitter and a mobile receiver in a signal-input single-output (SISO) channel, while combining both the line-of-sight (Los) components and non-LoS (NLoS) components. The overall expression channel impulse

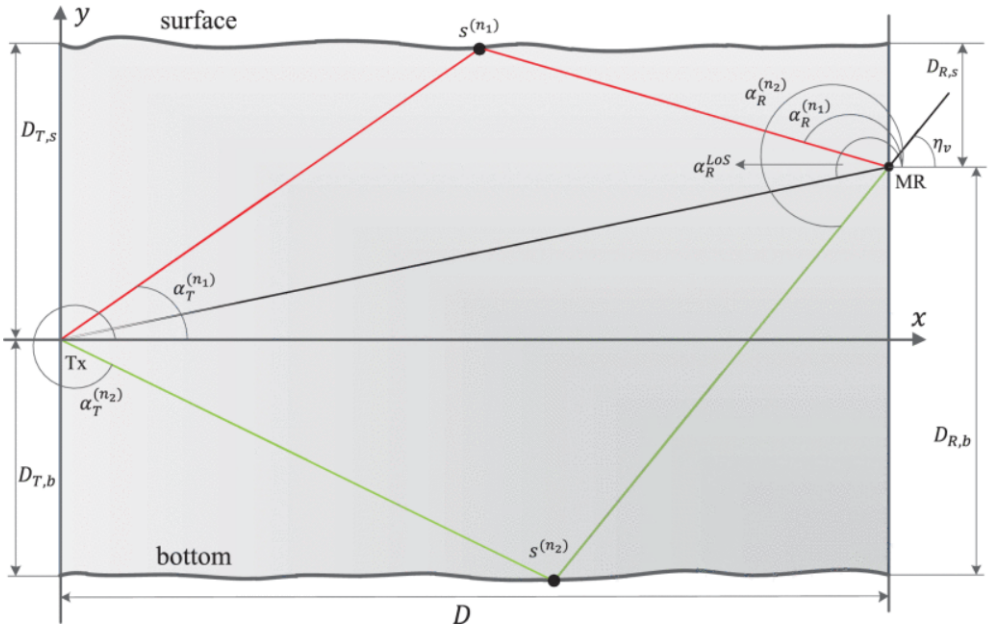

Figure 1.6: Illustration of path propagation for LoS and NLoS. Copied from [53]

response is given by:

$$h(t,\tau') = h_0(t,\tau') + \sum_{l=0}^{2} h_l(t,\tau') \tag{1.30}$$

The complex term $h_0(t,\tau')$ represents the LoS component can be expressed as:

$$h_0(t,\tau') = \sqrt{\frac{K}{1+K}} A_s(D_0) A_a(D_0) \times e^{j(2\pi f_0 t + \phi_0)} \delta(\tau' - \tau'_0) \tag{1.31}$$

with K is the rice factor, τ'_0 is the propagation delay of the LoS component, ϕ_0 is the initial phase generated as random parameter using uniform distribution $[-\pi, \pi)$ and f_0 designs the Doppler frequency of LoS component. Based on the geometry of the Los component the parameters τ'_0, f_0 and the absorption coefficients $A_s(D_0)$, $A_a(D_0)$ can be expressed as:

$$f_0 = \frac{v_r}{c} cos(\alpha_R^{LoS} - \eta_v) \tag{1.32}$$

$\alpha_R^{LoS} = \pi + arctan(\frac{D_{T,s} - D_{R,s}}{D_0})$ is the angle of arrival.

$$\tau'_0 = \frac{1}{c}\sqrt{D_0^2 + (D_{T,s} - D_{R,s})^2} \tag{1.33}$$

and,

$$\begin{cases} A_s(D_0) = \frac{1}{D_0} \\ A_a(D_0) = 10^{-\frac{1}{2000} \times D_0 \kappa} \end{cases} \tag{1.34}$$

where κ is a parameter that depends on the salinity, carrier frequency, temperature, and depth. An approximation of this parameter is introduced in [54]. For NLoS component the expression of $h_l(t,\tau')$ is defined as:

$$h_l(t,\tau') = \lim_{N_l\to\infty} \sum_{n_l=1}^{N_l} \frac{1}{\sqrt{2N_l(1+K)}} \times A_s(D_{n_l})A_a(D_{n_l}) \times e^{j(2\pi f_{n_l}+\phi_0)}\delta(\tau'-\tau'_{n_l}) \quad (1.35)$$

where τ'_{n_l} is the propagation delay of l-th path, $f_{n_l} = \frac{v_r}{c}cos(\alpha_R^{(n_l)} - \eta_v)$ is the Doppler frequency, and D_{n_l} is the propagation delay of the acoustic wave from the transmitter that crosses the scatters $s(n_l)$ then reach the arriving point. Geometrically, the parameter D_{n_l} can be expressed as:

$$D_{n_l} = \frac{D_{T,s}}{sin(\alpha_T^{(n_l)})} + \frac{D_{R,s}}{sin(\alpha_R^{(n_l)})} \quad (1.36)$$

Based on this model, [53] proposed the expressions of the probability density functions of the angle of departure and angle of arrival statistics. Moreover, they introduced the spatial correlation function (1.37) using the transfer function impulse response $H(t,\tau')$ while assuming that the UWA channel is stationary in both frequency and time domains.

$$\rho_{HH}(\tau,\nu') = \frac{\mathbb{E}\{H(t,\nu')H(t+\tau,t+\nu')^*\}}{|\mathbb{E}\{H(t,\nu')\}|^2} \quad (1.37)$$

To perform the proposed model, the spatial correlation function has been compared to the time-varying spatial correlation function introduced in [55] defined as:

$$\hat{\rho}_{HH}(\tau,\nu') = \frac{K}{1+K}e^{j2\pi(f_0\tau-\tau'_0\nu')} + \frac{K}{1+K} \times \sum_{n_l=1}^{N_l} c_{n_l}^2 e^{j2\pi(f_{n_l}\tau-\tau'_{n_l}\nu')} \quad (1.38)$$

c_{n_l} is the channel gain of path l defined as:

$$c_{n_l} = \frac{A_s(D_{n_l})A_a(D_{n_l})}{\sqrt{2\sum_{n_l=1}^{N_l} A_s^2(D_{n_l})A_a^2(D_{n_l})}} \quad (1.39)$$

The comparison is made using two methods dedicated to calculating the model parameters of the simulation channel for both models, namely the MESS and the Lp-norm. The result shows better performance of the model proposed in [53] compared to the underlying reference model.

1.2.4.4 Stochastic Replay of Non-WSSUS underwater acoustic channel

Another mean to compute stochastically the underwater acoustic channels is proposed by Socheleau in [56]. Unlike the previous approaches, this method is not based on the assumption of

(quasi-) WSSUS. Indeed, after analyzing the collected data from the Mediterranean Sea (2004) and the Atlantic Ocean (2007), it has been concluded that on the one hand, the wide sense stationary assumption is not always verified. On the other hand, the estimated channel impulse responses are more $trend$ stationary. Consequently, they used the empirical mode decomposition (EDM) process to propose a model called stochastic replay. From one single observation, the purpose is to generate an infinite number of realizations of the same process.

As introduced in [56] the UWA channel h_l is a $trend$ stationary random process if for each tap l it satisfies the following conditions:

$$h_l(k) = d_l(k) + w_l(k) \tag{1.40}$$

and, for all k, k_1 and $k_2 \in \mathbb{Z}$

$$\mathbb{E}\{h_l(k)\} = d_l(k) \tag{1.41}$$

$$\begin{aligned}\mathbb{E}\{(h_l(k_1) - \mathbb{E}\{h_l(k_1)\})(h_l(k_2) - \mathbb{E}\{h_l(k_2)\})^*\} &= \mathbb{E}\{w_l(k_1)w_l(k_2)\} \\ &= \mathbb{E}\{w_l(k)w_l(k + k_2 - k_1)\}\end{aligned} \tag{1.42}$$

with $d_l(k)$ is a pseudo-coherent element that represents the contribution as if the channel is deterministic and $w_l(k)$ is a wide sense stationary random process with a zero mean. Using the empirical mode decomposition, the estimated UWA channel can be expressed as [57]:

$$h_l(k) = \underbrace{\sum_{q=0}^{S_l-1} m_{l,q}(k)}_{w_l(k)} + \underbrace{\sum_{q=S_l}^{Q_l-1} m_{l,q}(k) + r_l(k)}_{d_l(k)} \tag{1.43}$$

where $m_{l,q}$ is q-th of the Q_l modes resulting from the EMD of the tap h_l, S_l is the decomposition order leading to the separation of two components, and r_l is the decomposition residue.

The principle of stochastic reply of measured impulse responses is based on the generation of new realizations of the process $\Omega(k) = [w_l(k)]_{l\in[0\ldots L]}$ (for all taps) while keeping their intrinsic second-order statistics. Indeed, from a given observation, a new multiple-variate complex random Gaussian process $\Psi(k) = [\lambda_l(k)]_{l\in[0\ldots L]}$ can be defined as follows:

$$\lambda_l(k) = \frac{1}{\sqrt{N}} \sum_{n=0}^{N-1} W_l(n) e^{\frac{2j\pi nk}{N}} e^{j\theta_l(n)} \ , \ \forall\, 0 \leq l \leq L \tag{1.44}$$

with $W_l(n) = \frac{1}{\sqrt{N}} \sum_{k=0}^{N-1} w_l(k) e^{\frac{-2j\pi nk}{N}}$, $\theta_l(n)$ is an independent and identically distributed random variable chosen to be uniformly distributed in $(0, 2\pi]$ and N is the observation window. In order to ensure that the generated $\Psi(k)$ respect the second-order statistics criteria, it is proposed to create dependence between the random phase shifts more precisely, they fixed $\theta_l(n) = \theta_p(n)$

and suppose that $\{e^{j\theta_l(n)}\}_n$ is independent and identically distributed that satisfies:

$$\begin{cases} \mathbb{E}[e^{j(\theta_l(n)-\theta_p(n))}] = 1 \\ \mathbb{E}[e^{j(\theta_l(n)-\theta_p(m))}] = 0\ ,\ m \neq n \end{cases} \tag{1.45}$$

Consequently, the correlation matrix of $\Psi(k)$ can be written as

$$\mathbb{E}[\lambda_l(k)\lambda_p^*(k-u)] = \frac{1}{N}\sum_{k=0}^{N-1} w_l(k)w_p^*([k-u]N) \tag{1.46}$$

Finally, for a probed channel composed of $(L+1)$ taps over an observation window of N samples, the l^{th} tap can be generated by computing the following steps:

- Apply the EMD to obtain $h_l(k) = d_l(k) + w_l(k)$,
- Calculate $W_l(n) = \frac{1}{\sqrt{N}}\sum_{k=0}^{N-1} w_l(k)e^{\frac{-2j\pi nk}{N}}$,
- Calculate $\lambda_l(k) = \frac{1}{\sqrt{N}}\sum_{n=0}^{N-1} W_l(n)e^{\frac{2j\pi nk}{N}}e^{j\theta_l(n)}$,
- Compute the new l-th tap channel as $\hat{h_l}(k) = d_l(k) + \lambda_l(k)$

The main advantage of the proposed model is providing realistic conditions of underwater acoustic channels, which can greatly assess communication in diverse environments. However, this model is limited to a narrow validation scope because of the probe channels used in certain locations.

1.2.4.5 Conclusion

Driven by the huge demand to reproduce the close possible model of underwater acoustic channels, statistical models are proposed as the most intuitive solution since it is possible to generate the physical properties of the channel (fluctuations, scattering, etc.) randomly. The aforementioned approaches can provide a good approximation to UWA channels. However, it should be noted that most of them are based on the WSSUS assumption, which is not always verified. Moreover, the non-WSSUS solution relies on the measured impulse responses, which makes it an environment-dependent solution.

1.3 Underwater acoustic channel simulators

In this section, we aim to provide the most used open-source simulators for UWA channels.

1.3.1 BELLHOP

BELLHOP is a static channel modeling simulator for UWA channels available as part of the Acoustics Toolbox [20]. This simulator is based on ray and beam tracing theory to solve the wave equation (1.2). As already explained in section 1.1.2, the acoustic wave is introduced in the medium as a set of rays, depending on the starting angle of transmission, each ray travels a different path which is governed by the speed profile. The concept of the beam is more precise than the rays since it includes intensity profile to ray trajectory. Practically, the BELLHOP model utilizes various inputs, including the speed profile at a specific location (which can be gathered from the NOAA database), a set of nodes, frequency bandwidth, bathymetry, and surface profiles (for simulating scattering at the top and bottom). As a result, it provides a multipath impulse response and the channel's gain for each deployed receiver.

1.3.2 KRAKEN

KRAKEN is another static model for the UWA channels [58]. This simulator is based on normal mode theory to solve the wave equation (1.2). Unlike the ray solution, the normal mode method allows the sound field to be calculated at any location between the source and the receiver. The normal mode method is most suited to a channel where the number of modes is small, i.e., relatively shallow water channels with low-frequency signals. An enhancement of the attenuation calculation of the propagating media and the surface roughness is proposed by Porter in [59].

1.3.3 VirTEX

Timeseries EXperiment (VirTEX) is a simulator based on Bellhop channel modeling to provide a time-varying channel impulse response for an underwater acoustic environment [60]. It takes into account the Doppler effect caused by the node and the sea surface motions. This simulator is considered more adapted to physical layer communication assessment since it includes the physical phenomena that could occur in such channels, and more importantly, it introduces different configurations through time variability.

1.3.4 Watermark

The Underwater Acoustic channEl Relpay benchMARK (Watermark) [61] simulates a virtual underwater acoustic transmission using sea measurements of the time-varying impulse response. The first release of this simulator has been established using different locations (Norway, France, and Hawaii) at different frequency bands (4-8 kHz, 10-18 kHz, and 32.5-37.5 kHz). The large number of estimated channel impulse responses provide highly realistic and reproducible conditions of UWA channels, including the hardware parts. This model is suitable for performing the physical layer algorithms

1.3.5 conclusion

For the rest of this work, we choose the Watermark simulator to perform the proposed algorithms for communication and Bellhop for localization. The Watermark simulator is mainly based on measured channels which introduce the acoustic propagation effects and also hardware effects. It will allow a better assessment of a transmitted signal in the medium. For the localization part, the Bellhop is most adapted to our case because it has the ability to generate CIRs from a given geometry position of transmitters and receivers.

1.4 Characterization of UWA channel

The purpose of this section is to provide the methodology to characterize an UWA channel. Firstly, we focus on estimating the channel impulse response using probe signals. Then, we introduce its derived functions, such as the scattering function, power delay profile, and Doppler spread. Finally, we give an example of a real UWA channel measured during this thesis.

1.4.1 Estimation of the impulse response of UWA channel

The commonly used method to estimate the time-varying impulse response is based on the correlation method [62]. Usually, probe signals with a wide frequency spectrum are used in this method. Among the most used probing signals, there are Pseudo-Random Binary Sequence (PRBS), Binary Phase Shift Keying (BPSK), linear frequency modulation (LFM), and Hyperbolic frequency modulation (HFM).

If we note $s(t)$ the transmitted signal and $h(t, \tau)$ the time-variant impulse response defined in a window of observation t and delay τ, then the received signal $r(t)$ can be expressed as the convolution between $s(t)$ and $h(t, \tau)$ with an additional noise $w(t)$ (equation (1.18)). The frame structure of transmitted signal $s(t)$ used to estimate the impulse response of the channel

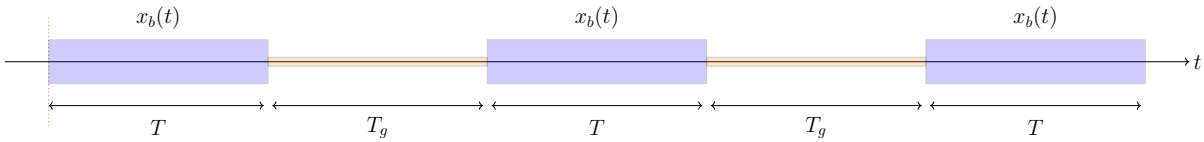

Figure 1.7: structure of transmitted signal

$\hat{h}(t,\tau)$ over time, is composed of a set of a probe signal $x_b(t)$ defined within a bandwidth B and at time T, spaced in time with time guard T_g as shown in Figure 1.7. By applying the cross-correlation function to the received signal $r(t)$ and the signal $x_b(t)$, the estimated time-variant impulse response of the channel $\hat{h}(t,\tau)$ can be obtained.

$$\hat{h}(t,\tau) = (r * x_b)(t) = (x_b * h * x_b)(t) + (w * x_b)(t) = (h * R_{x_b})(t) + (w * x_b)(t) \quad (1.47)$$

where $w(t)$ is the noise and $R_{x_b}(t)$ the auto-correlation function of $x_b(t)$. As mentioned in the equation (1.47) the estimated impulse response includes the noise term, which could strongly impact the estimation process. For better computation of the channel, it is recommended to filter the received signal and, in terms of hardware, to use a high-power transmitter and a hydrophone with good sensitivity to minimize the noise contribution.

1.4.2 Channel characteristics

After the computation of the time-varying channel impulse response, it is now possible to retrieve its characteristics such as multipath delay spread τ_m, Doppler spread ν_m, coherence time T_c and coherence bandwidth B_c [63]. It should be noted that the calculation is made while assuming the channel is WSSUS.

1.4.2.1 Power delay profile

The power delay profile (PDP) gives the average power output over the time variable t as a function of the time delay τ.

$$P(\tau) = \int_t |h(t,\tau)|^2 dt \quad (1.48)$$

This function is used to follow the variability of the power at each tap of the channel during the period of measurement, which can be used to study the frequency selectivity of the channel. More precisely, it allows calculating the multipath delay spread τ_m as the first and the last received component.

1.4.2.2 Doppler spread function

The Doppler spread function is calculated as the Fourier transform of the impulse response $h(t, \tau)$ as expressed by equation (1.49).

$$S(\nu, \tau) = \mathfrak{F}(h(\tau, t)) = \int_{-\infty}^{\infty} h(t, \tau) e^{-2j\pi\nu t} dt \tag{1.49}$$

with $-\frac{1}{2T} \leq \nu \leq \frac{1}{2T}$. This function presents the deterministic distribution of signal power in the frequency domain. The integration of the delay axis provides an estimate of the Doppler spectrum $P_v(\nu)$.

$$P_v(\nu) = \int_{\tau} |S(\nu, \tau)|^2 d\tau \tag{1.50}$$

Hence, using this formula, the maximum Doppler spread can be obtained as the width of $P_v(\nu)$.

1.4.2.3 Auto-correlation of the channel impulse response

As mentioned in section 1.2.2 under the WSSUS assumption, the auto-correlation function R_h depends only on Δt and $\Delta\tau$ variables, which simplifies its computation. By performing Fourier transform to R_h, we obtain the auto-correlation of the channel transfer function (1.51).

$$R_H(\Delta t, \Delta f) = \mathfrak{F}(R_h(\Delta t, \Delta\tau)) = \int_{-\infty}^{\infty} R_h(\Delta t, \Delta\tau) e^{-2j\pi f \Delta\tau} d\Delta\tau \tag{1.51}$$

where $-\frac{B}{2} \leq \Delta f \leq \frac{B}{2}$. The time correlation function $R_H(\Delta t)$ can be obtained by fixing Δf at 0. Thus the time coherence T_c can be retrieved by calculating the width of this function. Likewise, the frequency correlation function $R_H(\Delta f)$ can be calculated by fixing Δt at zero. Therefore the coherence bandwidth can be computed as the width of this function.

1.4.3 Example of UWA channel

In this section, we provide an example of UWA channel characterization in a lake trial. The experiment is conducted in "Bassin à Flot" lake in Bordeaux during July 2022.

1.4.3.1 Setup of experiment

The setup of this experiment was as follows: the distance between the transmitter and the receiver was 140 m. The depth of the lake was around 16 m, and both transmitter and receiver were fixed at a depth of 4 m. The breakdown of the parameters used to generate the probe signal is listed in table 1.4.

Table 1.4: Parameters of the transmitted signal

Parameter	Value
Carrier frequency	18 kHz
Bandwidth	5 kHz
Type	Single input single output
Probe signal type	Hyperbolic frequency modulation
Delay coverage	102.4 ms
Doppler coverage	9.76 Hz
Total play time	60 seconds

1.4.3.2 Experiment results

The characteristics of the experiment are expressed in Figure 1.8. As we can see, the channel has three major paths that vary slightly over time for approximately 4 ms. Besides, the Doppler effect is present in the channel, and it introduces a frequency shift between -1 and 1 Hz.

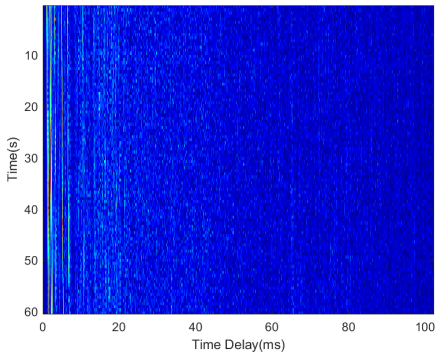

(a) Channel impulse response

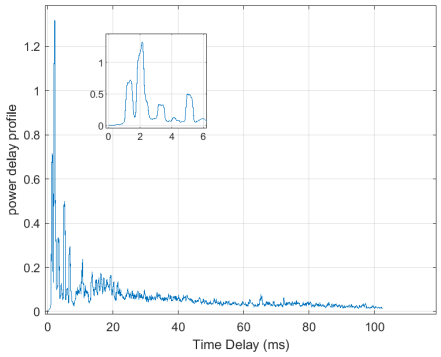

(b) Power delay profile

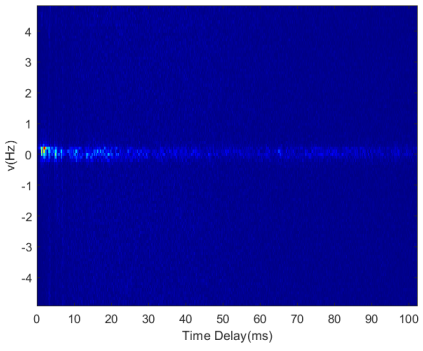

(c) Doppler Spreading function

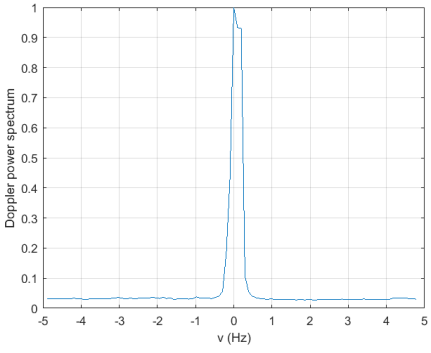

(d) Doppler power spectrum

Figure 1.8: Characteristics of "Bassin à Flot" lake

1.5 Conclusion

In this chapter, we presented the fundamental aspects of the underwater acoustic channel. Firstly, we started by providing a global understanding of the physical properties of the medium. By means of ray tracing theory we showed the propagation of the acoustic wave underwater. Secondly, we introduced the phenomena of the UWA channels, such as the multipath effect due to the surface and bottom scattering. Moreover, considering the low speed of the acoustic wave, we highlight that the medium can be subject to the Doppler effect because of the moving transmitting and receiving elements and the waves' motion. Consequently, a frequency shift can be introduced to the propagated wave and could also be stretched or compressed in time because of the Doppler spread. So far, the UWA channel is characterized by high temporal and spatial variability.

As we are interested in establishing a communication and localization system in such channels, our first task was choosing the most adapted model to reproduce the close possible environment. To do so, we listed the existing statistical models for the UWA channel while considering the phenomena previously mentioned. In the literature, we concluded that there is no standard model for channel modeling, and the statistical approaches are ongoing research. However, it is possible to have a robust model to assess the transmission systems in many different propagation environments. Namely, we choose Watermark as a simulator to perform developed algorithms for communication and Bellhop for localization introduced in chapters 2 and 3, respectively.

Finally, to conclude the study of the UWA channel, we explained the methodology to characterize the medium while assuming the WSSUS condition. More precisely, we used the correlation method to estimate the channel impulse response and retrieve its characteristics that can be summarized in the multipath delay spread, the Doppler spread, coherence time, and coherence bandwidth. In our case, these parameters would help to analyze recorded data and propose adapted processes to enhance communication and localization. An example of a measured channel in a lake trial is provided as part of experiments to perform the proposed system.

CHAPTER 2

Chirp-based signals for underwater acoustic communication

In the previous chapter, we provided an overview of the UWA channel. We showed that the channel is a subject of multiple phenomena, such as the multipath effect, Doppler effect, intense transmission loss, and high time variability. Thus, the transmitted signals in such channels require adapted processing at the receiver to overcome the severe characteristics of the channel and retrieve the carried data. In this chapter, we start by introducing the acoustic link budget for passive communication. Based on this analysis, we present an overview of the most used techniques for underwater acoustic communication at low signal-to-noise ratio (SNR) levels. These techniques have environmental merit because of the ability to use low-power transmitting systems. After that, we explain in detail the proposed scheme of communication, the differential chirp spread spectrum technique (DCSS), as a potential solution to preserve marine animals from acoustic pollution. In section 2.3.1, we present the developed system to carry out experiments in underwater acoustic environments. Finally, we present and discuss the obtained experimental results of DCSS in both lake and ocean trials.

2.1 Introduction

Driven by the huge demand to explore natural resources, conduct ocean research, and warn from natural disasters, underwater acoustic communications (UAC) have become a fast-growing field in recent decades. Many researchers have tackled this topic to overcome the severe characteristics of the UWA channel and propose reliable and adapted techniques ensuring data link. The choice of the most suitable modulation can be made depending on the range of communication, the data rate, and the power consumption. As seen in the previous chapter, the communication frequency band greatly depends on the attenuation of the acoustic wave in the medium. Hence,

ensuring communication in high frequencies requires high transmitting power. As depicted in Figure 2.1, the sound produced by marine animals is mainly used by underwater acoustic systems. Therefore, deploying boosting power systems will pollute the ocean environment acoustically and participate in species migration, as mentioned in [64].

Moreover, a behavioral study on harbor Porpoise carried out by [65] showed that for a fixed transmitting power (171 $dB\ re\ 1\ \mu Pa\ @1m$), the discomfort zones changes depending on the waveform of signals (DSSS, LFM, FSK ...) used in the experiments and the frequency range. Similarly, [66] studied the impact of seven types of modern commercial ships on marine life. The result showed that the acoustic power and spectral content affect the biotopes.

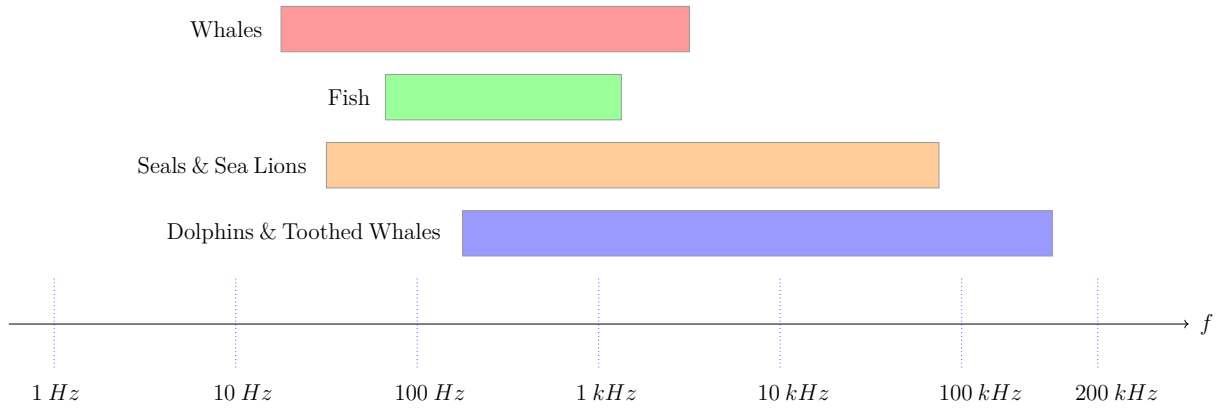

Figure 2.1: Frequency range of sound produced by marine animals according to OSPAR 2009b

In order to reduce the impact of propagated signals in UWA channels, it is mandatory to communicate below the background noise or at least at low SNR values. This way, the transmitted signals in the medium will be almost inaudible for marine animals. To achieve this, we establish an acoustic link budget and identify the parameters that would make communication at a low level of SNR possible. Then, we introduce the existing techniques for low SNR underwater acoustic communication. Finally, we focus on chirp-based signals as a likely solution for UAC to protect the biotopes from pollution.

2.1.1 Acoustic Link Budget

Acoustic link budgeting is an essential tool for studying the performance of communication underwater. It considers transmitter power, the directivity of transmitter and receiver, and channel parameters such as propagation loss and noise to predict the SNR at the receiver [67]. The strong frequency dependence of underwater acoustic propagation requires a link budget analysis within the communication bandwidth to estimate the SNR and predict the distance where the communication can be established. The acoustic link budget underwater can be simplified

to the following equation:

$$SNR = PSL - TL(d, f) - N(f) + DI_{Tx} + DI_{Rx} \tag{2.1}$$

where $TL(d, f)$ is the transmission loss in the medium (see section 1.1.3), $N(f)$ is the ambient noise (see section 1.1.4), DI_{Tx} and DI_{Rx} represents the gain of directivity of the transmitter and the receiver. Finally, PSL is the pressure spectrum level. It is a function of input power and transmission bandwidth. For a pure broadband signal defined within a bandwidth B, its PSL is given by:

$$PSL = SL - 10\ log_{10}(B) \tag{2.2}$$

It should be noted that the formula (2.2) can be changed depending on the nature of the transmitted signal. The power of an acoustic source SL is expressed in dB referenced to a pressure of 1 μPa at a distance of 1 meter from the source. As a reference, an acoustic power of 171 $dB\ re\ 1\ \mu Pa\ @1m$ is equivalent to an electrical power of 1 W.

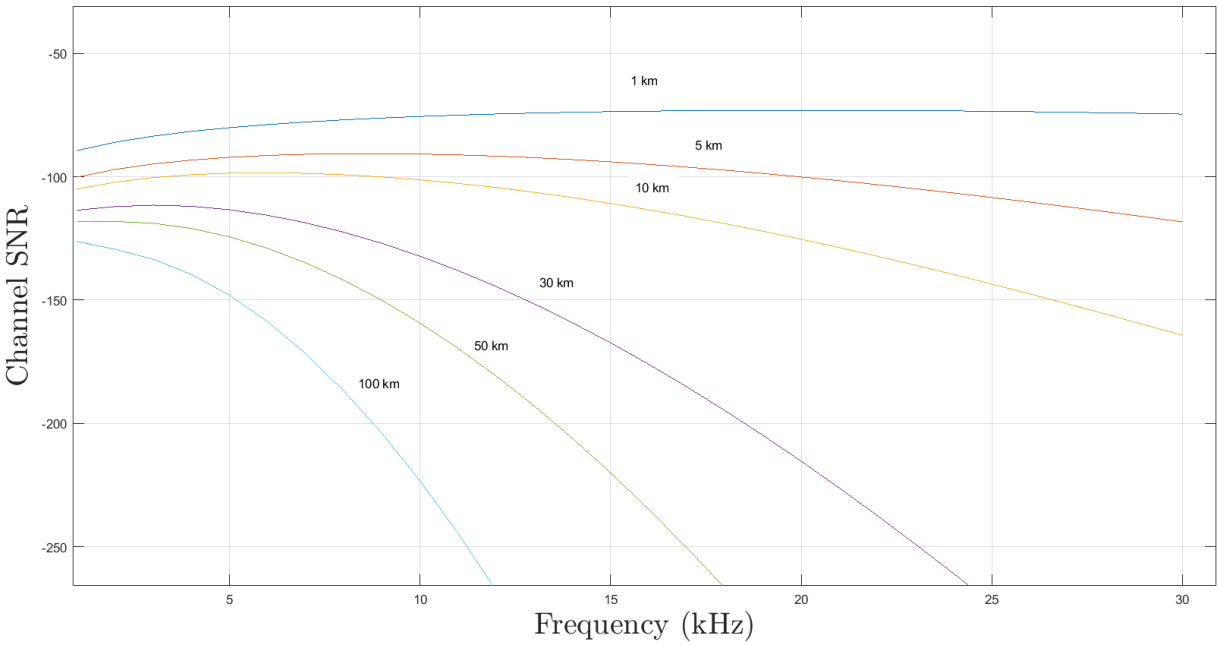

Figure 2.2: Illustration of the channel contribution in SNR calculation using Thorp model ($k = 1.5$); and noise spectrum ($s_a = 0$, $v = 0$)

Figure 2.2 illustrates the channel's impact in the SNR calculation. The parameter $SNR_{channel} = -TL(d, f) - N(f)$ is computed using the formulas introduced in the previous chapter. This parameter depends on the frequency and the distance where the communication is established. Based on this result, ensuring communication requires using low frequencies, especially for long ranges. In addition, the available bandwidth is automatically another parameter that suits

this requirement, implying only low-rate communication will be possible for long ranges.

According to (2.1), minimizing the SNR level involves reducing the acoustic power at the transmitter. In this context, [68] showed that regardless of the duration of exposure to sound, the accumulated effect is negligible when the pressure level is low. However, targeting low SNR systems requires adapted techniques able to demodulate the received signal. In this case, the low probability of detection (LPD) signals are more suitable for such applications. In the next paragraph, we highlight the existing LPD for underwater acoustic communications as a potential technique for biotope friendly communications.

2.1.2 Underwater acoustic communications for friendly environment

In recent years, several modulation schemes have been tested to communicate underwater at low SNR levels. The most studied schemes are mainly used for covert acoustic communications manner [69, 70]. In light of the most existing techniques, there is the spread spectrum. By sacrificing spectral efficiency, it is possible to communicate at a low level of SNR. The transmitted signals in UWA channels are expected to be below the background noise. Through de-spreading the received signal, it is possible to retrieve the carried data. In addition, other techniques based on multicarrier, such as orthogonal frequency division multiplexing (OFDM) and multicarrier spread spectrum scheme (MCSS), achieved low levels of SNR at a low data rate. For the rest of this section, we cite the most used techniques and their performance.

2.1.2.1 Multiband orthogonal frequency division multiplexing

The multiband OFDM technique has been widely used in frequency-selective channels because of its capacity to reduce the inter-symbol interference caused by the multipath effect. Usually, the OFDM technique improves throughput and error rate performance through channel estimation and equalization processes [71, 72]. However, for covert applications, multiband OFDM achieved up to -17 dB at a range of 52 km using a data rate of 4.2 bit/s [73]. Besides, using a data rate of 78 bit/s at the same distance, the SNR was -8 dB. Although the interest of this technique in achieving low SNR levels, it is a subject of multiple phenomena. A long symbol duration in OFDM could deteriorate the sub-carriers' orthogonality and create inter-carrier interference (ICI) due to the Doppler spread effect [74].

2.1.2.2 Multicarrier spread spectrum

Another multicarrier technique promoting good covert underwater acoustic communication is called the multicarrier spread spectrum scheme (MCSS). An example of use has been performed in [75]. In this work, they generated turbo-coded symbols using phase-shift key modulation

and spread them on multiple carrier frequencies. Regarding the performance of the proposed scheme, it achieved 75 bit/s at -12 dB at ranges up to 52 km.

2.1.2.3 Direct sequence spread spectrum

The dominant method used for covert communications is the direct sequence spread spectrum (DSSS). This technique exploits frequency diversity in frequency-selective channels. It spreads the communication symbols in frequency through spreading codes. In terms of performance, DSSS is considered resilient to inter-symbol interference but limited to a low data rate [76]. Some works proposed enhancing the DSSS system by adding time-synchronization and Doppler estimation and compensation [77]. In [78], the DSSS is performed using turbo equalization. The result showed that for a fixed bandwidth of 3.5 kHz and at a distance of 52 km, this technique recorded a level of SNR of - 14 dB for 4 bit/s and -6.5 dB for 75 bit/s. Moreover, [79] proposed an orthogonal-hybrid spread spectrum communication scheme with direct sequence spread spectrum (DSSS)-BPSK modulation and DSSS-MFSK modulation to face severe phenomena of the UWA channel and improve the bandwidth efficiency. The experiment in shallow water in South Sea China shows that BER is under 10^{-3} for a data rate of 317 bit/s for both schemes.

2.1.2.4 Frequency hopping spread spectrum

Another known form of spread spectrum based on frequency scheduling is the frequency hopping spread spectrum (FHSS). In this method, the frequency band of the transmitted signal is shifted using a hopping pattern. The receiver exploits the known pattern to reconstruct the signal and retrieve the information [80]. This technique is more resilient to inter-symbol interference. In [81], FHSS is combined with a chirp signal to transmit symbols, and a fractional Fourier transform is applied at the receiver to estimate symbols and compensate the Doppler shift. The simulation result using the watermark for the UWA channel showed that the bit error rate is 5×10^{-2} for a zero level of SNR. For an SNR of 5 dB, the bit rate is 4×10^{-3}.

2.1.2.5 Chirp spread spectrum

The chirp spread spectrum (CSS) technique is proposed as a reliable method for communication, given its low Doppler sensitivity and multipath robustness [82, 83]. This method consists of using a particular waveform to constitute symbols. Instead of a constant frequency carrier, a random signal having a spectral width (spread function) is used; the modulation is reversed at the receiver by multiplying with the spread function. The commonly used waveform is the linear frequency modulation. However, different works propose other waveforms to improve

communication compared to the conventional method (LFM-based signals) [84, 85, 86].

Numerous works proposed chirp-based signals combined with digital modulations such as multi-level M-ary, DQPSK, and PN codes to constitute orthogonal symbols. [87] proposed a scheme combining LFM based-chirp and M-ary modulation using different slope rates to make communication robust to the Doppler effect in underwater acoustic environments. This work is performed using SNR below 0 dB in the presence of the Doppler effect (relative speed up to 18 m/s). The simulation result showed that the system achieved uncoded bit error around 10^{-3} using a data rate of 300 bit/s.

In addition, a non-linear frequency modulation waveform is proposed as an alternative to the conventional CSS [85]. In this work, the generalized sinusoidal function is used to define the instantaneous frequency of transmitted symbols. Four combinations of the constellation are introduced to constitute symbols. A demodulation process based on cross-correlation is applied at the receiver to identify each symbol in the frame. The simulation result using VirTex for underwater channel modeling showed that the uncoded bit error rate was 0 at -8 dB SNR for a data rate of 100 bps. Experimental results in a lake trail using the same configuration as the simulation showed that the bit error rate was 3.52×10^{-2} at a range of 200 m.

Recently, CSS communication based on differential coding and matched filter processing has been proposed to communicate in a long-range underwater acoustic channel [88]. This work used differential encoding for modulation, considering two symbol periods and applying cross-correlation at the receiver to estimate symbols. In the lake trial, the proposed technique achieved a BER of 2.38×10^{-2} at 1.9 dB of SNR while using a data rate of 100 bit/s and a bandwidth of 2 kHz. However, the spectral efficiency of the proposed method is very low because the used period overhead is much longer than the payload, and only two bits are transmitted within a symbol time.

2.1.2.6 Conclusion

For the rest of this work, we focus on the chirp-based waveform as a solution to connect the fishing net. This choice is motivated by the ability to have a robust system face the Doppler effect and the multipath by exploiting the orthogonality of chirps. Meanwhile, we preserve the biotopes from acoustic pollution since it is possible to demodulate the received signals at a low level of SNR. The proposed method is called the differential chirp spread spectrum. Unlike the work introduced in [88], we propose an enhancement of the conventional CSS modulation and the data rate. In the next section, we explain in detail the proposed technique and its performance.

2.2 Differential chirp spread spectrum

This section is dedicated to the proposed DCSS technique for underwater acoustic communication. Firstly we introduce the conventional CSS technique and study its limitation in the UWA channel. Then, we explain our proposed approach to face the severe characteristics of the channel. Through the Watermark simulator, we perform and analyze the DCSS modulation in time-varying underwater acoustic channels.

2.2.1 Study of CSS in UWA channels

In this paragraph, we explain the CSS modulation and emphasize its limitation because of the time and frequency dispersion of UWA channels.

2.2.1.1 CSS principle

Initially, the binary information to transmit is divided into several sub-sequences, each of length SF bits that constitute a symbol. The number of possible symbols is hence equal to $M = 2^{SF}$. To distinguish M different symbols of the constellation, M orthogonal chirps are generated by applying a temporal cyclic shift (see Figure 2.3) to the raw chirp $x_{ref}(t)$ defined within a bandwidth B and symbol time T.

$$x_{ref}(t) = e^{j2\pi(\int_0^t f_c^0(u)\,du)} \tag{2.3}$$

with,

$$f_c^0(t) = B(\frac{t}{T} - \frac{1}{2}),\ for\ t \in [0, T) \tag{2.4}$$

Where $f_c^0(t)$ represents the frequency of the raw chirp signal, when it increases in time (proceeded by the '+' sign), the chirp is defined as up-chirp, whereas it is down-chirp if its instantaneous frequency decreases over time. The parameter SF is referred to as Spreading Factor, and it is related to the bandwidth B and symbol time T as:

$$B \times T = 2^{SF} \tag{2.5}$$

Let m_p denotes the p^{th} symbol to transmit at time pT, the modulated chirp instantaneous frequency of the symbol m_p can be expressed as:

$$\begin{cases} f_c^{m_p}(t) = \frac{B}{T}t + \frac{m_p}{T} - \frac{B}{2} \ \ for\ t \in [0, T - \tau_p) \\ \\ f_c^{m_p}(t) = \frac{B}{T}t + (\frac{m_p}{T} - \frac{3B}{2}) \ \ for\ t \in [T - \tau_p, T) \end{cases} \tag{2.6}$$

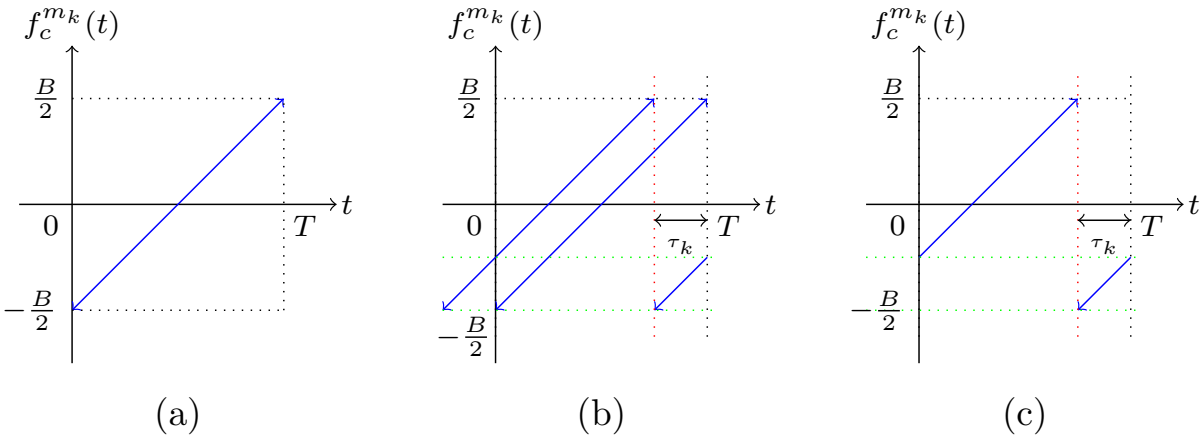

Figure 2.3: Symbol $\rightarrow$ chirp association process - (a) up raw chirp - (b) process principle - (c) associated chirp.

where $\tau_p = \frac{m_p}{B}$ represents the temporal cyclic shift for the symbol m_p. Using the equation (2.6), the complex envelope of the transmitted signal can be expressed as:

$$s(t) = \sum_{k=1}^{N_s} e^{j\phi_p(t-(k-1)T)} \mathbb{1}_{[(k-1)T,kT)}(t) \tag{2.7}$$

with,

$$\phi_p(t) = 2\pi \int_0^t f_c^{m_p}(u)\, du \tag{2.8}$$

$\phi_p(t)$ is the instantaneous phase of the symbol m_p, N_s is the total number of transmitted symbols and $\mathbb{1}_x(t)$ is the indicator function.

To explain the demodulation process, we consider a perfect time and frequency synchronization of the received signal, and we don't consider the noise term. The expression of the discrete received signal at sampling time $T_s = \frac{1}{B}$ is:

$$y(nT_s) = \sum_{k=1}^{N_s} e^{j\phi_p(nTs-(k-1)T)} \mathbb{1}_{[(k-1)M,kM]}(nTs) \tag{2.9}$$

The estimation of symbols consists of multiplying the received signal by the conjugate of the raw chirp $x_{ref}(nT_s)$, then applying the Fast Fourier Transform (FFT) to each symbol time. Thus, the estimation of the p^{th} symbol can be obtained using the following equation:

$$Y_p[k] = \frac{1}{\sqrt{M}} \sum_{n=0}^{M-1} y_p(nT_s)(x_{ref}(nT_s))^* e^{-j2\pi\frac{nk}{M}} \tag{2.10}$$

where $f(t)^*$ is the conjugate of the function $f(t)$, $y_p(nT_s) = y(nT_s + pT)$ is the complex

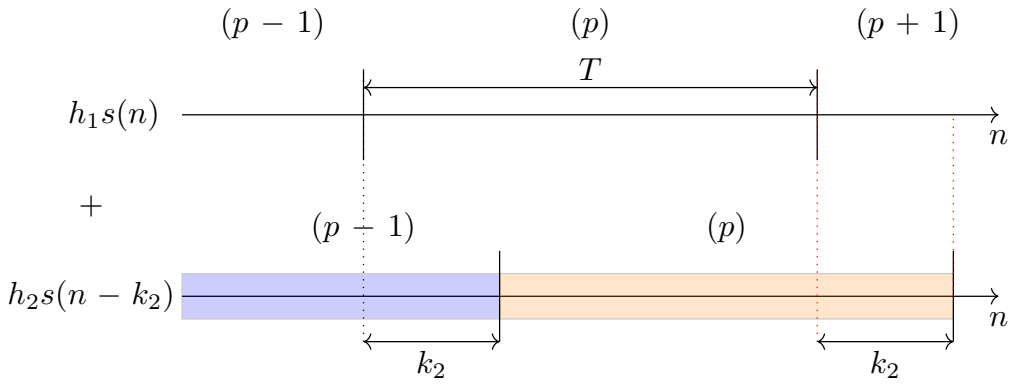

Figure 2.4: Illustration of ISI in case 2 paths channel synchronized on the first path ($k_1 = 0$).

envelope of the p^{th} transmitted symbol. Therefore, in a non-coherent receiver, a symbol $\tilde{m}_p$ is obtained as the argmax of the module of FFT.

$$\tilde{m}_p = \underset{k \in [\![0, M-1]\!]}{\text{argmax}} \left(|Y_p(k)| \right) \tag{2.11}$$

In a coherent receiver, the symbol is estimated using the real part of the FFT as follows:

$$\tilde{m}_p = \underset{k \in [\![0, M-1]\!]}{\text{argmax}} \left(Real(Y_p(k)) \right) \tag{2.12}$$

2.2.1.2 Impact of the multipath channel on CSS signals

In UWA channels, the multipath formation is governed by the reflection of the sound at the surface and the seafloor. Considering only the multipath effect, the temporal impulse response can be simplified to (1.22). We suppose here that the used symbol time is larger than the delay spread of the channel (i.e., $T \geq \Delta\tau = \tau_{N_p} - \tau_1$). However, inter-symbol interference is produced between the current and previous symbols. To understand this effect more, let's consider a simple case of two paths channel. The received signal sampled at T_s can be written as:

$$y(nT_s) = h_1 s((n-k_1)T_s) + h_2 s((n-k_2)T_s) + w(nT_s) \tag{2.13}$$

$w(nT_s)$ represents the complex noise assumed white and Gaussian. We suppose the synchronization is made on the first path ($k_1 = 0$). As illustrated in Figure 2.4 at time pT, the expression of the received signal introduces the symbol p from both paths and the symbol $(p-1)$ from the second path. Therefore, depending on the gain and the delay of the second path, the estimation of symbols could be distorted.

Figure 2.5 shows the result of transmitted symbols (SF= 7, B= 5 kHz) through two paths channel ($h_1 = 1$, $h_2 = 0.8$) received at different time delay. When the delay is significant, the

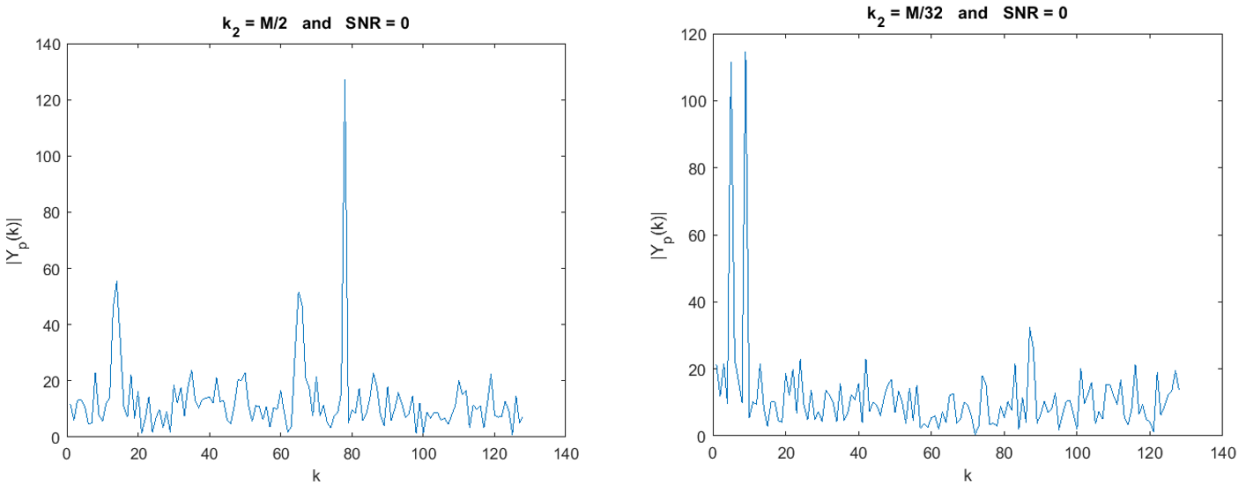

Figure 2.5: Illustration of the impact of ISI on symbol estimation process

energy will be distributed over the two symbols, allowing a good estimation. However, when the delay between the two paths is small and the difference in energy is low, the result of the symbol estimation process is strongly impacted.

2.2.1.3 Impact of Doppler effect on CSS signals

Because of the low propagation speed of sound, underwater acoustic communication observes a significant Doppler scaling. This effect is mainly caused by the relative motion of the transmitting and receiving elements and the platform and sea surface motion. Unlike terrestrial communication, where the Doppler effect is usually modeled only as carrier frequency offset (CFO), in underwater acoustic communication, the Doppler effect can be interpreted as the extension or compression of the waveform. Since the UWA channel involves multipath signals, multiple Doppler scales stretch or compress the received signal in time.

To understand the impact of the Doppler effect on CSS signals, we assume that each path's relative speed is the same. The transformation of raw chirp $x_{ref}(t)$ by Doppler effect (1.17) is then:

$$z_{chirp}(t) = e^{j[2\pi(f_c - \frac{B}{2})(1+\Delta)t + \pi\frac{B}{T}(1+\Delta)^2 t^2]} \tag{2.14}$$

where f_c is the carrier frequency, $\Delta = \frac{v_r}{c}$ is the Doppler coefficient defined as the ratio of the relative speed between transmitter and receiver v_r, and the speed of sound underwater c.

Using the equation (2.14) three aspects are produced by the Doppler effect [89] to a chirp signal $x_{ref}(t)$:

- Depending on the sign of Δ, the time domain is widening or compressing. The duration

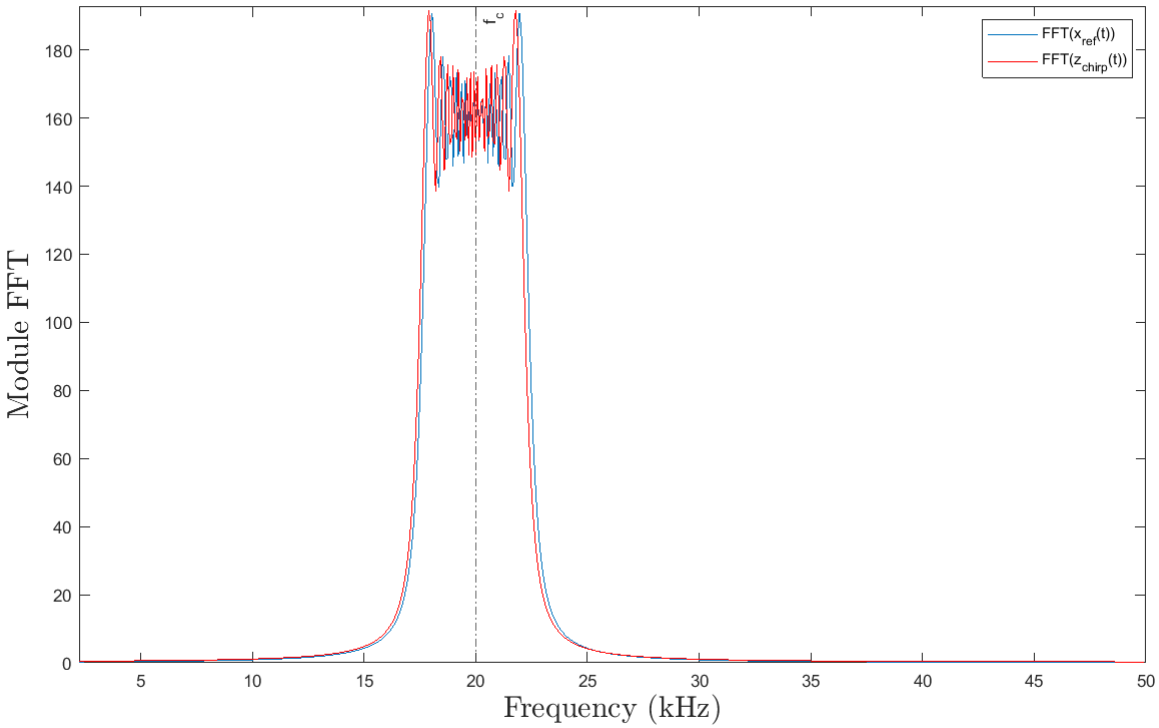

Figure 2.6: FFT applied to a raw chirp $x_{ref}(t)$ and to a chirp signal with Doppler effect $z_{chirp}(t)$

of the received signal becomes $\frac{T}{1+\Delta}$, and the observed bandwidth is $(1+\Delta)B$.

- The carrier frequency is shifted by an offset of Δf_c. The new center frequency becomes $(1+\Delta)f_c$.
- Chirp rate $\frac{B}{T}$ changes into $(1+\Delta)^2\frac{B}{T}$.

Figure 2.6 illustrates the Doppler effect's impact on the frequency domain chirp signal. The simulated signal is defined at $f_c = 20$ kHz within a bandwidth of 5 kHz and has a spreading factor of $SF = 6$. The Doppler effect is generated by a relative speed between the transmitter and receiver of $v_r = 5$ m/s. As shown in Figure 2.6, the carrier is shifted by an offset of 66 Hz, and the bandwidth is expanded. Consequently, without compensation, the Doppler effect can lead to a high error rate for communication based on such signals.

2.2.2 Architecture of DCSS

The overall architecture of DCSS is mentioned in Figure 2.7. This technique is based mainly on CSS with differential encoding and additional processes to eliminate the Doppler and multipath effects caused by the channel. Moreover, the orthogonality of chirps is exploited to generate the

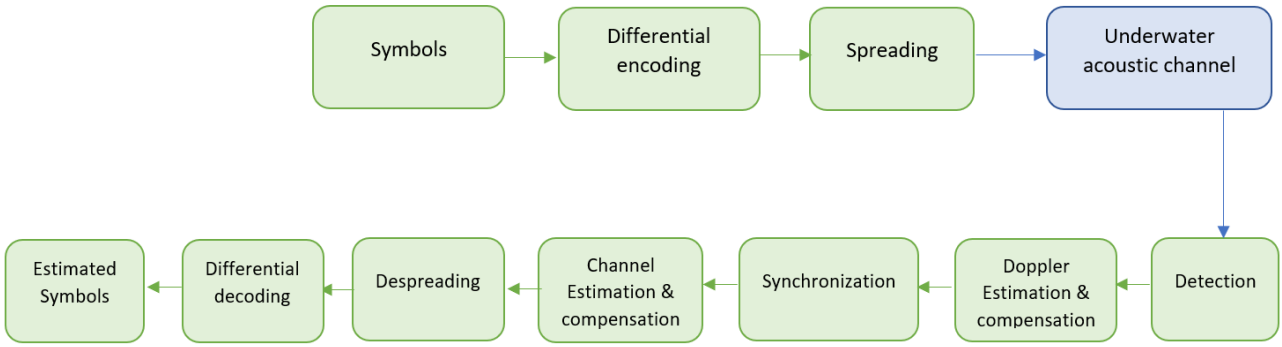

Figure 2.7: Architecture of differential chirp spread spectrum

payload, which deals with the inter-symbol interference and improves the spectral efficiency because no silence time or cyclic prefix is needed.

2.2.3 Differential encoding

Based on the same principle as CSS modulation, the key idea of the DCSS technique is to generate the transmitted symbols using differential encoding. Indeed, instead of directly associating a symbol m_k to a chirp, we generate a new symbol defined as the sum of two consecutive symbols, then associate it with a chirp. The original symbol can be obtained at the receiver through differentiation [90, 91]. The new symbol to be transmitted S_k at kT can be expressed in function of the symbol m_k and the previous transmitted symbol S_{k-1} by the following equation:

$$S_k = (m_k + S_{k-1}) \mod M \ , \ k \geq 0 \tag{2.15}$$

To initiate the integration process, we set the value of S_{-1} at 0. At the receiver, the symbol $\tilde{S}_k$ is estimated using the equation (2.11), and the original symbol can be retrieved by differentiation using the equation (2.16).

$$\tilde{m}_k = (\tilde{S}_k - \tilde{S}_{k-1}) \mod M \ , \ k \geq 0 \tag{2.16}$$

The main advantage of using differentiation in DCSS is to make the communication more resilient to Doppler shift since the additional frequency offset caused by the Doppler effect is compensated through differentiation applied to the estimated symbols.

2.2.4 Transmitted signal

The frame structure of the transmitted signal (Figure 2.8) is composed of a long chirp used to estimate the Doppler scaling factor, a time guard greater or equal to the delay spread of the chan-

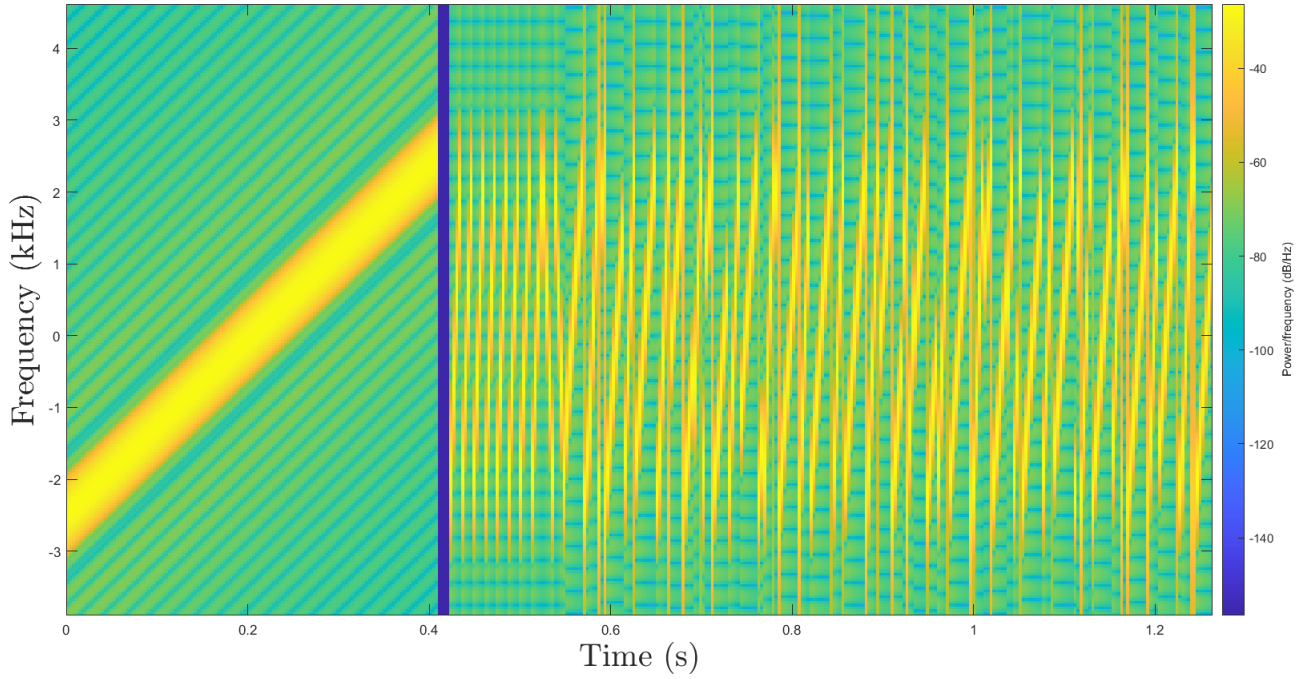

Figure 2.8: Spectrogram of the transmitted signal

nel, and a set of raw chirps composed of consecutive up-chirps followed by consecutive down-chirps for synchronization and channel estimation. Moreover, the payload is generated using two different symbol times ($SF = 6$ and $SF = 7$) to face the multipath problem mentioned in section (1.1.5) through the orthogonality of chirps. This way, we overcome the insertion of cyclic prefixes or silence times in the frame and improve spectral efficiency.

In practice, we use two consecutive spreading factors to constitute the payload. Let SF denote the low value of the spreading factor and T its associated symbol time, then the data rate of the proposed technique can be defined as:

$$R_b = \frac{SF + SF + 1}{T + 2\,T} = \frac{2\,SF + 1}{3\,\frac{2^{SF}}{B}} \tag{2.17}$$

2.2.5 Proposed receiver

Using the approximation of the UWA channel introduced in subsection 1.2.3. The received signal can be written as:

$$r(t) = \sum_{p=1}^{N_p} h_p(t) s(t - \tau_p(t)) + w(t) \tag{2.18}$$

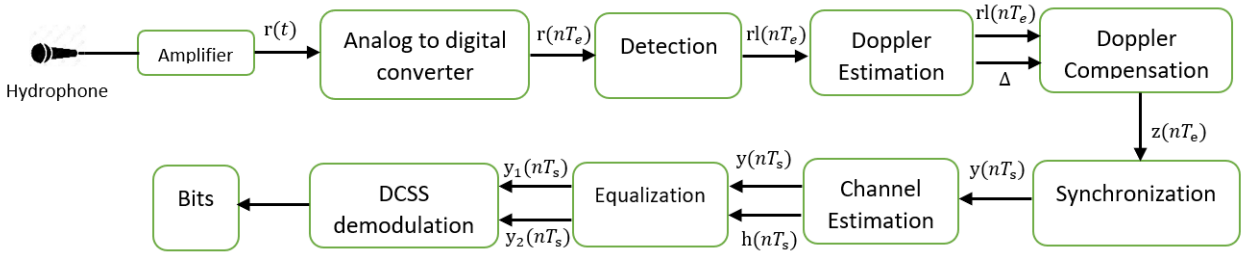

Figure 2.9: Diagram bloc of DCSS receiver

N_p is the number of paths in the channel, $h_p(t)$ and $\tau_p(t)$ are the complex gain and the relative delay of p^{th} path, respectively.

$$\tau_p(t) = \tau_p - \int_0^t \frac{v_r(u)}{c} du \tag{2.19}$$

Under the assumption of having constant amplitudes throughout the frame $h_p(t) \approx h_p$ and the relative speed at each path is constant $\tau_p(t)$ can be simplified to:

$$\tau_p(t) = \tau_p - \Delta t \tag{2.20}$$

Thus, the received signal can be expressed as follows:

$$r(t) = \sum_{p=1}^{N_p} h_p s(t(1+\Delta) - \tau_p) + w(t) \tag{2.21}$$

The received signal is sampled at time T_e using analog to digital converter and processed in several blocs to retrieve the carried data as mentioned in Figure 2.9. It should be noted that T_e differs from T_s introduced in the previous paragraphs. For the rest of this chapter, We note $\gamma = \frac{T_s}{T_e}$ the oversampling sampling ratio. In the following paragraphs, we provide an explanation of each bloc.

2.2.5.1 Detection

Firstly, the received signal $r(nT_e)$ is down-sampled at rythm T_s, then divided into several blocs of length M, referring to the low spreading factor SF value. Secondly, the signal is multiplied by the conjugate of the raw chirp $x_{ref}(nT_s)$. After that, the FFT is performed at each symbol time as indicated in equation (2.10). The $argmax$ of the first peak in the frequency domain allows a coarse detection of the first raw up chirp after the time guard in the preamble. Algorithm 1 summarizes the main steps to compute this process.

Algorithm 1: Detection

Data: $r(nT_s)$ received signal, $x_{ref}(nT_s)$ raw up chirp, $M = 2^S F$, N_b number of chirps and T_h threshold
Result: k_α index of the first chirp sample
for $k = 0$ *to* $(N_b - 1)$ **do**
  $r_k \leftarrow r(T_s(n + kM))$
  $Y_k \leftarrow FFT(r_k \times x^*_{ref})$
  $M(k) \leftarrow max(Y_k)$
$k \leftarrow 0$
while $M_p(k) \leq T_h$ **do**
  $k \leftarrow k + 1$
return $k_\alpha \leftarrow k \times M$

2.2.5.2 Doppler Estimation

As depicted in paragraph 2.2.1.3, in the presence of the Doppler effect in UWA channels, a chirp may undergo a compression (or extension) of the symbol time and its rate changes. This deformation can be produced at different paths in the UWA channel. Under the assumption of having the same Doppler scale at each path, we can estimate the Doppler effect by exploiting the waveform of the transmitted signal. As mentioned in [92], the Doppler scale can be deducted from the chirp rate by applying the Fractional Fourier Transform (Frft). Therefore, we apply this process to the long chirp used in the preamble to estimate the Doppler scale.

If we note T_{ch} is the duration of the long chirp in the preamble and T_g is the time guard, then the Frft operator is applied to the signal $x(nT_e)$ defined as

$$x(nT_e) = r(k_\alpha \gamma T_e - T_g + (n - K)T_e)\mathbb{1}_{[\![0,K-1]\!](n)}(nT_e) \tag{2.22}$$

k_α is the index obtained from the detection process and $K = \lceil \frac{T_{ch}}{T_e} \rceil$ with $\lceil . \rceil$ is a rounding operation. Let $\phi = p\frac{\pi}{2}$ and p denote the angle of rotation and the order of Frft operation. The optimal order p_{opt} applied to the first chirp in the frame corresponds to the rate of the chirp η, and the relationship between the rotation angle and the chirp rate can be written as:

$$\phi_{opt} = -arctan(\frac{1}{\eta}) \tag{2.23}$$

On the one hand, the optimal order p_{opt} can be calculated as the order maximizing the Frft function (2.24). A digital version of the $Frft$ operator is proposed in [93] to simplify its computation.

$$p_{opt} = \underset{p\in[0.5,1.5]}{argmax}(max|Frft^p(x(n))|) \tag{2.24}$$

On the other hand, as mentioned in (2.14), the rate of a chirp after crossing the channel is expressed as:

$$\eta = \frac{B}{T_{ch}}(1+\tilde{\Delta})^2 \tag{2.25}$$

Thus, combining the equation (2.23) and equation (2.25) the estimated value of Doppler coefficient $\tilde{\Delta}$ can be written as:

$$\tilde{\Delta} = \sqrt{\frac{-cot(p_{opt}\frac{\pi}{2})}{\frac{B}{T_{ch}}}} - 1 \tag{2.26}$$

To reduce the complexity of the Doppler coefficient computation, it is possible to use only a part of the chirp of length N_c. Thus, the equation to execute is simplified to:

$$\tilde{\Delta} = \sqrt{\frac{-cot(p_{opt}\frac{\pi}{2})}{\frac{B}{T_{ch}}\ N_c T_e^2}} - 1 \tag{2.27}$$

As the Doppler factor is now calculated, the long chirp and time guard can be removed from the received signal. Thus, the received signal becomes:

$$rl(nT_e) = r(T_e(n + k_\alpha \gamma)) \tag{2.28}$$

2.2.5.3 Doppler Compensation

The compensation of the Doppler effect is made by re-sampling the received signal at $\frac{Te}{1+\tilde{\Delta}}$. Indeed, the linear interpolation between every two consecutive samples is applied to regenerate a new sample [86]. Using the signal $rl(nT_e)$, the compensated signal $z(nT_e)$ can be defined as follows:

$$z(nT_e) = (m + 1 - \frac{n}{1+\tilde{\Delta}})\ rl(mT_e) + (\frac{n}{1+\tilde{\Delta}} - m)\ rl((m+1)T_e) \tag{2.29}$$

for all (n, m) that satisfies the following condition:

$$m \leq \frac{n}{1+\tilde{\Delta}} < (m+1) \tag{2.30}$$

2.2.5.4 Synchronization

The purpose of this bloc is to synchronize accurately with the first up chirp in the frame, referring to the most significant path of the UWA channel. An illustration of time synchronization is shown in Figure 2.10. This process will estimate the close possible sample to the strongest path. To do so, the first step is to down-sample the signal $z(nT_e)$ at rythm T_s and despread it

using the signal $x_{ref}(nT_s)$.

After Doppler compensation process, the observed signal $z(nT_s)$ can be expressed as follows:

$$z(nT_s) = \sum_{p=1}^{N_p} h_p \; s(nT_s - \Delta t_p) \; e^{j2\pi\Delta f \; nT_s} + w'(nT_s) \tag{2.31}$$

We introduced to the signal $z(nT_s)$ a frequency shift to ensure an accurate synchronization in case the previous processes do not compensate completely for the frequency shift from the signal. Otherwise, the estimation of time desynchronization will be strongly impacted. The formulation of the synchronization process can be summarized as determining the desynchronization amounts Δf and Δt and compensating them. The time desynchronization amount can be defined as follows.

$$\Delta t = \Delta t_{p_{max}} \; , \; p_{max} = \underset{p}{argmax}(|h_p|) \tag{2.32}$$

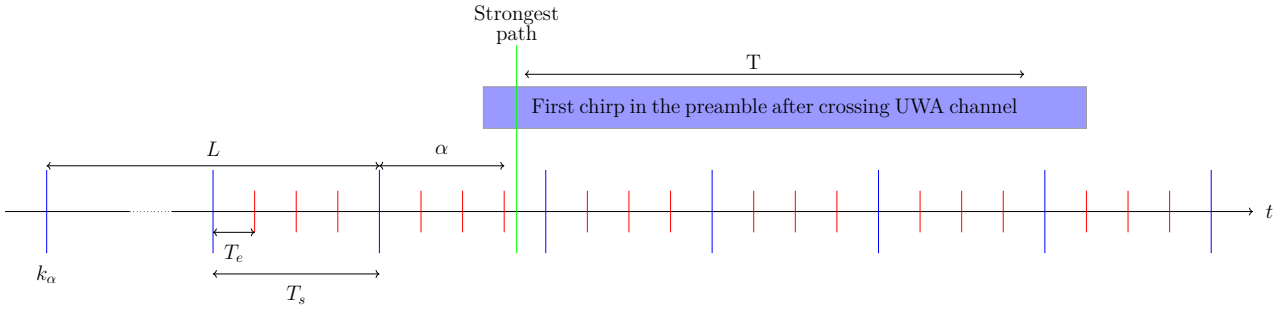

Figure 2.10: Illustration of time synchronization

Solving the desynchronization problem involves determining ΔfT and $\frac{\Delta t}{T_s}$ the corresponding indexes of Δf and Δt after dechirping the signal $z(nT_s)$. This operation consists of dividing the signal $z(nT_s)$ into several blocs, each of length M. Then, multiply each bloc by the conjugate of $x_{ref}(nT_s)$. To achieve this, two processes are computed. In the first one, which is a coarse synchronization, the integer amounts L and C parts of ΔfT and $\frac{\Delta t}{T_s}$ are estimated. Whereas the fractional parts α and β are estimated using fine synchronization.

$$\frac{\Delta t}{T_s} = L + \alpha \tag{2.33}$$

$$\Delta fT = C + \beta \tag{2.34}$$

It should be noted that we refer to the integer part as the multiple of T_s and the fractional part as the multiple of T_e.

Coarse Synchronization

Given that the raw chirps of the preamble can be seen as symbols equal to zero. Hence, after de-chirping up chirps of the preamble by multiplying each up chirp by the conjugate of x_{ref}, the observed FFT of each chirp (2.11) will be a shift to the main peak by the quantity l_{up}:

$$l_{up} = -\hat{C} + \hat{L} \mod M \tag{2.35}$$

The same operation applied to down chirps leads to a shift to the main peak by the quantity l_{down}:

$$l_{down} = \hat{C} + \hat{L} \mod M \tag{2.36}$$

Therefore, combining equation (2.35) and equation (2.36), we can obtain the integer amounts as follows:

$$\hat{C} = \lceil \frac{l_{down} + l_{up}}{2} \rceil \mod M \tag{2.37}$$

$$\hat{L} = \lceil \frac{l_{down} - l_{up}}{2} \rceil \mod M \tag{2.38}$$

Algorithm 2 describes step by step the computation of the coarse synchronization process.

Algorithm 2: Coarse synchronization

Data: $z(nT_s)$ received signal, $x_{ref}(nT_s)$ raw up chirp, M the number of constellation, N_{up} number of up chirps in the preamble and N_{down} number of down chirps in the preamble

Result: L and C

for $k = 0$ *to* $(N_{up} - 1)$ **do**

- $r_k \leftarrow z(T_s(n + kM))$
- $Y_k \leftarrow FFT(r_k \times x^*_{ref})$
- $l_{up}(k) \leftarrow argmax(Y_k)$

$\hat{l}_{up} \leftarrow repelem(l_{up})$ # returns repeated value in l_{up}

for $k = N_{up}$ *to* $(N_{up} + N_{down} - 1)$ **do**

- $r_k \leftarrow z(T_s(n + kM))$
- $Y_k \leftarrow FFT(r_k \times x_{ref})$
- $l_{down}(k) \leftarrow argmax(Y_k)$

$\hat{l}_{down} \leftarrow repelem(l_{down})$ # returns repeated value in l_{down}

$C = round(\frac{l_{down}+l_{up}}{2}) \mod M$

$L = round(\frac{l_{down}-l_{up}}{2}) \mod M$

Fine Synchronization

After compensating the integer parts of desynchronization from the signal $z(nT_e)$, we resampled this letter at rythm $T_{s2} = \frac{1}{2B}$. In this process, we consider only up chirps to estimate the

fraction amounts α and β. Indeed, the preamble of signal $z(nT_{s2})$ dechirped by performing multiplication to the conjugate of signal $x_{ref}(nT_{s2})$. The fractional part of the frequency amount is obtained using the Schmidl-Cox method [94, 95] as the average of the phase at each $2M$ point.

$$\hat{\beta} = \frac{1}{N_{up}-1}\sum_{k=0}^{N_{up}-2}\frac{1}{2\pi}arg\left(\sum_{n=0}^{2M-1} zl(T_{s2}(n+2kM))\ \ zl(T_{s2}(n+2(k+1)M))^*\right) \mod 1 \tag{2.39}$$

with,

$$zl(T_{s2}(n+2kM)) = z(T_{s2}(n+2kM))[x_{ref}(nT_{s2})]^* \tag{2.40}$$

where $p \in [\![0, N_{up}-1]\!]$ and $n \in [\![0, 2M-1]\!]$. The value of α is obtained by performing the FFT at each 2M point to the dechirped signal $zl(nT_{s2})$. If we note $\tilde{l}_{up}(k)$ the argument of the maximum value of FFT applied to the k^{th} up chirp in the preamble, then α can be expressed as follows:

$$\hat{\alpha} = \frac{1}{N_{up}}\left(\lceil\sum_{k=1}^{N_{up}}\tilde{l}_{up}(k)\rceil - \lfloor(\sum_{k=1}^{N_{up}}\tilde{l}_{up}(k))\rfloor\right) \mod 1 \tag{2.41}$$

$\lfloor . \rfloor$ it rounds each element to the nearest integer less than or equal to that element.

Algorithm 3: Fine synchronization

Data: $zl(nT_{s2})$ dechirped signal, $x_{ref}(nT_{s2})$ raw up chirp, M the number of constellation, N_{up} number of up chirps in the preamble
Result: α and β
for $k = 0$ *to* $(N_{up}-2)$ **do**
  $r_k \leftarrow zl(T_{s2}(n+2kM)) \times [zl(T_{s2}(n+2(k+1)M))]^*$
  $val \leftarrow \sum_{n=0}^{2M-1} r_k(nT_s)$
  $f_{up}(k) \leftarrow \frac{angle(val)}{2\pi}$
$\beta \leftarrow mean(f_{up})$ # returns the mean value of f_{up}
for $k = 0$ *to* $(N_{up}-1)$ **do**
  $y_k \leftarrow zl(T_s(n+2kM))) \times e^{j2\pi\beta nT_{s2}}$
  $Y_k \leftarrow FFT(y_k)$
  $\tilde{l}_{up}(k) \leftarrow argmax(Y_k)$
$\alpha = round(mean(\tilde{l}_{up}) - floor(mean(\tilde{l}_{up})))$

Finally, the obtained values of Δf and Δt are used to synchronize with the first chirp in the frame.

$$y(nT_e) = z(nT_e + (L+\alpha)\gamma Te)e^{-j2\pi\frac{(C+\beta)}{T}nT_e} \tag{2.42}$$

For the rest of the processing, the signal $y(nT_e)$ is down-sampled at rhythm T_s.

2.2.5.5 Equalization

Equalization plays a crucial role in mitigating the multipath effect induced by the channel and ensuring the accuracy of received symbols. This process can be accomplished by either inverting the channel or minimizing the difference between the estimated and transmitted symbols. Existing equalization techniques can be categorized into two main classes: time domain equalization (TDE) [96, 97, 98] and frequency domain equalization (FDE) [99, 100, 101].

Regarding the most commonly used equalizer in the time domain, there is the decision feedback equalizer (DFE). It is a nonlinear equalizer that utilizes previously estimated symbols to improve the decision-making process for the current symbol. This approach has been employed in various studies. For instance, [96] introduced an adaptive DFE combined with digital locked loops, which yielded promising results in a shallow-water channel at a data rate of up to 40 kb/s. Typically, TDE equalization is considered to be computationally intensive in underwater acoustic communication due to the increased multipath delay. A reduction in computational complexity is proposed by employing the time reversal method [102, 103].

Moreover, FDE provides an alternative approach to mitigate the effects of the UWA channel. In DFE, suboptimal linear equalization methods such as zero-forcing (ZF) and minimum mean square error (MMSE) are commonly employed [104]. FDE involves applying FFT at each symbol time, followed by channel inversion and subsequent IFFT to rectify the signal. In contrast to time domain equalization (TDE) techniques, DFE-based methods offer reduced complexity and are better suited for channels with significant delay spread.

So far, turbo equalizers have emerged as sophisticated equalization methods that integrate the principles of turbo decoding and equalization to overcome the multipath distortion induced by the UWA channel [105, 101, 106]. These advanced techniques employ iterative algorithms to jointly estimate the transmitted symbols and the characteristics of the channel. An example of this equalization technique was demonstrated in [107]. They introduced a filtered multitone (FMT) modulation scheme for underwater acoustic communication, incorporating low-complexity channel-estimation-based MMSE turbo equalization. The outcomes of their study exhibit improved communication performance and higher bit rates compared to the utilization of traditional MMSE adaptive equalization in FMT modulation UWA communication.

For the rest of this work, we use the MMSE equalizer in the frequency domain to eliminate the impact of the UWA. This equalizer offers a good balance between performance and complexity. It significantly improves symbol recovery while maintaining a reasonable computational complexity compared to turbo equalization techniques.

Channel Estimation

The channel is estimated using the up chirps of the preamble as proposed in [108]. If we note X $(M \times M)$, the circulant matrix obtained from the raw up-chirp $x_{ref}(kT_s)$ for $k \in [\![0, M-1]\!]$, and A_v $(1 \times M)$ the average of the N_{up} received raw up chirps in the preamble, then the estimated channel impulse response $\hat{h}$ can be expressed as:

$$\hat{h} = (X^T X)^{-1} X^T A_v \tag{2.43}$$

with,

$$A_v(nT_s) = \frac{1}{N_{up}} \sum_{k=1}^{N_{up}} y(T_s(n + (k-1)M) \ , \ n \in [\![0, M-1]\!] \tag{2.44}$$

Finally, the preamble is removed from signal $z(nT_s)$. The estimated impulse response of the channel is used to rectify the payload by eliminating the multipath effect through frequency equalization, introduced in the next paragraph.

Channel Compensation

As shown before, the preamble is generated with the spreading factor SF, and the payload symbols are generated using two different spreading factors, SF and $SF+1$. To eliminate the multipath effect from each symbol, we divide the signal $y(nT_s)$ into two signals $y_1(nT_s)$ and $y_2(nT_s)$ in which the symbols have the same spreading factor.

$$y_1(nT_s) = \sum_{k=0}^{N_{s1}-1} y(T_s(n + 3kM)) \mathbb{1}_{[kT,(k+1)T]}(nT_s) \tag{2.45}$$

$$y_2(nT_s) = \sum_{k=0}^{N_{s2}-1} y(T_s(n + (3k+1)M)) \mathbb{1}_{[2kT,2(k+1)T]}(nT_s) \tag{2.46}$$

N_{s1} is the number of symbols generated with spreading factor SF and N_{s2} is the number of symbols generated with spreading factor $SF+1$. Finally, we apply the minimum mean square error (MMSE) equalizer [109] using the following steps:

- Divide the corresponding signal to several blocs. For signal $y_1(nT_s)$ the size of each bloc is M and for $y_2(nT_s)$ is $2M$.

- Apply the Fast Fourier transform (FFT) to each bloc.

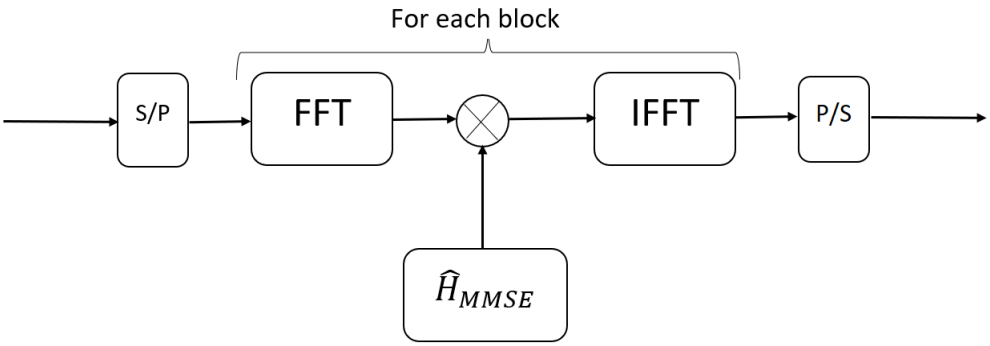

Figure 2.11: Equalization diagram block

- Multiply each bloc by the MMSE function transfer $\hat{H}_{MMSE}$ defined as:

$$\hat{H}_{MMSE} = \frac{(\hat{H})^*}{|\hat{H}|^2 + \sigma_n^2}$$

  σ_n is the variance of the noise. For the signal $y_1(nT_s)$, the transfer function of the impulse response is defined as $\hat{H} = \mathfrak{F}(\hat{h})$ with $\hat{h}(nT_s)$ for $n \in [\![0, M-1]\!]$ is the estimated CIR from the previous process. For the signal $y_2(nT_s)$, the transfer function of the impulse response is obtained as $\hat{H} = \mathfrak{F}(\hat{h_2})$ with $\hat{h_2} = [\hat{h} \;\; 0_{[\![0,M-1]\!]}]$.

- Apply the inverse Fast Fourier transform (IFFT) to each bloc.

Finally, the estimation of symbols is carried out by applying the three operations of dechirping, calculating the $argmax$ of FFT, and differentiation as mentioned in equations (2.10), (2.11) and (2.16), to each signal using the corresponding spreading factor.

2.2.6 Simulation results of DCSS

In this paragraph, we aim to evaluate the decoding performance of the proposed DCSS in an uplink scenario in order to measure the capacity of the demodulation at low SNR levels.

2.2.6.1 Bit error rate under AWGN channel

The purpose of this simulation is to perform DCSS generated using two spreading factors in a perfect synchronization case without any interference. We consider that the received signal is only disturbed by the AWGN signal. The simulation is made using a bandwidth of 5 kHz, and the payload is generated using different configurations of double SFs.

Figure 2.12 depicts the DCSS signal's BER as a SNR function. As we can see in all configurations, the signal can be demodulated at a negative value of SNR, and by increasing the SF

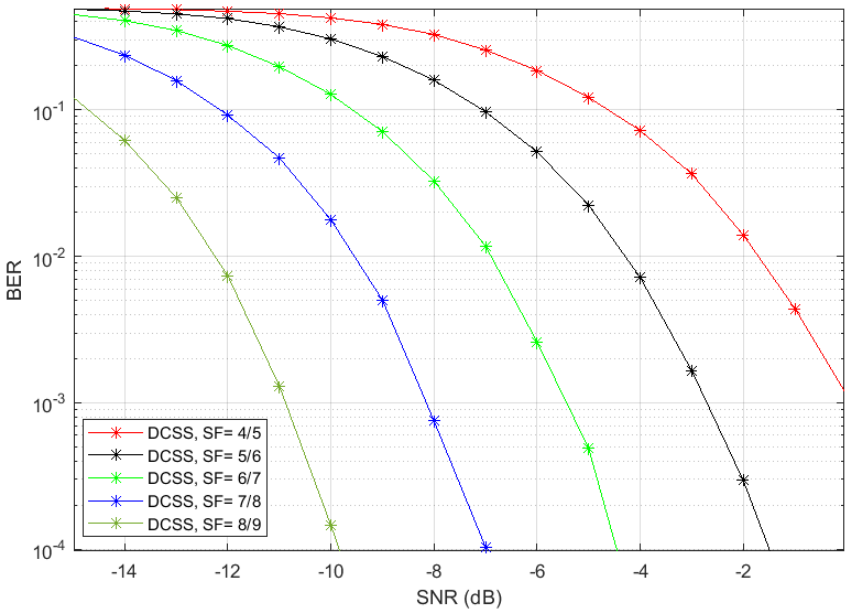

Figure 2.12: BER of DCSS in a perfect synchronization case

by 1, the processing gain of 3 dB. Hence, using high SF values improves the sensitivity of the system. However, considering the bandwidth of communication and the variability of the UWA channel, the transmitted symbols in the frame will be limited.

2.2.6.2 Bit error rate under UWA channel

In this paragraph, we aim to perform the proposed DCSS in the UWA channel. The Watermark channel modeling is used to simulate the time-varying channel impulse responses. This benchmark is based on gathered CIR in different locations. In this simulation, we performed the proposed DCSS using two channels BCH1 and NOF1 [61]. Based on the delay spread of the channels we set the transmitted signal at the configuration below:

Table 2.1: Parameters of the transmitted signal in Watermark simulator

Parameter	Value
Carrier frequency	14 kHz and 35 kHz
Sampling frequency	100 kHz
Spreading factor	6/7
Bandwidth	5 kHz
Preamble: Long chirp duration	1 s
Preamble: Number of up chirps	8
Preamble: Number of down chirps	2
Number of symbols	20

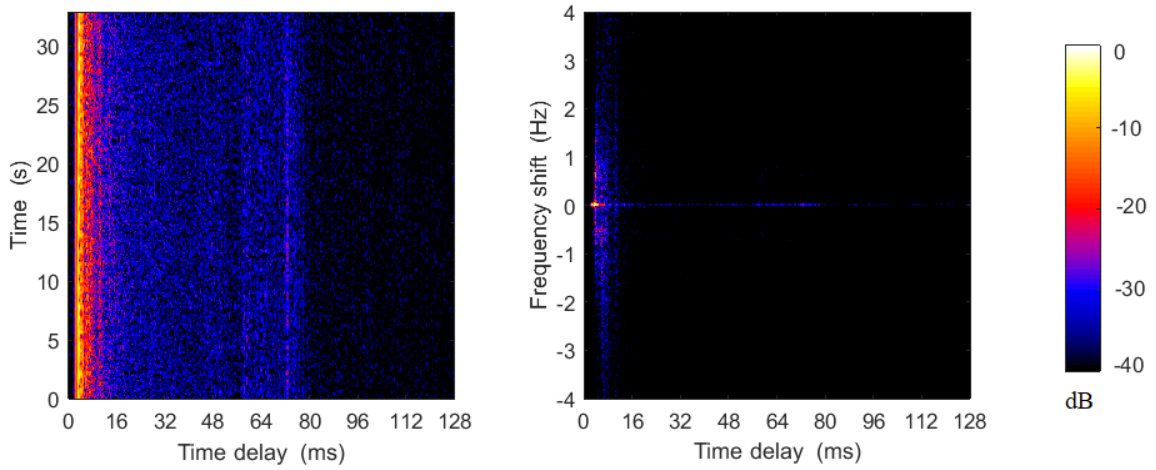

Figure 2.13: Charatecristics of NOF1 channel, copied from [61]

NOF1 is a channel measured in a shallow stretch of Oslofjorden using SISO configuration. The data consist of a TVIR measurement over 32.9 s, repeated 60 times. The CIRs are estimated using LFM-based signal defined at a carrier frequency of 14 kHz, within a bandwidth of 8 kHz and a duration of 128 ms. Figure 2.13 depicts the main characteristics of the channel during the first observation.

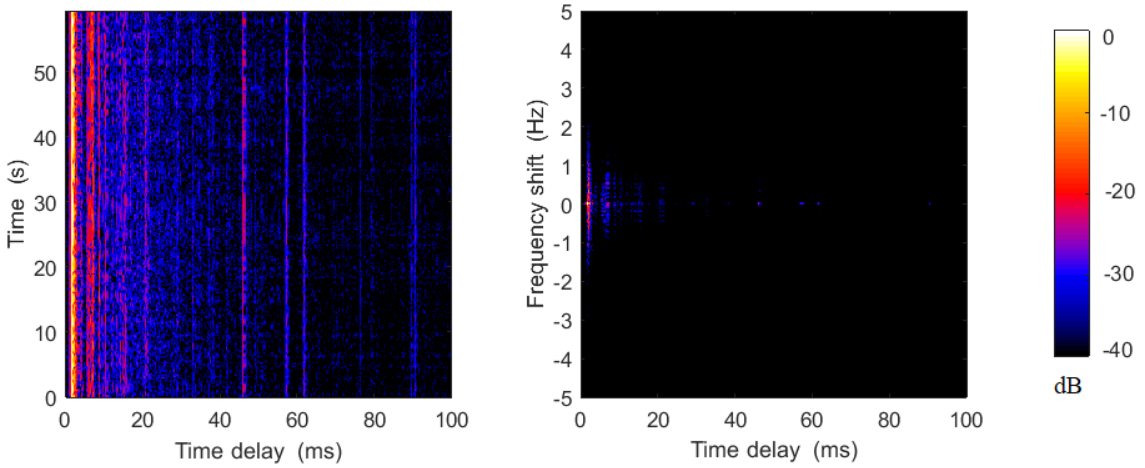

Figure 2.14: Charatecristics of BCH1 channel, copied from [61]

BCH1 is a SIMO channel measured in the commercial harbour of Brest, France. A source and a 4-element array were lowered into the water column from two docks. A single probe transmission over a range of 800 m resulted in a TVIR measurement over 59.4 s, simultaneously recorded on the four hydrophones. The CIRs are estimated using Pseudonoise signals defined at a carrier frequency of 35 kHz, within a bandwidth of 5 kHz and a duration of 102 ms. Figure 2.14 shows the main characteristics of the channel observed at the first receiver.

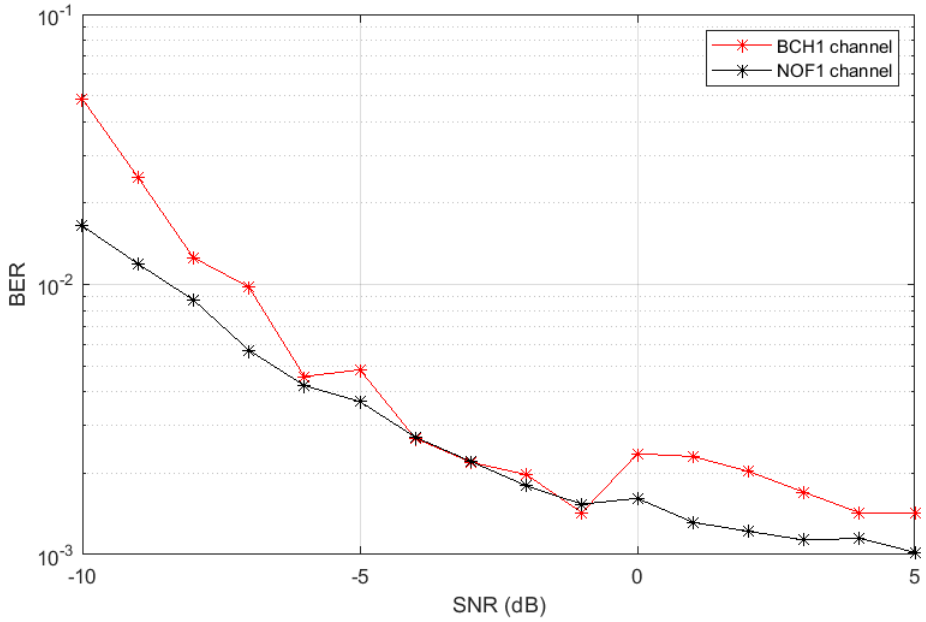

Figure 2.15: BER of DCSS in UWA channels

The chosen configuration respects the frequency selectivity of the channel. In other words, the duration of the chirp generated by the lowest SF (6 in this case) is greater than the channel delay spread. For a better assessment of DCSS communication, we performed it through all channels of observation whether they are estimated in NOF1 or BCH1. As shown in Figure 2.15, the BER of DCSS is presented as a SNR function. In terms of performance, the proposed DCSS can achieve a BER up to 10^{-3} for SNR between -3 and 5 dB. Compared to the performance of DCSS under AWGN (see Figure 2.12), we can easily notice that the channel's contribution is important, leading to a degradation in performance.

2.3 Implemented DCSS system

This section introduces the developed system for conducting experiments in UWA channels. The main purpose of this system is to test DCSS communication in lake and ocean environments. However, it can also perform various modulation types because the transmitted signals are pre-stored in a micro-SD card. In the first subsection, we present the breakdown of the system and the principle of working. We dedicated the second subsection to study the system's performance, more precisely defining the receiver's sensitivity and calculating its maximum achievable distance.

2.3.1 Hardware

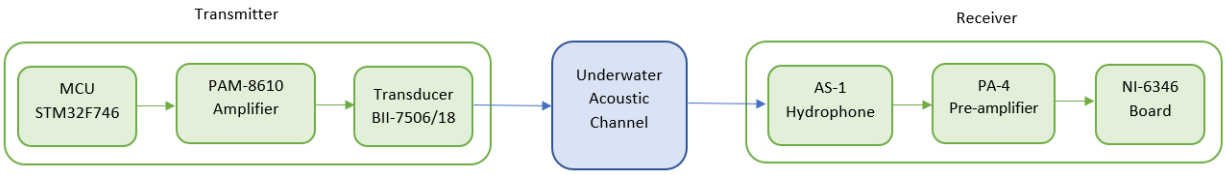

Figure 2.16: Block diagram of DCSS system

In terms of hardware, the system's transmitter consists of a signal generator, a power amplifier, and a transducer. The receiver is equipped with a hydrophone to detect signals, a pre-amplifier, and a data acquisition board. The overall diagram block of the system is shown in Figure 2.16.

2.3.1.1 Transmitter

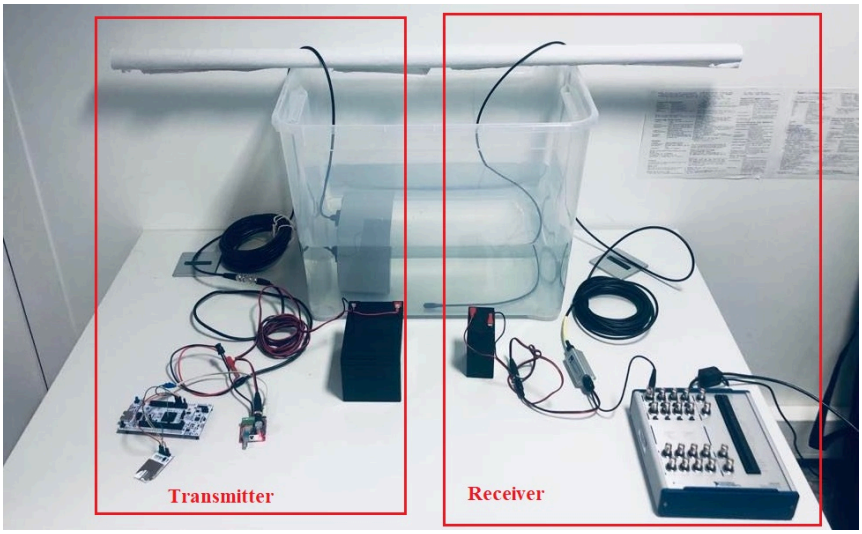

Figure 2.17: Illustration of the assembled system in a tank

As depicted in Figure 2.17, the communication starts from the microcontroller STM32F746. This microcontroller reads stored data frames, encoded as wav files, from the micro SD card. Then it decodes the data and generates the frame using the integrated digital-to-analog converter. When transmitting over short ranges, the analog signal is amplified using the PAM-8610 module to ensure 15 V_{RMS} at the output. However, when transmitting over long ranges, the KROHN-HITE 7500 amplifier ensures up to 160 V_{RMS} at the output to drive the transducer. Finally, the transducer $BII - 7506/18$ propagates the signal with a power up to 157.6 dB 1 $\mu Pa/V$ @1m. The main features of this transducer are listed in Table 2.2.

Table 2.2: Transducer Specification

Parameter	Value
Resonant frequency f_c	18 kHz
Transmitting voltage response at f_c	157.6 dB 1 $\mu Pa/V$ @1m
Maximum driving voltage	600 V_{RMS}
Maximum input pulse power	2000 Watts
Maximum continuous input power	60 Watts

Using the transmitting voltage response of the transducer and the voltage at its input V_{in}, the effective acoustic power for the broadband signal can be calculated as follows:

$$SL = 157.6 + 20\ log_{10}(V_{in}) \tag{2.47}$$

2.3.1.2 Receiver

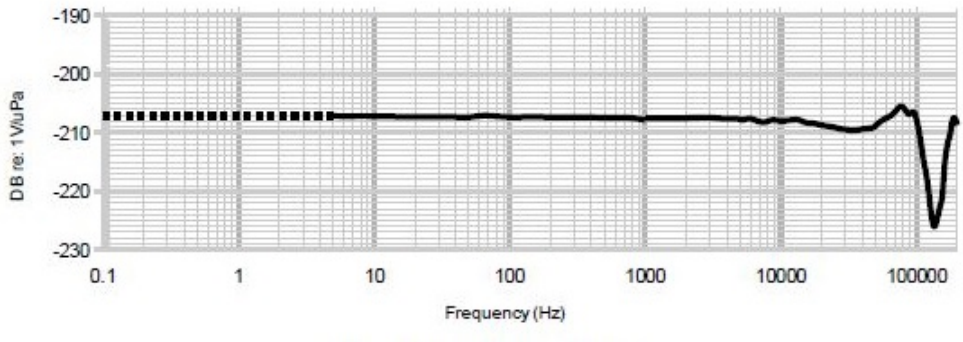

Figure 2.18: The open circuit receiving response

The hydrophone AS-1 receives the signal with a sensitivity of around -208 $dBV\ re\ 1\ \mu Pa$ (refer to Figure 2.18). The signal is then amplified with a gain of 50 dB (PA-4) before being recorded using the NI USB-6364 board and a laptop. The sampling frequency is programmable and limited to 500 kHz, and the resolution of samples is 16 bits.

2.3.2 Characterization of DCSS system

Before performing DCSS in UWA channels, our first task consisted in characterizing the system that had been designed. Indeed, we connected the signal generator to the acquisition board. Then, we generated 500 packets of DCSS signals spaced with a silence time of 1 second. After that, we stored them in a wav file. Each frame included a preamble made up of 10 raw chirps (8 up-chirps followed by 2 down-chirps) and 30 symbols with SF=6 and SF=7 and a 5 kHz bandwidth. The carrier and the sampling frequency were set at 18 and 100 kHz, respectively.

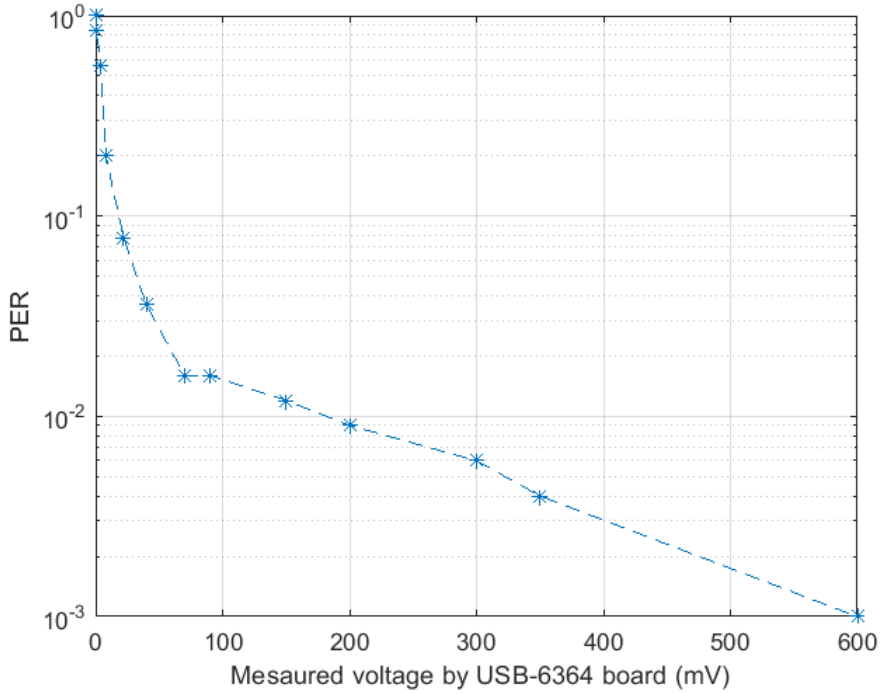

Figure 2.19: Packet error rate

The result is presented as the packet error rate (PER) for different voltage values of the received signal. As mentioned in Figure 2.19, from 150 mV, the PER is around 10^{-2}. We set this voltage value as the minimum acceptable value to process the received signal properly. So far, we designed this value as a threshold to calculate the achievable distance of the DCSS system. As we have seen previously, the hydrophone has a sensitivity of -208 $dBV\ re\ 1\ \mu Pa$, and the pre-amplifier has a gain of 50 dB. Hence, the receiver's source intensity level (SIL) can be calculated as follows:

$$SIL = V_f(dB) - GAIN_{dB} - OCCR(f_c) \tag{2.48}$$

where $V_f(dB)$ is the input voltage of the acquisition board expressed in decibels, $GAIN_{dB}$ is the amplifier gain in dB, and $OCCR(f_c)$ is the Open Circuit Receiving Response at the carrier frequency $f_c = 18\ kHz$. On the one hand, by fixing $V_f = 150\ mV$ at the threshold value, we obtain the corresponding minimum acoustic power value $SIL \approx 150\ dB\ re\ 1\ \mu Pa$. On the other hand, the SIL can be expressed as a function of the source level and the attenuation losses in the medium as mentioned in equation (2.49).

$$SIL_{min} = SL - TL(d_{max}, f_c) \tag{2.49}$$

According to the datasheet of the transducer, for a signal defined at $f_c = 18\ kHz$ within

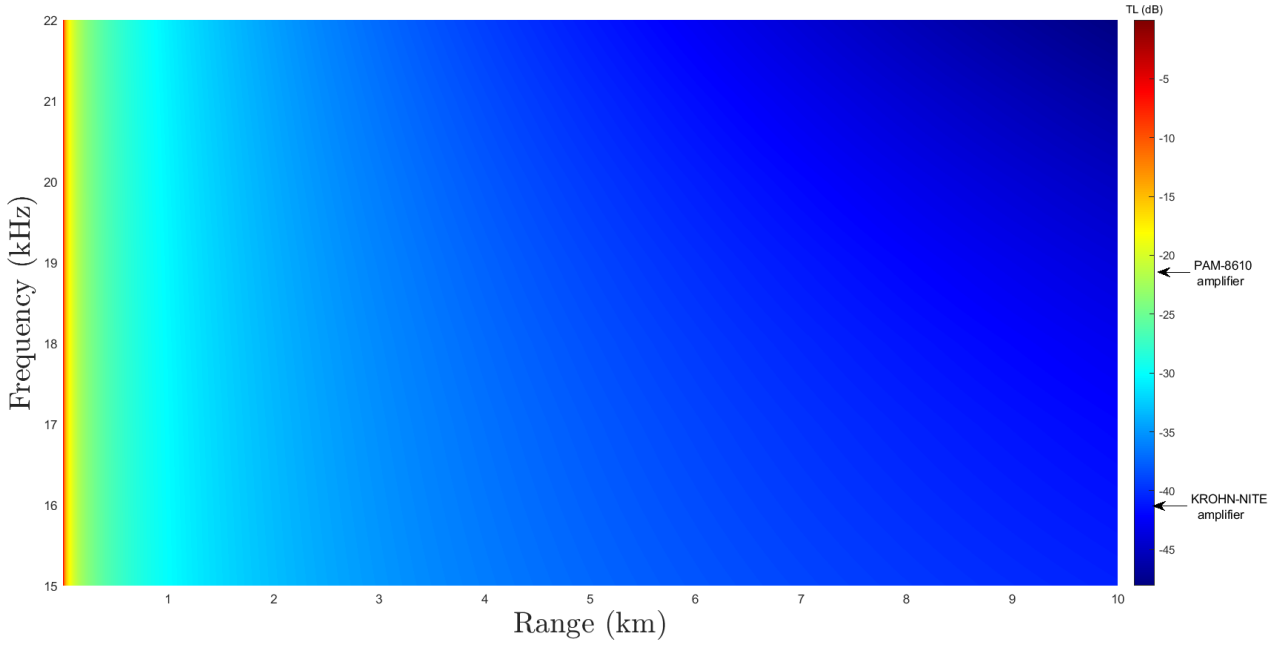

Figure 2.20: Transmission loss (TL) Thorp model

a bandwidth of 5 kHz its TVR drops by almost 10 dB. Thus, applying the equation (2.47), the effective acoustic source power for the PAM-8610 and KROHN-HITE 7500 modules is 171.12 $dB\ re\ 1\ \mu Pa\ @1m$ and 191.68 $dB\ re\ 1\ \mu Pa\ @1m$ respectively.

Based on the source level value and the Thorp model for transmission loss calculation, we can estimate the maximum achievable distance of the DCSS system. Figure 2.20 illustrates the TL using the Thorp model. The simulation setting used to generate the TL in a frequency band of 15 and 22 kHz and an index of propagation $m = 1$ (see section 1.1.3). According to this figure, the proposed DCSS system can achieve a distance of 160 m using the PAM-8610 amplifier and up to 7 km using the KROHN-HITE 7500 amplifier. It should be noted that this estimation is based on the Thorp model, which is more adapted to the horizontal configuration of communication. Moreover, it considers only the frequency as a metric of calculation. Therefore, the result could change in a vertical configuration in which depth is an important parameter to assess. So far, the transmission loss caused by the scatters is not included, which could also limit the communication range.

2.4 Experimental results

This section is dedicated to the performance of the proposed DCSS system in various environments.

2.4.1 Lake trial

2.4.1.1 Setup of experiment

Figure 2.21: Setup of the experiment

The experiments were conducted in Bordeaux "Bassin a Flot" lake in September 2022 (Figure 2.21). The distance between the transmitter and the receiver was 140 m. The lake's depth was about 16 m, and both transmitter and receiver were fixed at a depth of 4 m. The breakdown of the parameters used to generate the signal is listed in table 2.3.

Table 2.3: Parameters of the transmitted signal

Parameter	Value
Carrier frequency	18 kHz
Sampling frequency	100 kHz
Source level	171.12 $dB\ re\ 1\ \mu Pa\ @1m$
Spreading factor	5/6 and 6/7
Bandwidth	2.5 kHz and 5 kHz
Preamble: Long chirp duration	1 s
Preamble: Number of up chirps	8
Preamble: Number of down chirps	2
Number of symbols	30
Number of bits	165 (for SF5/SF6) and 195 (for SF6/SF7)

2.4.1.2 Result and discussion

The underwater channel is characterized using a set of hyperbolic frequency modulations (bandwidth of 5 kHz and carrier frequency of 18 kHz) to constitute pings, each of length 120 ms. The signal is repeated for 1 minute to observe precisely the variability of the channel. The methodology introduced in section 1.4 is applied to obtain the characteristics of the channel. The result is expressed in Figure 2.22. As we can see, the channel has three central taps that vary slightly over time for approximately 4 ms. Besides, the Doppler effect is present in the channel, and it introduces a slight frequency shift around 0 Hz.

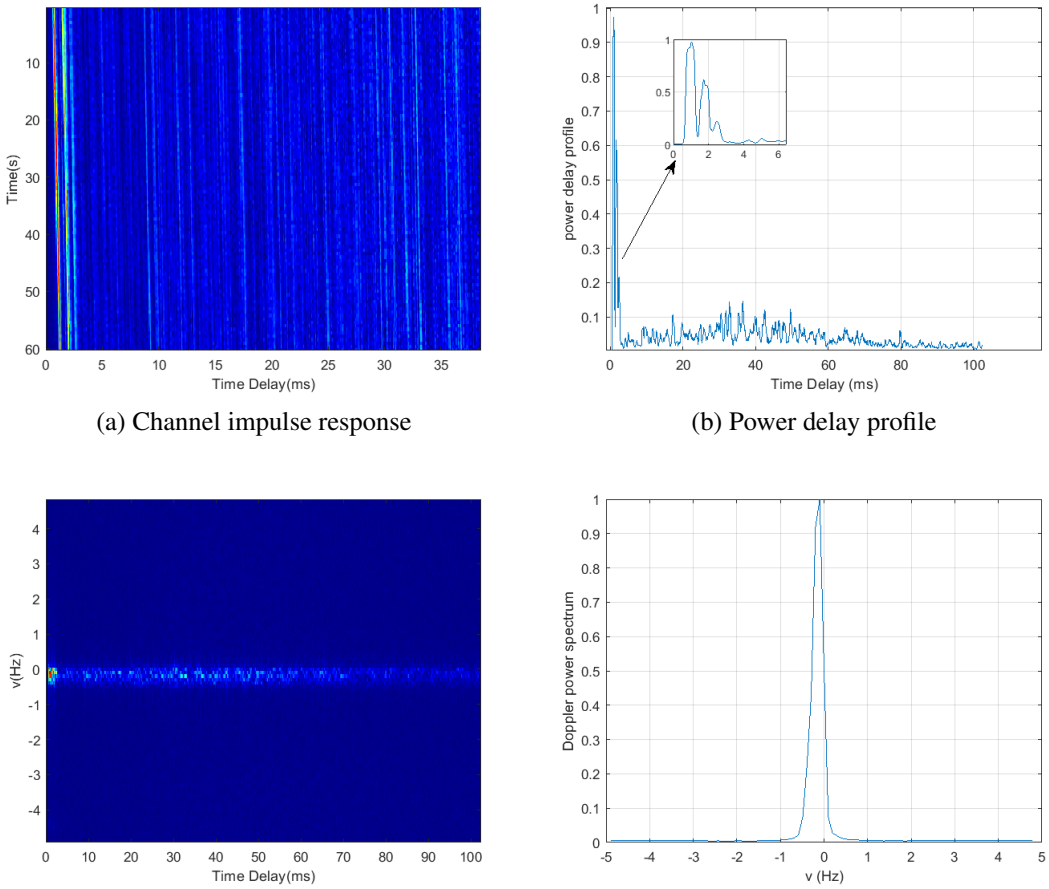

(a) Channel impulse response

(b) Power delay profile

(c) Doppler Spreading function

(d) Doppler power spectrum

Figure 2.22: Characteristics of "Bassin à Flot" lake

Spreading factor		Bandwidth	Bit rate	BER
Preamble	Payload			
6	5 and 6	5 kHz	572 bps	$4.16\ 10^{-2}$
6	5 and 6	2.5 kHz	286 bps	$3.33\ 10^{-2}$
7	6 and 7	5 kHz	338 bps	$1.17\ 10^{-1}$
7	6 and 7	2.5 kHz	169 bps	$9.87\ 10^{-2}$

Table 2.4: BER performance of DCSS in lake

Table 2.4 summarizes the performance of the DCSS system for different payload configurations. In all experiments, the payload is generated with two spreading factors, and the number of symbols is 30. At a distance of 140 m, the results show that the configuration SF5/SF6 is better than SF6/SF7. However, the obtained values of BER are low compared to the material characterization study, where the BER is expected to be at 0. Indeed, the estimated channel presents a high level of noise. As a result, both the frequency equalization and demodulation processes are impacted.

2.4.2 Ocean trial

2.4.2.1 Setup of experiment

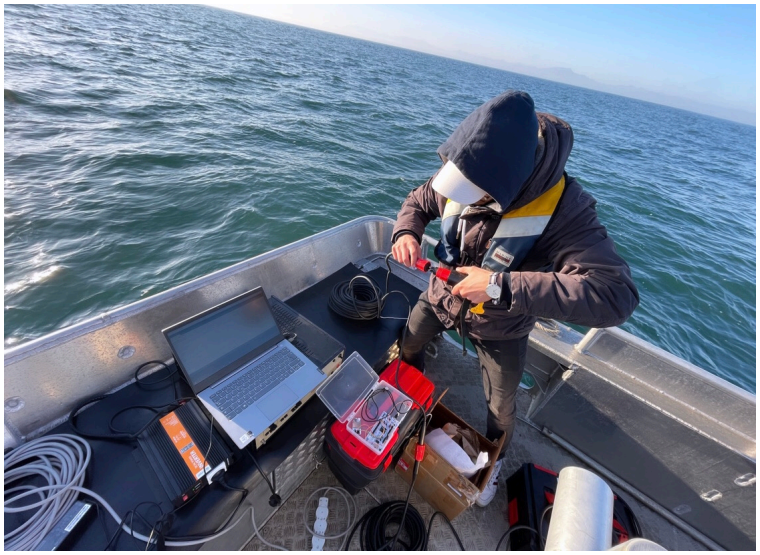

Figure 2.23: Illustration of transmitter deployment

The experiments were conducted off the Bay of "Gasgogne" in April 2023. In terms of hardware, we performed the system using a SIMO system composed of one transmitter and four hydrophones. The distance between the transmitter and the receivers was 250 m, and the ocean's depth was about 80 m. The transmitter was fixed at a depth of 4 m. The hydrophones were fixed at 3 m (2 hydrophones) and 5 m (2 hydrophones). The payload is generated using 20 symbols divided into 10 for $SF = 6$ and 10 for $SF = 7$ which represents a total bits of 130. The preamble is composed of a long chirp of length 1 s, 8 up chirps, and 2 down chirps. The bandwidth was 2 kHz, and the carrier frequency was 18 kHz. Finally, the acoustic power used to send the frame is fixed at $191.68\ dB\ re\ 1\ \mu Pa\ @1m$.

2.4.2.2 Result and discussion

The channel is characterized similarly to the study carried out in the lake environment. During 60 seconds, a set of hyperbolic frequency modulation (bandwidth of 5 kHz and carrier frequency of 18 kHz) pings, each of 120 ms, are transmitted in the medium. The characteristics of the ocean channel are shown in Figure 2.24. The channel has two major taps, where the first one is dominant. That tap varies quickly over time within an interval of 10 ms. In the frequency domain, we can observe an intense Doppler effect. It varies quickly and introduces a frequency shift that is more dominant from 1 to 3 Hz.

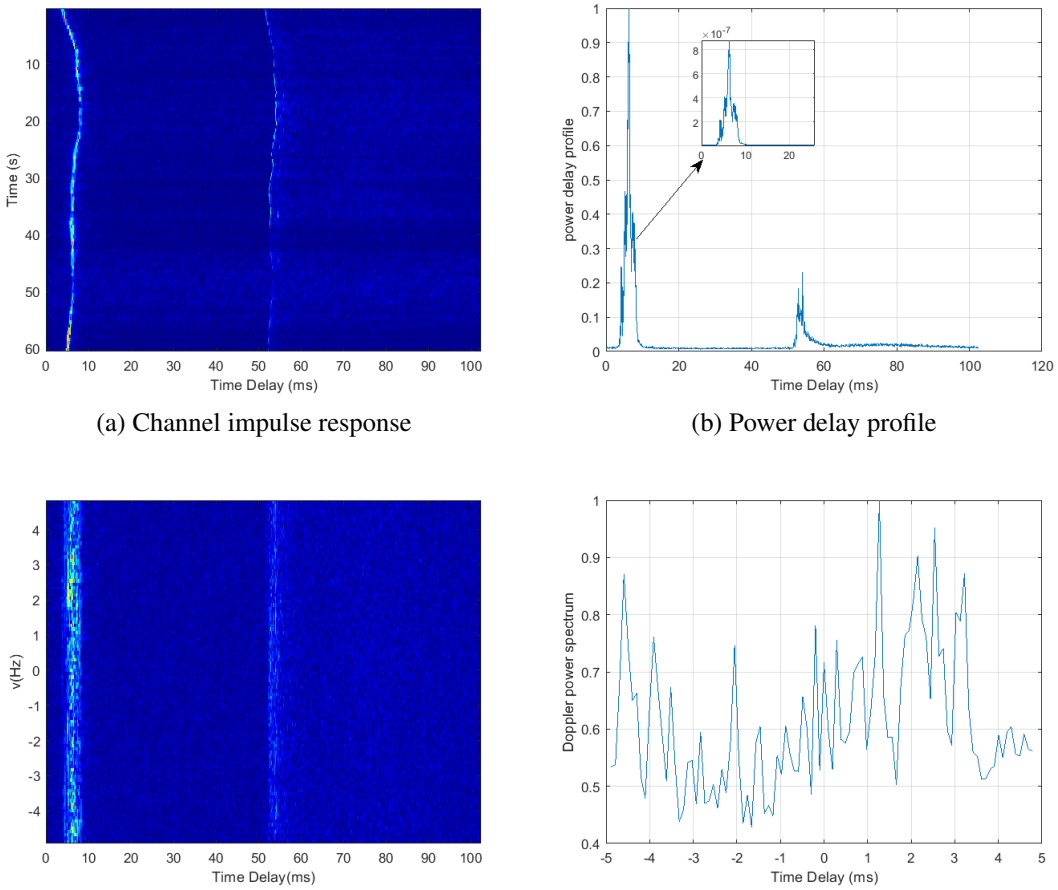

(a) Channel impulse response

(b) Power delay profile

(c) Doppler Spreading function

(d) Doppler power spectrum

Figure 2.24: Characteristics of the bay of "Gasgogne"

Hydrophone	BER	SNR (dB)
1	8.1×10^{-3}	2.25
2	0	2.7
3	0	8.51
4	8.06×10^{-2}	3.8

Table 2.5: BER performance of DCSS in the ocean

The performance of this experiment is listed in Table 2.5. As we can see, hydrophones 2 and 3 have a good performance with a BER of 0. Whereas hydrophone 1 has a less efficient result and hydrophone 4 is even lower with BER of 8.06×10^{-2}. The investigation of the corresponding frames leads to an error of 1 or -1 between the transmitted and the received symbols. This problem occurs when the fractional part of the CFO is not well compensated during the synchronization process. An enhancement of the performance is possible by encoding the transmitted symbols. However, the data rate will be reduced, which is not practical since the data rate is by default low. In addition, using correlation-based synchronization would enhance

performance. Nevertheless, it should be noted that the computation complexity is much higher than the proposed method based on despreading the received signal.

2.5 Conclusion

In this chapter, we explained the proposed UAC to connect the fishing nets while preserving the biotopes from acoustic pollution. We introduced at first the acoustic link budget and highlighted that marine animals mostly use the frequency band of communication. In this context, we focused on modulation schemes that ensure communication underwater at low SNR levels. By reducing the transmitting acoustic power of the UWA channel, it will be possible to ensure data link without disturbing the environment. We presented existing works of acoustic communication at a low SNR level, and we focused on the chirp-based waveform as a likely solution to establish communication without introducing additional noise to the environment or at least not disturbing the biotopes. After that, we introduced the proposed DCSS scheme of communication. We started by studying the conventional CSS and its limitation in UWA channels. Then, we introduced the differential encoding to overcome the frequency shift problem. Besides, we used the FrfT operator to reduce the Doppler effect. Furthermore, we exploited the orthogonality of the chirps to enhance the data rate and bypass the insertion of cyclic prefixes. We also added a channel estimator and equalization to demodulate the signal. Finally, we performed the system using the Watermark simulator before conducting experiments in various underwater environments.

Next, we presented the developed system to assess the proposed communication scheme in real conditions. We characterized the hardware to determine the achievable distance using different acoustic amplifiers. Throughout several tests in lake and ocean environments we performed the DCSS system. The result indicates that the system can achieve a BER up to 10^{-3} at 2 dB of SNR. So far, we have shown that an enhancement is possible by applying channel encoding.

CHAPTER 3

TDOA-Based localization in UWA channel

In the previous chapter, we focused on the communication part of the proposed hybrid system to connect and localize the filling nets underwater. Firstly, we established the acoustic link budget to assess communication schemes underwater, and we cited the existing works of underwater acoustic communication operating at low transmitting power. Based on this analysis, we chose the chirp-based waveform to overcome the severe characteristics of the UWA channel. More precisely, we proposed DCSS modulation to make communication at low SNR levels. This way, we ensure communication and preserve the environment from acoustic pollution. In this chapter, we describe the localization part of the proposed system. We start by providing the underwater acoustic localization techniques. Then, we focus on TDOA approach to ensure localization underwater. By means of the hyperbolic based technique we explain the localization principle. Moreover, we introduce the existing methods to compute TDOA-based positioning technique in case of noised measurements.

In order to minimize the error of TDOA calculation, we present various methods of computation using chirp signals and provide a performance comparison in UWA channels. Finally, we present and discuss the result of the proposed system in a scenario of source localization using Bellhop-Based channel modeling for network simulation.

3.1 Introduction

In recent years, the development of underwater acoustic sensors enabled numerous applications in both civil and military fields. As a result, accurate localization of underwater acoustic devices has become a popular focus of research in the scientific community. Various underwater applications have been thoroughly investigated, including systems to detect natural catastro-

phes such as tsunamis, ecosystem monitoring, oil drilling operations, and military surveillance [110]. Generally, localization approaches can be classified into two classes: range-free and range-based ones. Ranging in wireless networks can be achieved through a variety of methods, such as the measurement of time of arrival (ToA), time difference of arrival (TDoA), received signal strength indicator (RSSI), or angle of arrival (AoA) of received signals.

3.1.1 Range-based schemes for underwater acoustic localization

In this paragraph we emphasize the commonly used methods for range-based underwater acoustic localization.

3.1.1.1 Received signal strength indicator

Received signal strength indication is a widely used characteristic for underwater acoustic localization. The RSSI method does not require clock synchronization, which bypasses the high cost of synchronization imperfections. This method measures the power in a signal sent from an acoustic source. As acoustic waves attenuate according to the frequency and range of transmission (see subsection 1.1.3), the distance can be approximated based on the relationship between the transmitted and received signal strengths. According to [111], the measured RSSI in the UWA channel can be expressed as follows:

$$RSSI(l) = SL - TL(l) + \eta \tag{3.1}$$

SL is the source level, $TL(l)$ is the transmission loss at a distance l, and η is a random noise assumed to be a zero-mean Gaussian random variable. Due to the high variability of UWA channels, the RSSI value is vulnerable to environmental disturbances. Thus, it is difficult to perform precise ranging by directly exploiting the absolute RSSI value. To overcome this problem, [112] proposed an assisted RSSI-based localization from a mobile anchor node. They introduced a scheme based on support vector regression (SVR) to estimate the projection of sensor nodes on the linear trajectory of the mobile anchor node.

3.1.1.2 Time of arrival

Time of arrival represents the time a signal travels between the transmitter and receiver. Multiplying the TOA value by the speed of the acoustic wave underwater, allows the estimation of the range between the receiver and the transmitter. As the direction is unavailable, multiple receivers are usually deployed in the network to determine the source position accurately. This technique requires time synchronization between receivers and transmitters. Practically,

the source location using a TOA-based algorithm is a subject of time synchronization imperfection or error in TOA calculation. Thus, various optimization algorithms could be applied to enhance the source estimation. [113] analyzed different positioning algorithms, including the least-squares method, the Taylor-series method, the approximate maximum likelihood method, the two-stage maximum likelihood method, and the genetic algorithm.

3.1.1.3 Time difference of arrival

The time difference-of-arrival method determines the location of an acoustic source by calculating the time difference between signals received by each device. The TDOA method lessens the need for precise time synchronization between the acoustic source and receiver sensor. However, it requires synchronization between the receivers. In light of the existing works using the TDOA approach for underwater localization, [114] proposed a network of receivers to estimate the TDOA of acoustic signals. The analysis of the proposed method is carried out using cross recurrence plot analysis (CRPA), which involves studying the similarities between different segments of the received signals. Unlike the traditional approaches where the complete signal is analyzed for TDOA estimation, this method involves the initial step of detecting similar sample series on each hydrophone pair within the array using cross-recurrence plot analysis. The TDOA is accurately estimated by exclusively focusing on these shared sample series. However, it should be noted that the proposed network may require more processing time and is susceptible to error multiplication.

3.1.1.4 Angle of arrival

Angle of arrival (AoA) measurement is a method for determining the direction of propagation of acoustic wave incident using an array of hydrophones. AoA determines the direction of an acoustic source by measuring the path length difference at each element of the array. As an example, this method combined with Doppler shift processing is proposed in [115] to localize a mobile node in an underwater environment.

As introduced in Chapter 1, it is challenging to design an accurate attenuation model for the UWA channel because of the multiple calculation metrics, such as salinity and temperature. Thus, the performance of RSSI methods will change from one model to another. Moreover, AoA methods involve the deployment of multiple hydrophones in the network acting like anchor nodes, which makes it an expensive solution for localization. Therefore, most approaches for underwater acoustic localization rely on ToA or TDoA for distance estimation. However, time synchronization error is one of the factors that degrade their performance. In this work we focus on TDOA based technique since we are deploying passive communication system.

3.1.2 Underwater positioning

This paragraph introduces the conventional positioning systems used for underwater acoustic localization. These systems can be distinguished into three categories defined by the distance separating the acoustic network's sensors.

3.1.2.1 Ultra-short baseline (USBL)

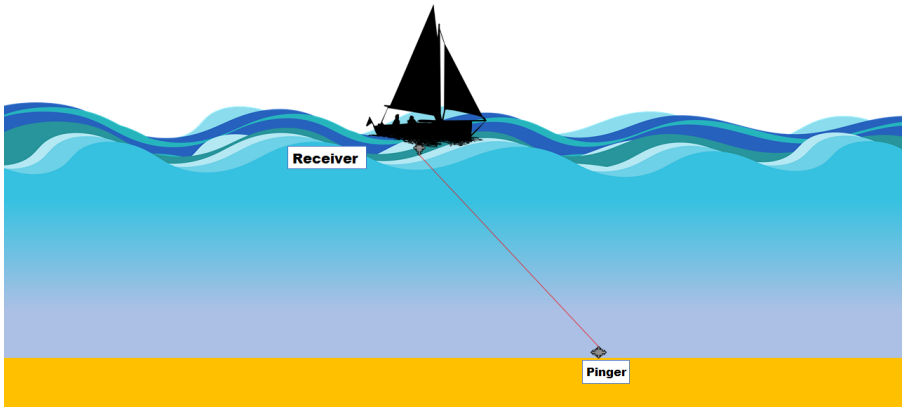

Figure 3.1: USBL system

Also known as the Super-short Baseline (SSBL), the USBL comprises an array of sensors (or acoustic antenna) separated from each other by very short distances (of the order of a few centimeters), which are typically installed under a pole attached to the underside of a boat [116]. This system determines the position of a source by measuring the TDOA between receivers. AOAs are also measured to provide additional information on the source location.

3.1.2.2 Short baseline (SBL)

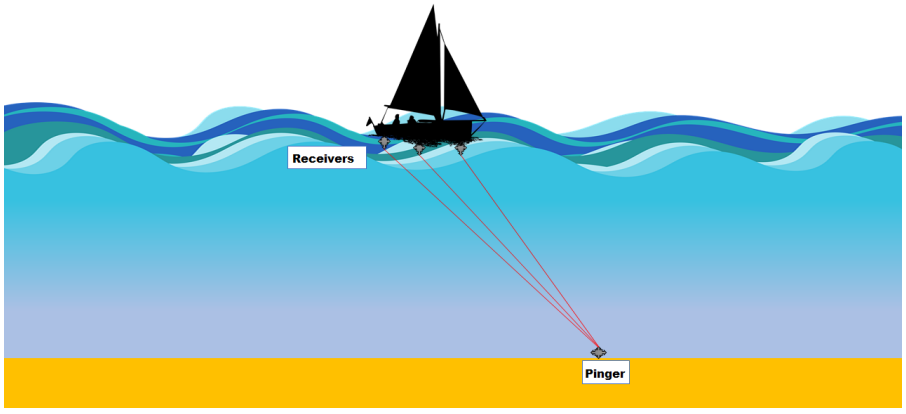

Figure 3.2: SBL system

This system uses two or more sensors separated from each other by a certain distance. Figure 3.2 shows the configuration of this system. The distance separating the sensors from each other defines the system's performance. Indeed, the greater the distance, the more accurate the location measurements will be [116]. Thus, the performance of this system will depend on the size of the boat or platform where the reception system is deployed. Similar to the USBL system, this system uses the TDOA as a calculation method to locate the source. This system is more precise than USBL since it involves multiple receivers, which make it more suitable for short and medium ranges of localization.

3.1.2.3 Long baseline (LBL)

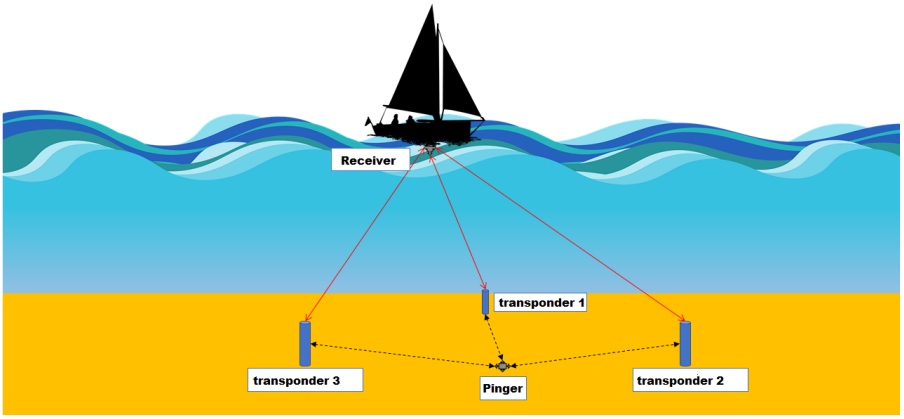

Figure 3.3: LBL system

This system is the most accurate of the three categories. It comprises several transponders deployed on the seabed, acting as references or cardinal points. The source in the area bounded by the transponders sends an acoustic signal. Next, the time of reception of the signal at each transponder is used to determine the source's position relative to the transponders' position. This system is very accurate, giving low errors in source distance. However, this system is at a disadvantage compared with other configurations due to the complexity of deploying all the equipment and the associated expenses in terms of time and cost. [116]. Figure 3.3 shows the architecture of LBL configuration.

Based on the previous consideration and on practical constraints, the proposed system is based on SBL configuration to localize filling nets underwater. Indeed, an antenna in tetrahedral form composed of 5 hydrophones is used to calculate TDOA between receivers, and through TDOA-based positioning algorithms, we estimate the acoustic source supposed to be attached to the filling net. To explain the proposed localization scheme, we start by providing the TDOA-based technique for underwater acoustic localization.

3.2 TDOA-based techniques for underwater acoustic localization

In this section, we provide the underlying theory of underwater acoustic localization based on TDOA measurements. Then, we present the most used algorithms to compute the source localization in case of noised measurements.

3.2.1 Positioning technique based on TDOA measurements

The technique of positioning is known as a Hyperbolic lateration or multilateration technique. It uses measured TDOA between receivers to determine the relative position of the transmitter. Based on measured differential distances, it traces geometrically a set of hyperbolas. As mentioned in Figure 3.4, the intersection of these hyperbolas indicates the transmitter's position.

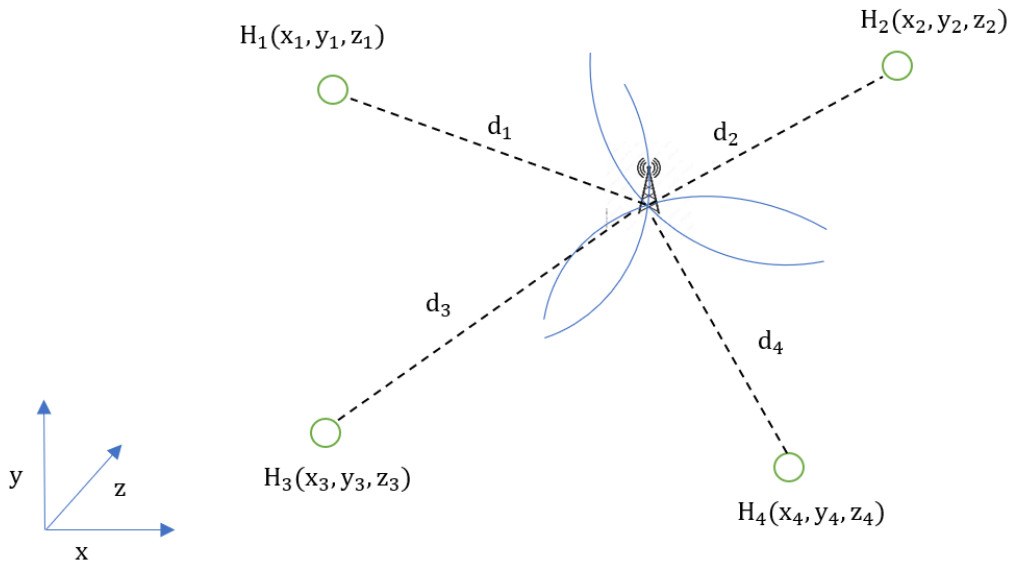

Figure 3.4: Illustration of TDOA-based positioning

To understand the principle of the TDOA-based positioning, we consider a system composed of a transmitter and several receivers ($N \geq 5$) in three-dimensional (3-D) space. We suppose that the receivers are synchronized in time. Let $p\ (x, y, z)$ denotes the position of the source and $H_k\ (x_k, y_k, z_k)$ the position of the k^{th} receiver (for $k \in [\![1, N]\!]$). We set the receiver H_1 as a reference of calculation. On the one hand, the difference in range between the k^{th} and 1^{st} receivers ($r_{k,1}$) can be obtained from the measured TDOA ($\Delta t_{k,1}$) between these receivers as follows:

$$r_{k,1} = c\ \Delta t_{k,1} = c\ (t_k - t_1) \tag{3.2}$$

c is the speed of the sound underwater. On the other hand, using the distance of 1^{st} and k^{th} receivers from the transmitter, we obtain the difference in range $r_{k,1}$ (for $k \in [\![2, N]\!]$) as mentioned in equation (3.3).

$$r_{k,1} = \sqrt{(x - x_k)^2 + (y - y_k)^2 + (z - z_k)^2} - \sqrt{(x - x_1)^2 + (y - y_1)^2 + (z - z_1)^2} \quad (3.3)$$

Substituting the equation (3.3), we have

$$r_{k,1} + \sqrt{(x - x_1)^2 + (y - y_1)^2 + (z - z_1)^2} = \sqrt{(x - x_k)^2 + (y - y_k)^2 + (z - z_k)^2} \quad (3.4)$$

By squaring both sides of (3.4) and introducing $d_1 = \|p - H_1\|_2$ we obtain:

$$\begin{aligned} (x_k - x_1)(x - x_1) + (y_k - y_1)(y - y_1) + (z_k - z_1)(z - z_1) + r_{k,1}d_1 \\ = \frac{1}{2}[(x_k - x_1)^2 + (y_k - y_1)^2 + (z_k - z_1)^2 - r_{k,1}^2] \end{aligned} \quad (3.5)$$

Formulating (3.5) in matrix form we have:

$$A\theta = b \quad (3.6)$$

with,

$$A = \begin{bmatrix} x_2 - x_1 & y_2 - y_1 & z_2 - z_1 & r_{2,1} \\ . & . & . & . \\ . & . & . & . \\ x_N - x_1 & y_N - y_1 & z_N - z_1 & r_{N,1} \end{bmatrix}, \ \theta = \begin{bmatrix} x - x_1 \\ y - y_1 \\ z - z_1 \\ d_1 \end{bmatrix}$$

$$b = \frac{1}{2} \begin{bmatrix} (x_2 - x_1)^2 + (y_2 - y_1)^2 + (z_2 - z_1)^2 - r_{2,1}^2 \\ . \\ . \\ (x_N - x_1)^2 + (y_N - y_1)^2 + (z_N - z_1)^2 - r_{N,1}^2 \end{bmatrix}$$

In the particular case where the noise is not introduced in the TDOA measurements, the source position can be deducted by inversion of the matrix A as follows:

$$\theta = (A^T A)^{-1} A^T b \quad (3.7)$$

In practice, the noise is always included in the TDOA measurements and consequently in the difference in ranges $r_{k,1}$. Hence, calculating the source position requires solving the non-linear system introduced in (3.6). In the next paragraph, we present the most used approaches to estimate the source's position while considering the noise contribution.

3.2.2 Estimation of TDOA-based position

In this part, we present the existing techniques to solve the system (3.6). The main idea is to minimize the noise in TDOA measurements to obtain the optimal estimation of the transmitter position. These algorithms are based on the assumption that the signal propagates in a straight line between the transmitter and each receiver. Moreover, the range difference errors n_k are independent Gaussian random variables with zero mean and variance σ_k^2.

3.2.2.1 Non-linear approaches

Several nonlinear approaches have been performed to determine the target location. The most used methods are least squares (LS) and maximum likelihood (ML). These methods have demonstrated their success in numerous applications by transforming the localization problem into an optimization problem. LS estimator minimizes the sum of squared residuals between the estimated and measured distances. On the other hand, the ML estimator can be seen as a weighted version of the LS method by introducing the noise covariance [117, 118, 119].

LS estimator can be divided into two classes: nonlinear least squares (NLS) and linear least squares (LLS). In this paragraph, we focus on the NLS solution to determine the target position. The purpose of the NLS estimator is to optimize the objective function defined as:

$$J_{NLS}(\tilde{p}) = min \sum_{k=2}^{N} R_k(\tilde{p})^2 \tag{3.8}$$

where $\tilde{p} = [\tilde{x}, \tilde{y}, \tilde{z}]^T$ is the optimization variable vector, $R_k(\tilde{p}) = \tilde{r}_{k,1} - r_{k,1}$ is residual with the $\tilde{r}_{k,1}$ is the measured value using the formula (3.2). Thus, the optimal position can be obtained from the vector $\tilde{p}$ as follows:

$$\hat{p} = \underset{\tilde{p}}{argmin} J_{NLS}(\tilde{p}) \tag{3.9}$$

The principle of the NLS estimator consists of solving the equation (3.9) using two methods. The first one is by performing global research using random search techniques, such as the genetic algorithm (GA) [120] and the Firefly algorithm [121]. An example based on this solution is introduced in subsection 3.2.2.3. The second method consists of computing the optimal value of the target from an initial position using an iterative procedure. To do so, an optimization of the cost function is applied to define the new position of the target at each iteration. By means of the stopping criterion, the optimal position can be estimated. Namely, Newton-Raphson (NR), Gauss-Newton (GN) [122, 123] and Levenberg-Marquardt [124] are among the most used methods for optimization. Usually, the first position value is fixed using the linear least squares approximation, which is introduced in the next paragraph. The Cramer-Rao Lower bound (CRLB) for TDOA measurements provides a lower bound on the covariance of the un-

biased estimator of the source position, and it is often used as a benchmark for performance comparison [125].

Newton-Raphson optimization method

NR is one of the widely used optimization methods to solve the non-linearity problem using Taylor series expansion to the objective function. Through linear approximation, the objective function at a slight variation from the position p can be written as:

$$J_{NLS}(p+\delta p) \approx f(p) = J_{NLS}(p) + \delta p^T[\nabla J_{NLS}(p)] + \frac{1}{2}\delta p^T \nabla^2 J_{NLS}(p)\delta p \tag{3.10}$$

Exploiting (3.10), the optimal value of the objective function satisfies the following condition:

$$\nabla f(p) = 0 \tag{3.11}$$

Solving this system yields

$$\delta p = -[\nabla^2 J_{NLS}(p)]^{-1} \nabla J_{NLS}(p) \tag{3.12}$$

Thus, the NR method requires the calculation of the gradient of the objective function and Hessian matrix to update the position value at each iteration as follows:

$$\nabla J_{NLS}(p) = \begin{bmatrix} \frac{\partial J_{NLS}(p)}{\partial x} \\ \frac{\partial J_{NLS}(p)}{\partial y} \\ \frac{\partial J_{NLS}(p)}{\partial z} \end{bmatrix}, \ \nabla^2 J_{NLS}(p) = \begin{bmatrix} \frac{\partial^2 J_{NLS}(p)}{\partial^2 x} & \frac{\partial^2 J_{NLS}(p)}{\partial x \partial y} & \frac{\partial^2 J_{NLS}(p)}{\partial x \partial z} \\ \frac{\partial^2 J_{NLS}(p)}{\partial y \partial x} & \frac{\partial^2 J_{NLS}(p)}{\partial^2 y} & \frac{\partial^2 J_{NLS}(p)}{\partial y \partial z} \\ \frac{\partial^2 J_{NLS}(p)}{\partial z \partial x} & \frac{\partial^2 J_{NLS}(p)}{\partial z \partial y} & \frac{\partial^2 J_{NLS}(p)}{\partial^2 z} \end{bmatrix} \tag{3.13}$$

Finally, the position is updated at $(k+1)^{th}$ iteration using the following formula:

$$p^{k+1} = p^k + \delta p^k \tag{3.14}$$

According to [123], stopping the computation of the position can be made using a criterion that checks the gradient norm of the objective function at each iteration (3.15).

$$\|\nabla J_{NLS}(p^k)\| \leq \epsilon \tag{3.15}$$

Newton-Gauss optimization method

Unlike the NR optimization method, the GN is limited to the first order in the linearization process of the objective function. Hence, it has a low complexity computation compared to the NR method. The coefficient of correction δp used to rectify the target position at each iteration

is defined as follows:

$$\delta p = -[\mathbb{J}(p)^T \mathbb{J}(p)]^{-1} \mathbb{J}(p)^T [R_2(p) \ ... \ R_N(p)]^T \tag{3.16}$$

where $[R_2(p) \ ... \ R_N(p)]$ is the residual vector and $\mathbb{J}(p)$ is the Jacobian matrix defined as follows:

$$[\mathbb{J}(p)]_k = [\frac{\partial R_k(p)}{\partial x} \ \ \frac{\partial R_k(p)}{\partial y} \ \ \frac{\partial R_k(p)}{\partial x}] \ , \ k \in [\![2, N]\!] \tag{3.17}$$

$$\mathbb{J}(p) = - \begin{bmatrix} \frac{\partial(\|H_2-p\|-\|H_1-p\|)}{\partial x} & \frac{\partial(\|H_2-p\|-\|H_1-p\|)}{\partial y} & \frac{\partial(\|H_2-p\|-\|H_1-p\|)}{\partial z} \\ . & . & . \\ . & . & . \\ \frac{\partial(\|H_N-p\|-\|H_1-p\|)}{\partial x} & \frac{\partial(\|H_N-p\|-\|H_1-p\|)}{\partial y} & \frac{\partial(\|H_N-p\|-\|H_1-p\|)}{\partial z} \end{bmatrix} \tag{3.18}$$

As mentioned in the NR method, the updated position can be calculated using the equation (3.14), and the stopping criterion (3.15) can be applied to obtain the optimal position of the target.

The non-linear approaches can ensure good accuracy in determining the target position. However, their performance strongly depends on the selection of the initial point. Therefore, it is not guaranteed to converge to the global optimal solution. Alternatively, linear least squares are proposed to overcome this problem.

3.2.2.2 Linear least squares

LLS methods are widely used in TDOA-based positioning because of their efficiency in computing the source position. The conventional method of LLS determines the target position through LS estimator. The location estimate is found from [126]

$$\hat{\theta}_{LS} = \underset{\tilde{\theta}}{argmin}(A\tilde{\theta} - b)^T (A\tilde{\theta} - b)^T = (A^T A)^{-1} A^T b \tag{3.19}$$

An enhancement to this approximation is proposed in [127] by introducing a constraint condition between the components of the vector θ. This condition is exploited to rectify the position $\hat{\theta}_{LS}$. The proposed technique is known as the linear correction least squares (LCLS). It solves the LS cost function (3.19) while considering the following constraint condition:

$$\tilde{\theta}^T S \tilde{\theta} = (\tilde{x} - x_1)^2 + (\tilde{y} - y_1)^2 + (\tilde{z} - z_1)^2 - \tilde{d_1}^2 = 0 \tag{3.20}$$

where $S = diag(1, 1, 1, -1)$.

Weighted least squares

Chan and Ho have presented the weighted least squares algorithm (WLS) technique as an alternative to the conventional LS-based estimator [128, 129]. Unlike the conventional formula used in LS to define range differences $r_{k,1}$ (3.3), this technique includes the noise term in $r_{k,1}$ as follows:

$$r_{k,1} = d_{k,1} + n_{k,1} \ , \ k \in [\![2, N]\!] \tag{3.21}$$

with,

$$d_{k,1} = d_k - d_1 \ , \ k \in [\![2, N]\!] \tag{3.22}$$

and,

$$d_k = \sqrt{(x - x_k)^2 + (y - y_k)^2 + (z - z_k)^2} \tag{3.23}$$

Given (3.23), we can rewrite (3.21) for $k \in [\![2, N]\!]$ as follows:

$$r_{k,1} + \sqrt{(x - x_1)^2 + (y - y_1)^2 + (z - z_1)^2} = \sqrt{(x - x_k)^2 + (y - y_k)^2 + (z - z_k)^2} + n_{k,1} \tag{3.24}$$

By squaring both sides of (3.24) and introducing d_1 we obtain:

$$\begin{aligned} (x_k - x_1)(x - x_1) + (y_k - y)(y - y_1) + (z - z_1) + r_{k,1} d_1 = \\ \frac{1}{2}[(x_k - x_1)^2 + (y_k - y_1)^2 + (z_k - z_1)^2 - r_{k,1}^2] + e_{k,1} \end{aligned} \tag{3.25}$$

where $e_{k,1} = d_k n_{k,1} + \frac{1}{2} n_{k,1}^2$. Using the matrix from we can express (3.25) as follows:

$$A\theta = b + e \tag{3.26}$$

A, b and θ are defined in (3.2.1). The parameter $e = [e_{2,1} \ ... \ e_{N,1}]^T$ represents the noise vector. The basic idea of the WLS approach is to determine θ by optimizing the objective function defined as:

$$J_{WLS}(\tilde{\theta}) = (A\tilde{\theta} - b)^T W (A\tilde{\theta} - b) \tag{3.27}$$

with $W = E(ee^T)^{-1}$ is the expectation weighting matrix. By neglecting the second-order error term in the expression of $e_{k,1}$ (for $k \in [\![2, N]\!]$) and using $n_{k,1} = n_k - n_1$ with n_k is zero mean AWGN, then the weighting matrix can be simplified to:

$$W \approx (\hat{D}^T \Sigma \hat{D})^{-1} \tag{3.28}$$

with,

$$\hat{D} = diag(\hat{d}_2, \hat{d}_3, ..., \hat{d_N}) \ , \ \Sigma = diag(\sigma_2^2, \sigma_3^2, ..., \sigma_N^2) + \sigma_1^2 \mathbb{1}_{N-1} \times \mathbb{1}_{N-1}^T$$

Finally, the unconstrained solution based on the weighted least algorithm simplifies the estimated θ into:

$$\hat{\theta}_{WLS} = (A^T W A)^{-1} A^T W b \tag{3.29}$$

As the matrix W depends on the distances d_k whose are not known, the position computation is usually made using two steps:

- First step: the matrix W is initially fixed to the identity matrix I_N to compute $\hat{\theta}_{WLS}$.
- Second step: the obtained result from the first step is inserted in the algorithm to get the accurate value of the position.

Constraint weighted least squares

Similarly to the LCLS method, an improvement of the WLS method is proposed while considering the constraint condition mentioned in (3.20). This approach is called constrained weighted least squares (CWLS) [130, 131]. The proposed solution rectifies the value of θ_{WLS} by introducing the constraint condition. More precisely, it minimizes the Lagrangian equation expressed as follows:

$$L(\tilde{\theta}, \lambda) = (A\tilde{\theta} - b)^T W (A\tilde{\theta} - b) + \lambda \tilde{\theta}^T S \tilde{\theta} \tag{3.30}$$

where λ is the Lagrangian scalar. The constrained weighted least squares solution is

$$\hat{\theta}_{CWLS} = (A^T W A + \lambda S)^{-1} A^T W b \tag{3.31}$$

The coefficient λ can be derived from (3.30) by applying the derivation:

$$\frac{\partial L(\tilde{\theta}, \lambda)}{\partial \tilde{\theta}} = 0 \tag{3.32}$$

The development of this equation leads to the following expression:

$$\sum_{i=1}^{4} \frac{u_i w_i}{(\lambda + \gamma_i)^2} = 0 \tag{3.33}$$

with

$$\begin{gathered} [u_1, u_2, u_3, u_4]^T = U^T S A^T W b \quad , \quad [w_1, w_2, w_3, w_4]^T = U^T A^T W b \\ A^T W A S = U diag(\gamma_1, \gamma_2, \gamma_3, \gamma_4) U^{-1} \end{gathered} \tag{3.34}$$

According to [130], λ is the real-valued root that minimizes the objective function $J_{NLS}(\hat{\theta})$.

3.2.2.3 Hybrid solution: WLS and firefly algorithm

Algorithms of optimizations have gained much interest in TDOA-based positioning because of their ability to seek efficiently the optimal position. So far, hybrid solutions have shown better performance compared to the classical methods [123]. Indeed, these approaches combine the algorithms of optimization with the objective function to obtain better estimation. As the implementation of these techniques is made in iterative way, the initial point is mostly set using LLS estimator. In this paragraph we introduce an example of hybrid-based solutions. The proposed technique improves the source computation through a combination of the WLS and the Firefly algorithm (FA) [132]. To explain this method, we start by introducing the Firefly algorithm. Then, we show the main steps to find the optimal position from a start guess obtained by the WLS method. The main idea of the FA can be summarized in three major points:

- The fireflies are attracted to each other regardless of their gender.
- A brighter firefly is more attractive than a less bright one. Thus, the less bright one will move towards the brighter one.
- The brightness of fireflies is related to the objective function.

FA exploits the attraction between the fireflies to gather at the end around the brighter one. In TDOA-based localization context, that means the algorithm will optimize the objective function defined in (3.8). The following paragraph introduces the main steps to localize the source using FA and an initial point obtained from WLS approach.

Firefly algorithm

In a general case, we consider the firefly position dimension equal to D. We assume that the total number of fireflies is equal to N. The distance between fireflies $f_i = (x_{i1}, x_{i2}, ..., x_{iD})$ and $f_j = (x_{j1}, x_{j2}, ..., x_{jD})$ for $i, j \in [\![1, N]\!]$, can be expressed as:

$$r_{ij} = \|f_i - f_j\| = \sqrt{\sum_{d=1}^{D} (x_{id} - x_{jd})^2} \tag{3.35}$$

with x_{id} and x_{jd} are the positions of the i^{th} and j^{th} fireflies respectively.The following function models the brightness metric:

$$I = I_0 e^{-\gamma r_{ij}^2} \tag{3.36}$$

where I_0 is the brightness of the firefly, supposed to be proportional to the objective function value. γ represents the absorption coefficient of the brightness intensity.

The attractiveness of the fireflies is defined as:

$$\beta = \beta_0 e^{-\gamma r_{ij}^2} \tag{3.37}$$

where β_0 designs the factor of maximum attraction level. Given (3.36) and (3.37), we can notice that when the distance is short, the brightness intensity increases. Consequently, the attractiveness factor also increases. In this case, the fireflies who have less brightness factor will move towards the others using the following formula:

$$x_{id}(t+1) = x_{id}(t) + \beta(x_{jd}(t) - x_{id}(t)) + \epsilon\alpha_i(t) \tag{3.38}$$

where $x_{id}(t)$ and $x_{jd}(t)$ represent the position of i^{th} and j^{th} fireflies at iteration t. $\alpha_i(t)$ is the step factor at t^{th} iteration and ϵ is random value generated uniformly within an interval of $[-0.5\ \ 0.5]$.

Hybrid-FA model

The purpose of this method is from pre-calculated value of the source using WLS approximation p_{wls}, apply FA to obtain the close possible point of the source position. More precisely, using fireflies principle in a region of interest which is around the calculated value of p_{wls}, to calculate the optimal value that represents an estimation of the desired location. According to [132], the main steps describing the implementation of this method are listed below:

1. Calculate the initial value of the source p_{wls} using WLS approximation [129].
2. Initialize the parameters of FA: the number of fireflies N, dimension $D = 3$, the factor of maximum attraction degree β_0, and the maximum iteration number.
3. Define the region of interest (around p_{wls} position).
4. Initialize the location of fireflies randomly and calculate the objective function.
5. Calculate the relative brightness of the fireflies using (3.36).
6. Calculate the attractiveness of the fireflies using (3.37).
7. Update the location of the fireflies in the region of interest.
8. Increment the iteration parameter. If it achieves the maximum value, run the next step. Otherwise, run back the step 5.
9. Get the optimal value of the source position.

The condition utilized to stop the computation of this technique could be the number of iterations or a criterion applied to the position or the objective function given by

$$\|J_{NLS}(p_{k+1}) - J_{NLS}(p_k)\| \leq \epsilon_1 \ , \ \|p_{k+1} - p_{k+}\| \leq \epsilon_2 \tag{3.39}$$

ϵ_1, ϵ_2 are positive small constants.

3.2.2.4 Development of Taylor series

The main idea of this method is to calculate an optimum position supposed to be near to an initial position through linearization of the distance between receivers and the target [133, 134]. The linearization is made by Taylor series expansion in the first order. If we note $\theta^0 = (x^0, y^0, z^0)$ the approximate point, then the source estimation can be defined as:

$$\hat{\theta} = \Delta\hat{\theta} + \theta_0 \tag{3.40}$$

The formulation of the position determination is to calculate the variation $\Delta\hat{\theta}$. Let's d_k^0 denotes the distance between receiver k and θ^0, so we have:

$$d_k^0 = \sqrt{(x^0 - x_k)^2 + (y^0 - y_k)^2 + +(z^0 - z_k)^2} \tag{3.41}$$

Geometrically, the difference in distance between the receiver $k \geq 2$ and the referring receiver 1 with the point of origin θ^0 is written as

$$d_{k,1}^0 = d_k^0 - d_1^0 \tag{3.42}$$

Applying the development of the Taylor series in the first order, we have

$$d_{k,1} = d_{k,1}^0 + \Delta x\frac{\partial d_k}{\partial x} + \Delta y\frac{\partial d_k}{\partial y} + \Delta z\frac{\partial d_k}{\partial z} - (\Delta x\frac{\partial d_1}{\partial x} + \Delta y\frac{\partial d_1}{\partial y} + \Delta z\frac{\partial d_1}{\partial z}) \tag{3.43}$$

Including the noise term in the TDOA measurements, we can express the difference in ranges as follows:

$$r_{k,1} = d_{k,1}^0 + (\frac{\partial d_k}{\partial x} - \frac{\partial d_1}{\partial x})\Delta x + (\frac{\partial d_k}{\partial y} - \frac{\partial d_1}{\partial y})\Delta y + (\frac{\partial d_k}{\partial z} - \frac{\partial d_1}{\partial z})\Delta z + n_{k,1} \tag{3.44}$$

This equation can be written as:

$$(\frac{\partial d_1}{\partial x} - \frac{\partial d_k}{\partial x})\Delta x + (\frac{\partial d_1}{\partial y} - \frac{\partial d_k}{\partial y})\Delta y + (\frac{\partial d_1}{\partial z} - \frac{\partial d_k}{\partial z})\Delta z = d_{k,1}^0 - r_{k,1} + n_{k,1} \tag{3.45}$$

Thus, the matrix form can be expressed as

$$G\Delta\hat{\theta} = \delta + e' \tag{3.46}$$

Where

$$\begin{gathered} G = \begin{bmatrix} (\frac{\partial d_1}{\partial x} - \frac{\partial d_2}{\partial x}) & (\frac{\partial d_1}{\partial y} - \frac{\partial d_2}{\partial y}) & (\frac{\partial d_1}{\partial z} - \frac{\partial d_2}{\partial z}) \\ \cdot & \cdot & \cdot \\ \cdot & \cdot & \cdot \\ (\frac{\partial d_1}{\partial x} - \frac{\partial d_N}{\partial x}) & (\frac{\partial d_1}{\partial y} - \frac{\partial d_N}{\partial y}) & (\frac{\partial d_1}{\partial z} - \frac{\partial d_N}{\partial z}) \end{bmatrix}, \ \Delta\theta = \begin{bmatrix} \Delta x \\ \Delta y \\ \Delta z \end{bmatrix} \\ \delta = \begin{bmatrix} d^0_{2,1} - r_{2,1} \\ \cdot \\ \cdot \\ d^0_{N,1} - r_{N,1} \end{bmatrix}, \ e' = \begin{bmatrix} n_{2,1} \\ \cdot \\ \cdot \\ n_{N,1} \end{bmatrix} \end{gathered} \tag{3.47}$$

The partial derivation of d_k yields $\frac{\partial d_k}{\partial x} = \frac{x^0 - x_k}{d_k^2}$, $\frac{\partial d_k}{\partial y} = \frac{y^0 - y_k}{d_k^2}$ and $\frac{\partial d_k}{\partial z} = \frac{z^0 - z_k}{d_k^2}$. Therefore, the least squares estimator of θ can be expressed as

$$\Delta\hat{\theta} = (G^T G)^{-1} G^T \delta \tag{3.48}$$

3.2.2.5 Conclusion

The estimation of the position using TDOA-based measurements is ongoing research. Several works are proposed in the literature to estimate the position. The NLR approaches have shown exemplary performance in diverse applications, but they are classified as high-complexity solutions, especially if a random search is involved in the calculation. Besides, they are not always guaranteeing global solutions. Alternatively, LLS or WLS approaches are proposed to ensure a global solution and are simple to implement.

Furthermore, in a dynamic case where the target is moving, other approaches are proposed in the literature to estimate accurately the position at each measured TDOA. Namely, the Kalman filter is one of the most suitable solutions for such applications [135]. It exploits the estimation of the source at each time to predict the next position and rectify it. As the system of localization depends on a non-linear function, a linearization of KF based on Taylor series expansion is often proposed to overcome the linearity problem of the system and calculate the position. The extended Kalman filter (EFK) is one of the linearization based methods.

As the error of TDOA measurement could strongly affect the localization process, we present in the following section diverse methods to compute TDOA using chirp-based signals and their performance in UWA channels. The method with low error in computation will be used in TDOA-based position estimation algorithms to perform the proposed system.

3.3 Proposed system for localization

In this section, we introduce the proposed system to localize the filling nets underwater using TDOA measurements. Firstly, we present the architecture of the system and the main steps to localize a target. As we are exploiting the synchronization process to calculate the TDOA between receivers, we study various calculation methods and provide a performance comparison in UWA channels. Then, we use the technique with the low error of TDOA calculation to perform the system using the aforementioned techniques of target estimation.

3.3.1 Architecture

In this work, we propose a hybrid system to localize and communicate filling nets underwater. Indeed, we exploit the same transmitted signal from an acoustic source to ensure communication and localization at the receiver. The main idea is to use an autonomous acoustic source attached to the filling net to send the information. At the vessel, we use a tetrahedron-shaped acoustic antenna composed of 5 hydrophones to record the transmitted signals. Then, we process these signals to retrieve the carried data using DCSS demodulation and also to localize the transmitter using a TDOA-based technique.

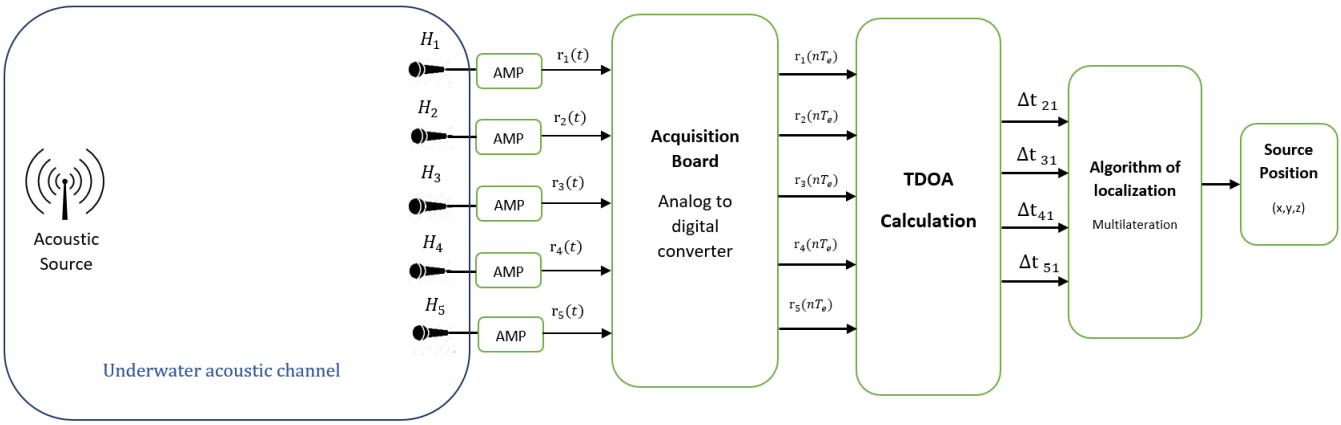

Figure 3.5: Architecture of localization

Let $s(t)$ denote the transmitted signal in the UWA channel. Using the same notation as the communication part (chapter 2), the received signal $r_i(t)$ by the hydrophone H_i can be expressed as follows:

$$r_i(t) = h_i \otimes s(t) + w_i(t) \tag{3.49}$$

$h_i(t)$ and $w_i(t)$ are the impulse response of the channel and the measured noise at receiver H_i. As mentioned in Figure 3.5, the localization process starts from the acoustic source that sends the DCSS signal (see the frame structure in Figure 2.8). At the receiver, the hydrophones are

placed in a tetrahedron structure which separates them with a distance d. Thus, the transmitted signal arrives at each hydrophone with a slight delay (Δt_{i1}) from others. This delay is calculated to launch the TDOA-based algorithm for source localization. The acquisition board record the hydrophone signals using a simultaneous analog-to-digital converter. This way, the sampled signals are time synchronized, a mandatory condition for TDOA calculation.

3.3.2 TDOA calculation

The proposed technique to calculate TDOA is based on four blocs of processing introduced in the DCSS receiver: detection, Doppler estimation, Doppler compensation, and synchronization (see subsection 2.2.5). The preamble of the transmitted signal is exploited to calculate the start time of the frame. It is composed of a set of raw up chirps followed by down chirps. The difference in start times between receivers allows the calculation of the TDOA.

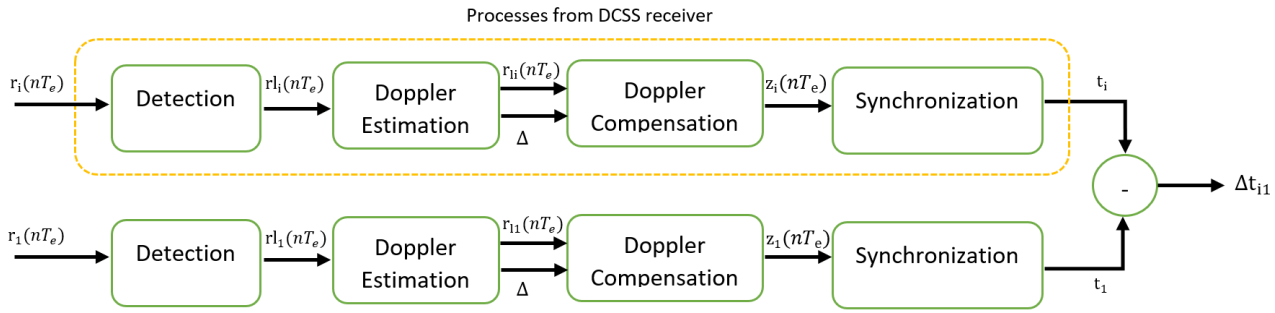

Figure 3.6: Principle of TDOA calculation between receivers H_i and H_1

After crossing the UWA channel, the received signal is sampled at T_e. We note $\gamma = \frac{T_s}{T_e}$ the oversampling ratio, with $T_s = \frac{1}{B}$ and B is the bandwidth of the transmitted signal $s(t)$. The overall diagram of TDOA calculation is shown in Figure 3.6. A reminder of each bloc is presented in the following stages:

Detection

It indicates coarsely the first chirp after time guard in the preamble for each recorded signal $r_i(nT_e)$, $i \in [\![1, 5]\!]$. Using Algorithm 1, the time of detection of receiver H_i can be expressed as follow:

$$t_{di} = k_{\alpha_i} T_s \tag{3.50}$$

where k_{α_i} is the index of the first sample of the up-chirp.

Doppler estimation and compensation

The recorded signal is rectified if a Doppler spread is introduced in the frame using Frft processing and linear interpolation for signal recovery. The main steps to execute these processes are mentioned in subsection 2.2.5.

Synchronization

It calculates the start time with high precision, referring to the most significant path in the UWA channel. Unlike the communication part, where the synchronization allows the identification of the close possible sample to the strongest path (multiple of T_e). In localization, a fine calculation is made to calculate the start time, even if it is located between two samples. Let Δt_{si} denote the synchronization time.

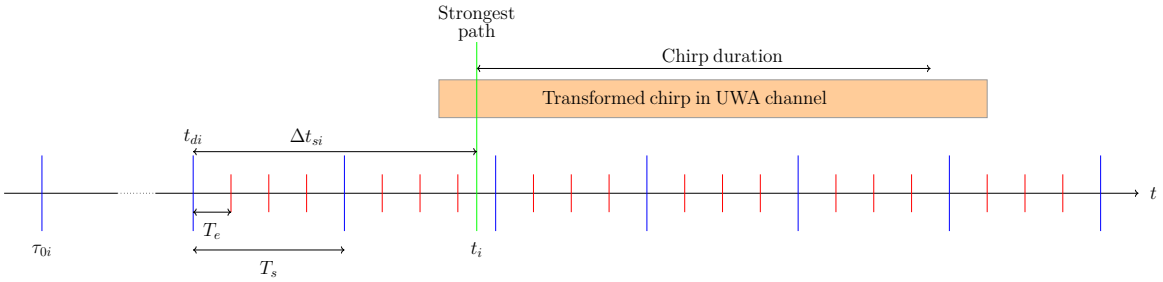

Figure 3.7: Illustration of start time calculation

A formulation of the start time calculation is presented in Figure 3.7. Based on this illustration, the start time of receiver H_i can be expressed as follows:

$$t_i = t_{di} + \Delta t_{si} \tag{3.51}$$

As presented in the DCSS receiver (subsection 2.2.5), the synchronization is made in two stages: coarse synchronization and fine synchronization. The up chirps followed by down chirps are exploited in this process to calculate Δt_{si}. After dechirping the signal $z(nT_s)$, by multiplying each bloc of length M by the conjugate of raw up chirp $x_{ref}(nT_s)$, we identify the desynchronization indexes in time and frequency domains as follows:

$$\frac{\Delta t_{si}}{T_s} = L_i + \alpha_i \tag{3.52}$$

and,

$$\Delta f_i T = C_i + \beta_i \tag{3.53}$$

with $T = \frac{M}{B}$ is the symbol time. Through coarse synchronization, L_i and C_i are estimated by implementing Algorithm 2. The amounts α_i and β_i are obtained using fine synchronization as

described in Algorithm 3. Finally, the start time of i^{th} receiver can be written as:

$$t_i = (k_{\alpha_i} + L_i + \alpha_i)\gamma T_e \tag{3.54}$$

Let H_1 be the reference receiver for TDOA calculation. Then, the TDOA between receivers H_i and H_1 can be deducted by applying the difference in start times.

$$\Delta t_{i1} = t_i - \tau_{0i} - (t_1 - \tau_{01}) = t_i - t_1 - (\tau_{0i} - \tau_{01}) \tag{3.55}$$

It should be noted that the calculation of TDOA is based on two major assumptions. The first one is that the received signals are synchronized in time. This condition involves $\tau_{0i} = \tau_{0j}$ for $i \neq j$ which simplifies the TDOA formula into:

$$\Delta t_{i1} = t_i - t_1 \tag{3.56}$$

The second assumption is that the energy of the direct path of the channel's impulse response corresponds to the strongest. According to [136, 137], this assumption is not always verified. As a result, the UWA channel could impact the accuracy of the source position.

As previously mentioned, the error introduced in TDOA measurements could strongly impact the calculation of the source position. In order to minimize the TDOA error, we focus on the synchronization process since it is responsible for the finest start time calculation. More precisely, we study various fine synchronization methods to calculate the start time and provide a performance comparison.

Focus on Fine synchronization

Usually, the frequency offset β is estimated using the Schmidl-Cox method [94, 95]. However, other methods could be applied for fractional frequency estimation. For example, [138, 139] proposed a difference in the phase between two consecutive chirps to retrieve the frequency amount. Compensating the frequency amount is mandatory to estimate α accurately. In addition to the method used for DCSS communication, we introduce in the following paragraphs different methods to estimate the time desynchronization.

3.3.2.1 Despreading method

Despreading method introduced in [140] consists of dechirping a signal composed of the up chirps of the received signal and zero padding, then performing the FFT operation to estimate the desynchronization amounts. As the processing is done in the frequency domain, insert-

ing the zero padding increases the computation resolution. To implement this method, we down-sample the received signal $z_i(nT_e)$ at rythm T_s. Then, we define the signals $\hat{zl}_i(nT_s)$ and $\hat{x}_{ref}(nT_s)$ as follows:

$$\hat{zl}_i = [[z_i]_1 \ ... \ [z_i]_{N_{up}-2} \ 0_{M\times N_{up}}] \tag{3.57}$$

and,

$$\hat{x}_{ref} = [x_{ref} \ ... \ x_{ref} \ 0_{M\times N_{up}}] \tag{3.58}$$

with $[z_i]_p = z_i(nTs + (p-1)M)$ for $p \in [\![1, N_{up}]\!]$ and $n \in [\![0, M-1]\!]$. The FFT of a dechirped signal can be written as:

$$Y = \mathfrak{F}(\hat{zl}_i \ [\hat{x}_{ref}]^*) \tag{3.59}$$

Performing the maximum value of Y and calculating q_α and q_{max}.

$$q_\alpha = \frac{M}{\pi} \frac{|Y_{q_{max}-1}|^2 - |Y_{q_{max}+1}|^2}{u(|Y_{q_{max}-1}|^2 - |Y_{q_{max}+1}|^2) + v|Y_{q_{max}}|^2} \tag{3.60}$$

with, $u = \frac{64M}{\pi^5+32\pi}$ and $v = u\frac{\pi^2}{4}$

$$q_{max} = \underset{q}{argmax}(|Y(q)|). \tag{3.61}$$

Therefore, the fractional parts α_i can be derived as follows:

$$\hat{\alpha}_i = \frac{q_{max} + q_\alpha}{2N_{up}} \ mod \ 1 \tag{3.62}$$

3.3.2.2 Correlation-based method

This method is based mainly on correlation operation to the received chirps in the frame [141]. For the fractional part of frequency desynchronization, we apply the Cox-Schmidt method. After frequency compensation, three configurations are proposed to estimate the time desynchronization amount.

- Cross-correlation: the correlation is applied to the first chirp in the frame $z_i(nT_e)$ and raw up chirp $x_{ref}(nT_e)$ for $n \in [\![0, \gamma M - 1]\!]$. Thus, $\hat{\alpha}_i = \underset{k}{\text{argmax}} \left(R_{z_i,x_{ref}}(k)\right)$
- Auto-correlation: the correlation is applied to the first chirp in the frame $x_{up1} = z_i(nT_e)$ and second raw up chirp $x_{up2} = zl_i(T_e(n + \gamma M))$ for $n \in [\![0, \gamma M - 1]\!]$.
  Hence, $\hat{\alpha}_i = \underset{k}{\text{argmax}} \left(R_{x_{up1},x_{up2}}(k)\right)$.
- Reverse-correlation: the correlation is applied to the last up chirp in the frame $x_{up} = z_i(Te(n + (N_{up} - 1)\gamma M))$ and conjugate of first down chirp in the frame $x_{down} =$

$z_i(Te(n + N_{up}\gamma M))$ for $n \in [\![0, \gamma M - 1]\!]$.
Therefore, $\hat{\alpha}_i = \underset{k}{\text{argmax}} \left(R_{x_{up},[x_{down}]^*}(k)\right)$

Finally, to seek the accurate value of the maximum argument, which is not always multiple of T_e, we perform the dichotomy research around the estimated fractional part α_i with a precision up to 10^{-6} for all introduced methods, whether the processing is made in the time domain or the frequency domain.

3.3.3 Performance of TDOA calculation in UWA channel

The performance of TDOA calculation is accomplished using time-varying UWA channels. This simulator is based on a library of channels measured in different locations [61]. To test TDOA, we focus on the channels measured using SIMO configuration. This way, we use each receiver to calculate the start time, and the difference between them allows the calculation of TDOA.

3.3.3.1 Brest Commercial Harbor

The Brest Commercial Harbor (BCH1) channel is estimated using one transmitter and array receiver composed of 4 hydrophones. The settings used to estimate the BCH1 channel at each receiver are given in Figure 3.8a and Table 3.8b.

(a) Geometric setting

Parameter	Value
Carrier frequency	35 kHz
Bandwidth	5 kHz
Probe signal	Pseudonoise
Number of hydrophones	4
Element spacing	1 m
Water depth	20 m
Range	800 m
Number of channels	582

(b) The breakdown of channel parameters

Figure 3.8: Setting of BCH1 channel copied from [61]

As depicted in Figure 3.9, the strongest path of the channel of receiver 1 is quite different from receiver 2. The difference in time between the strongest path is fixed as the real value of TDOA calculation. Besides, we can observe that the gain of the channel impulse response of receiver 1 is more significant than receiver 2. By fixing the SNR parameter, the power of the AWGN will be generated differently for each receiver. This way, we are ensuring a

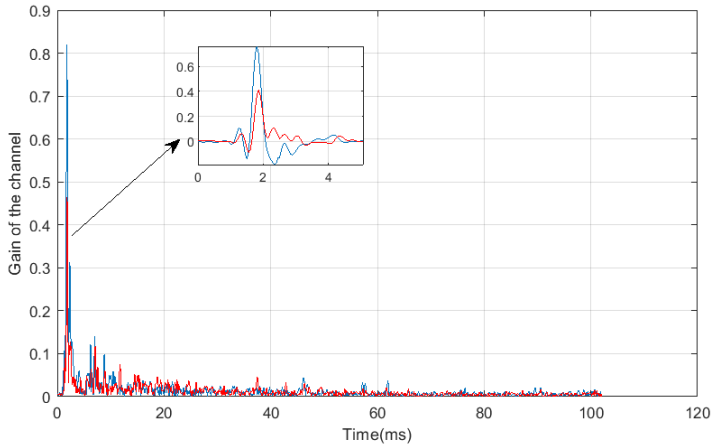

Figure 3.9: The first CIRs received by hydrophone 1 and hydrophone 4

good assessment of TDOA. The performance of TDOA is evaluated using mean absolute error (MAE) as a function of SNR. The MAE is calculated at each value of SNR using the following expression:

$$MAE(s) = \frac{\sum_{p=1}^{N_{max}} |(TDOA_{estimated})_p - TDOA|}{N_{max}} \tag{3.63}$$

N_{max} is the total number of iterations. The simulation is carried out using a preamble composed of 8 up chirps followed by two down chirps. These chirps are generated using $SF = 6$ and bandwidth of $5\ kHz$. The carrier frequency and sampling frequency were fixed at $35\ kHz$ and $500\ kHz$, respectively. Finally, the number of iterations was fixed at 500.

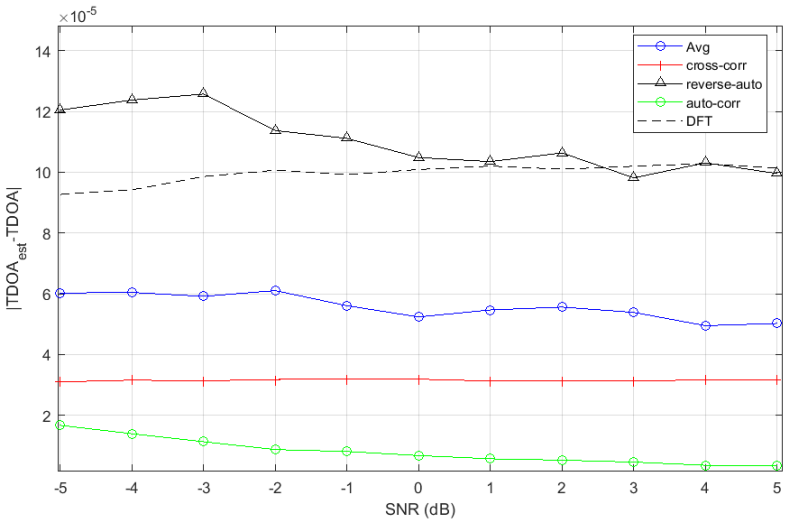

Figure 3.10: Mean absolute error of TDOA

Figure 3.10 shows the result of the TDOA error in seconds for different techniques of calculation. The blue curve corresponds to the proposed method in [90], and the DFT curve rep-

resents the despreading method [140]. The other curves represent the implementation of the correlation-based method [141]. As we can see, the auto-correlation method has a better performance compared to the other methods. It achieved an error of calculation with an order of 10^{-5} s for different values of SNR. The despreading-based methods showed less accuracy than the auto-correlation and the cross-correlation methods, with a ratio of exactness up to 10 times.

3.3.3.2 Kauai 2

Kauai (KAU2) channel represents a shallow water channel off the western side of Kauai, Hawaï, USA. This channel is estimated using one transmitter and an array receiver composed of 16 hydrophones. The settings used to estimate the KAU2 channel at each receiver are given in Figure 3.11a and Table 3.11b.

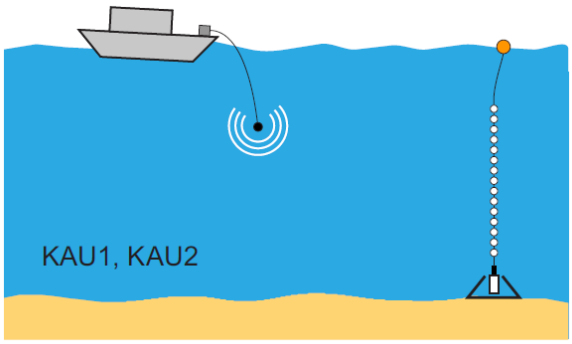

(a) Geometric setting

Parameter	Value
Carrier frequency	6 kHz
Bandwidth	4 kHz
Probe signal	LFM
Number of hydrophones	16
Element spacing	3.75 m
Water depth	100 m
Range	3160 m
Number of channels	258

(b) The breakdown of channel parameters

Figure 3.11: Setting of KAU2 channel copied from [61]

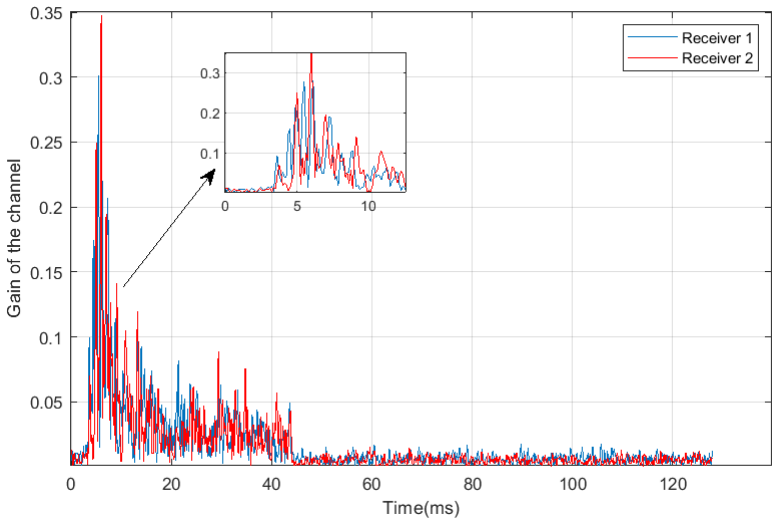

Figure 3.12: The first CIRs received by hydrophone 1 and hydrophone 3

Unlike the BCH1 channel, the KAU2 channel has multiple taps that vary quickly over time. As Shown in Figure 3.12, the energy of the channel is spreading in interval of 45 ms. The same principle of TDOA calculation is applied in the previous simulation. We set the difference in time between the strongest paths as a reference for TDOA calculation. The performance of TDOA calculation is evaluated using MAE as a function of SNR. The simulation is carried out using a preamble composed of 8 up chirps followed by two down chirps. These chirps are generated using $SF = 8$ and a bandwidth of 2 kHz. The carrier frequency and sampling frequency were fixed at 6 kHz and 500 kHz, respectively. Finally, the number of iterations was fixed at 200.

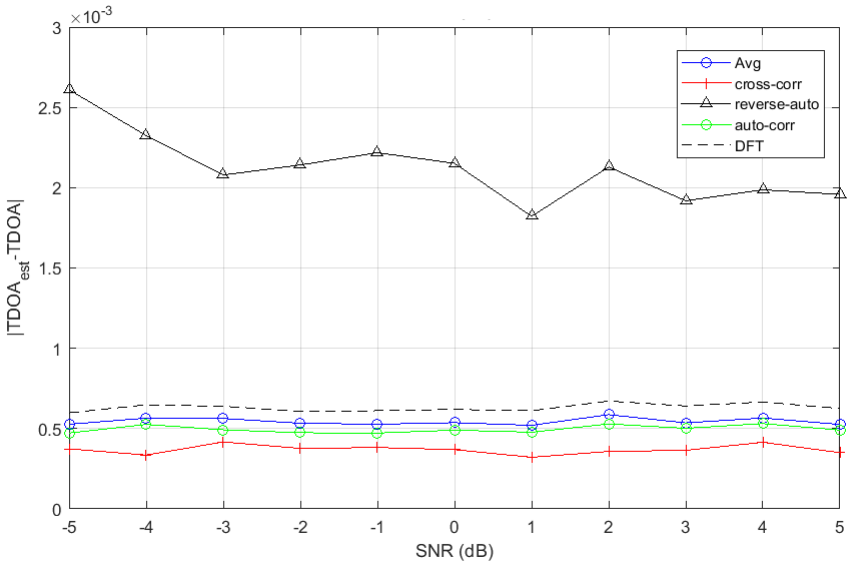

Figure 3.13: Mean absolute error of TDOA

The result of the TDOA error in KAU2 channel is depicted in Figure 3.13. As we can observe, the calculation of TDOA deteriorated compared with the result obtained in the BCH1 channel. This channel is characterized by high time variability and multiple taps. Consequently, the order of error is around 10^{-4} s for the most proposed method for TDOA calculation. However, the cross-correlation method achieved a low error in calculation. Referring to both simulations we have an interval of TDOA error between 3×10^{-5} s and 4×10^{-4} s. Using the speed of the acoustic wave underwater (approximately 1500 m/s) and the TDOA error, we obtain an error of the difference in range between 3 cm and 60 cm (formula 3.2), Therefore, in the case of a short distance between receivers, the error of TDOA could strongly impact the calculation of the difference in range and then the source position.

Namely, auto-correlation and cross-correlation achieved the low error in TDOA calculation in both simulations. Regarding the difficulties of the used channel for this simulation, we choose the cross-correlation method to compute TDOA for the proposed localization system.

3.3.4 Performance of proposed system in UWA channel

In order to evaluate the proposed system in the UWA channel, we simulate the scenario of locating a transmitter submerged underwater at a depth of 20 m and far 136 m from the antenna of reception (tetrahedron composed of 5 hydrophones). To do so, we used the simulator proposed in [142], which is a channel modeling for network simulations. This open software is based mainly on the Bellhop simulator for underwater acoustic channel modeling. From a fixed set of transmitters and receivers in 3D dimension underwater, it calculates the CIR for each receiver deployed in the network.

3.3.4.1 Setup of simulation

The UWA channels are generated using the north atlantic coast configuration for the speed profile and the channel bounce. The geometric setting of the simulation is an emitter located at $p\ (100, 100, -20)$ and the five receivers fixed respectively at $H_1\ (4, 4, -15)$, $H_2\ (4+\frac{d}{2}, 4, -15)$, $H_3\ (4-\frac{d}{2}, 4, -15)$, $H_4\ (4, 4+\frac{d}{2}, -15-\frac{d}{\sqrt{2}})$, $H_5\ (4, 4-\frac{d}{2}, -15-\frac{d}{\sqrt{2)}})$ with d = 4 m. We set the receiver H_1 as a reference of calculation. The breakdown of the parameters used to generate the transmitted signal is listed in table 3.1.

Table 3.1: Parameters of the transmitted signal

Parameter	Value
Carrier frequency	24 kHz
Sampling frequency	500 kHz
Bandwidth	5 kHz
Spreading factor	6
Number of up chirps	8
Number of down chirps	2
Total number of iterations	200

3.3.4.2 Simulation result

The obtained CIR at each receiver is shown in Figure 3.14. As depicted in this figure, the generated channels have two paths, where the first path has the strongest energy. We can also notice that the first path is received at different times at each receiver. By applying the calculation method of TDOA-based localization without introducing the noise (see subsection 3.2.1), we checked that we obtain the source position correctly. To perform the localization system in case of noise, we added to the received signals an AWGN, and we applied four algorithms of localization: LS [126], LCLS [127], NLS-ML [124], and NLS-GN [123]. The localization performance is evaluated using root-mean-square error (RMSE) as a function of SNR.

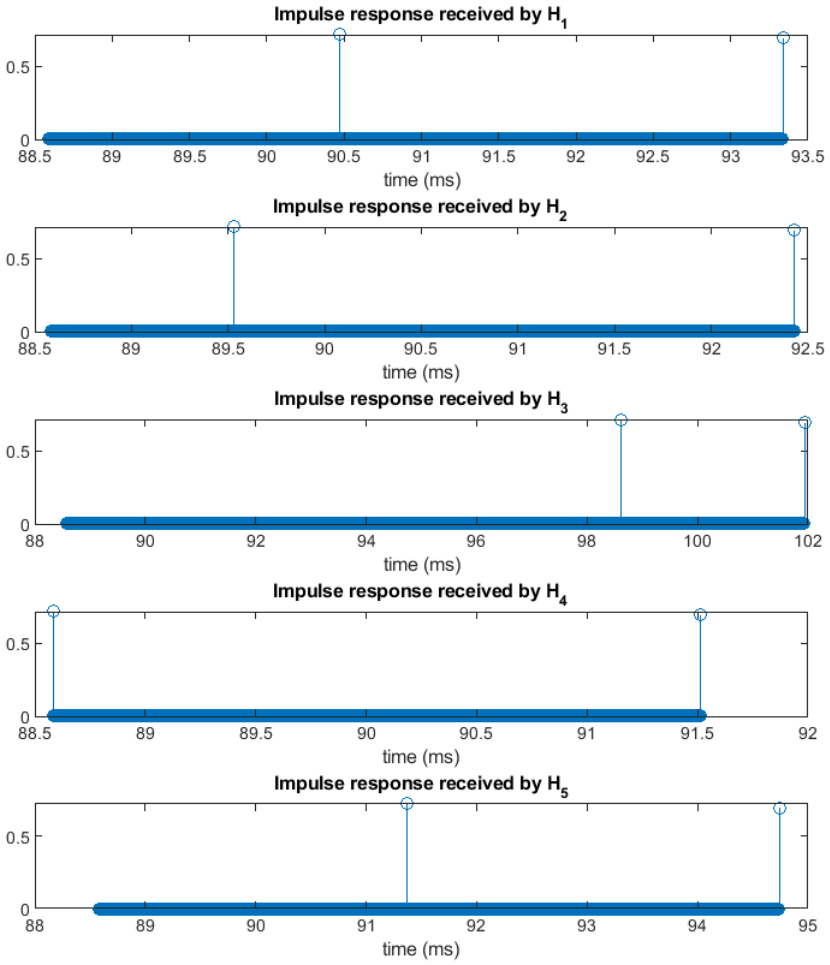

Figure 3.14: CIR at each receiver

The RMSE is calculated using the expression

$$RMSE = \sqrt{\frac{1}{N}\sum_{k=1}^{N}[(\hat{a}_k - x)^2 + (\hat{b}_k - y)^2 + (\hat{c}_k - z)^2]} \tag{3.64}$$

where N is the number of simulations, $p = (x, y, z)$ is the real position of the target, and $(\hat{a}_k, \hat{b}_k, \hat{c}_k)$ is the estimated position at the k^{th} simulation. The result of the simulation is presented in Figure 3.15. We can notice that in this particular geometric configuration, the LLS approaches for the source estimation have shown a better result compared to NLS methods. More precisely, the LCLS method converged rapidly to the source location and improved the obtained result of the LS estimator by integrating the distance between the source and the receiver H_1 as another metric in the calculation (see subsection 3.2.2.2).

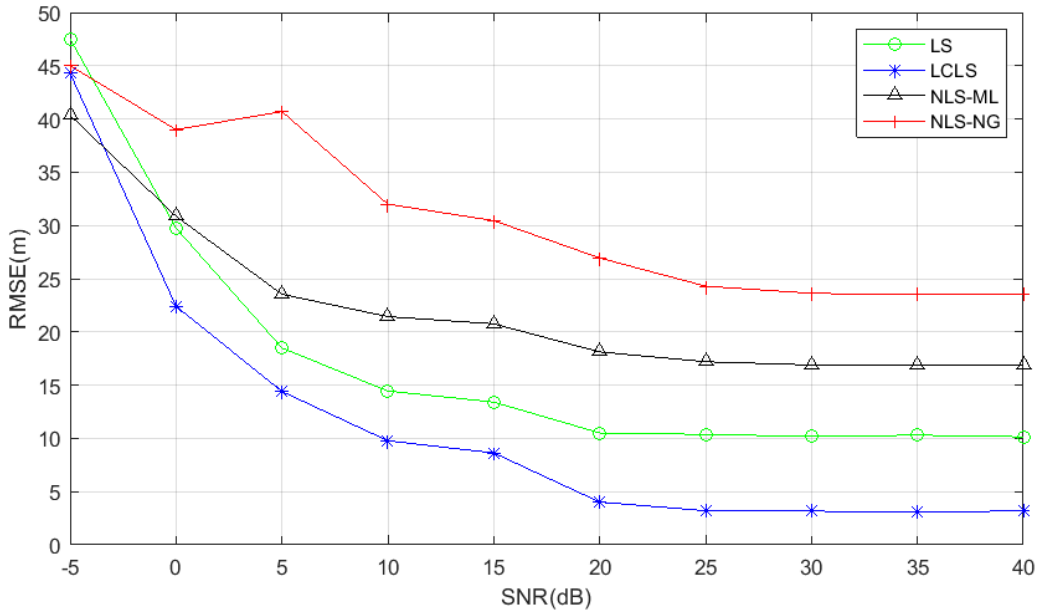

Figure 3.15: Performance of proposed localization system

In the context of localizing a missing fishing net equipped by an acoustic source, the proposed system would help to get closer to the source. Indeed, by exploiting the estimated source location at the beginning and moving toward the location, the accuracy of the source position will increase. As a result, when getting closer to the source, it is possible to design a zone of detection that simplifies the research process. Referring to the obtained simulation result using the LCLS method, the zone of research can be limited to a circle of radius 5 m.

To enhance the obtained result, it is recommended to enlarge the distance between receivers, which means geometrically increasing the difference in ranges between receivers and the source. As a consequence, minimizing the impact of TDOA error in the calculation. However, we pass from the short baseline positioning configuration to the long baseline positioning configuration, which is complex to deploy and costly.

3.4 Conclusion

In this chapter, we discussed the second part of our hybrid system, which is localization. We started by introducing the most commonly used methods to locate acoustic devices underwater. We explained that range-based methods, such as the RSSI method, use received signal strength to estimate the distance, considering transmission loss and source level. Another method, AOA, provides more precise location information for the acoustic emitter. Time-synchronized methods, like TOA and TDOA, are widely used because of their effectiveness in estimating the source location. We focused on the TDOA method for the proposed method since we are making passive communication and also for ease of receivers deployment.

The proposed system is composed of 5 hydrophones in a tetrahedron acoustic antenna to record a transmitted signal used initially for DCSS communication. We exploited the synchronization process proposed in the previous chapter to calculate TDOA between receivers. So far, we introduced an enhancement of TDOA calculation using cross-correlation for fine estimation. The performance of the TDOA calculation is carried out using the watermark benchmark of UWA channels. In two profiles of UWA channels, we showed that the proposed TDOA calculation has an error order ranging from 20 μs to 0.4 ms, which could impact the localization process, especially for nearby configurations.

Finally, by means of Bellhop channel modeling, we performed the system of localization and presented the result by RMSE as a function of SNR. The obtained results showed that the LCLS method achieved a low error in source estimation from 15 dB of SNR; the error was less than 10 m. During this work, we presented only simulation results for localization performance. Unfortunately, we couldn't conduct experiments to assess the proposed system in real environments because of the lack of resources. For a better assessment, more tests should be conducted in UWA channels.

Conclusion and perspectives

Conclusion

The research work carried out during this thesis focused on practical solutions that would make fishing sustainable. We proposed a hybrid acoustic system to ensure the communication and localization of fishing nets underwater. We chose the linear frequency modulation waveform to ensure data link because of its ability to demodulate the received signals at low levels of SNR. The chirp signals are also exploited to localize transmitters using the TDOA positioning technique.

Before introducing the proposed system, an understanding of the propagation environment was mandatory. In chapter 1, we showed that the UWA channel is a subject of multiple phenomena, such as the multipath effect, Doppler effect, intense transmission loss, and high time variability. To design a reliable model of UWA channels, we introduced the existing UWA channel modeling. We chose the watermark simulator for communication performance. This model allows a better assessment using estimated UWA channels in diverse locations with different setups of deployment. Besides, Bellhop for network simulation was more adapted for localization performance because of the possibility of generating CIRs for a geometry-fixed set of transmitters and receivers.

In chapter 2, we presented the DCSS scheme of communication as an enhancement of the conventional CSS modulation. We highlighted that the differential encoding makes the proposed scheme more resilient to Doppler shift since the carrier frequency offset introduced to the signal can be eliminated at the receiver through differentiation. Besides, to limit the Doppler spread, we exploited the Frft operator and rectified the received signal through interpolation. As the UWA implies a multipath effect, we introduced a channel estimator and MMSE equalizer to recover the received symbols. In terms of performance, DCSS achieved a BER up 10^{-3} at 2 dB of SNR in the ocean trial.

The localization part is presented in chapter 3. Indeed, we exploited the transmitted signal used for communication to ensure localization at the receiver using the TDOA positioning

technique. More precisely, we proposed a tetrahedron-shaped acoustic antenna composed of 5 hydrophones to record the transmitted signals. Through DCSS demodulation, we computed the start time at each receiver and then TDOA between receivers. As TDOA error could lead to high errors of source estimation, we presented various methods for fine synchronization. Using the watermark benchmark in two locations (BCH1 and KAUI2), we performed the TDOA calculation, which achieved an error between 20 μs and 0.4 ms. Finally, a scenario of localization is simulated to perform the proposed system using different methods for source estimation.

Finally, throughout the course of this thesis research, we have authored four papers in flagship international conferences like IEEE OCEANS and IEEE LASCAS. Furthermore, our latest work is currently under submission process in the journal IEEE TAFE.

Perspectives

Based on the obtained results, several potential research perspectives can be considered for further investigation.

1. In this work, we focused on a balance between complexity and performance to propose the DCSS receiver, which allows easy implementation in embedded systems. Nevertheless, there is scope for further improving performance by using high-complexity processing such as correlation-based synchronization and turbo equalization.

2. Instead of using the CSS method to define symbols, a reflection on the orthogonality of the chirp signals to constitute the payload would enhance the spectral efficiency.

3. A study of the time imperfection of the hardware to determine its contribution to TDOA calculation error is essential for the final solution. In this case, it is more relevant to use methods such as WLLS and ML for source estimation since the covariance of the noise is known.

4. Recently, a new approach has shown a promoting result in GNSS localization using M-estimators instead of classical LS or ML estimators [143]. This study is to investigate to perform underwater acoustic localization.

5. Since the acoustic transmitters are expected to be attached to the filling nets, an opportunity arises to use them to deter the cetaceans from entangling in the nets. Unlike commercial pingers or deterrent devices that usually use a random signal within a bandwidth of communication. The idea here is to use the reflection of the signal emitted by dolphins used for echo localization. This way, the signal will carry familiar information to prevent dolphins from danger. To investigate this further, an initial study can be conducted using a K-wave simulator to model the filling net underwater.

List of Publications

Journal Articles

[J-1] M. Rezzouki and G. Ferré, "Chirp-Based signals for underwater acoustic communication and localization," in IEEE Transactions on AgriFood Electronics 2023 (ongoing)

Conference Papers

[C-1] M. Rezzouki, S. Dubois and G. Ferré, "FIND project: Underwater Connected Objects for Sustainable Fishing," Global Oceans 2020: Singapore U.S. Gulf Coast, Biloxi, MS, USA, 2020, pp. 1-5, doi: 10.1109/IEEECONF38699.2020.9389114.

[C-2] M. Rezzouki, M. A. B. Temim and G. Ferré, "Differential Chirp Spread Spectrum to perform Acoustic Long Range Underwater Localization and Communication," OCEANS 2021: San Diego Porto, San Diego, CA, USA, 2021, pp. 1-9, doi: 10.23919/OCEANS44145.2021.9706010.

[C-3] M. Rezzouki and G. Ferré, "Design and Implementation of Differential Chirp Spread Spectrum System for Underwater Acoustic Communication," OCEANS 2022, Hampton Roads, Hampton Roads, VA, USA, 2022, pp. 1-7, doi: 10.1109/OCEANS47191.2022.9977293.

[C-4] Marwane Rezzouki, Guillaume Ferré. Performance of Differential Chirp Spread Spectrum in Underwater Acoustic Channel. LASCAS 2023 (WAFE session), Feb 2023, Quito, Ecuador. hal-04053983

List of Figures

List of Tables

Bibliography

[1] "Observatoire des mammifères et oiseaux marins coordinateur du réseau national Échouages." [Online]. Available: https://www.observatoire-pelagis.cnrs.fr

[2] "Ghost nets the silent killers of our oceans." [Online]. Available: https://oliveridleyproject.org/what-are-ghost-nets

[3] "Our oceans are haunted by ghost nets: Why that's scary and what we can do." [Online]. Available: https://www.worldwildlife.org/stories/our-oceans-are-haunted-by-ghost-nets-why-that-s-scary-and-what-we-can-do–23

[4] R. L. Lewison, L. B. Crowder, A. J. Read, and S. A. Freeman, "Understanding impacts of fisheries bycatch on marine megafauna," *Trends in ecology & evolution*, vol. 19, no. 11, pp. 598–604, 2004.

[5] S. M. D. S. Northridge, D. Waples, and A. J. Read, "To ping or not to ping: the use of active acoustic devices in mitigating interactions between small cetaceans and gillnet fisheries," *Endangered Species Research*, vol. 19, no. 3, pp. 201–221, 2013.

[6] G. V. Giardino, M. Cosentino, G. Buscaino, R. Bastida, and D. Rodríguez, "Acoustic detection of franciscana dolphins near artisanal fishing nets in argentina," in *The Effects of Noise on Aquatic Life: Principles and Practical Considerations*. Springer, 2023, pp. 1–12.

[7] A. Moan and A. Bjørge, "Pinger trials in norwegian commercial fisheries confirm that pingers reduce harbour porpoise bycatch rates and demonstrate low level of pinger-associated negative impacts on day-to-day fishing operations," *IWC Scientific Committee. Report number: SC*, vol. 68, 2021.

[8] E. B. Arnett, C. D. Hein, M. R. Schirmacher, M. M. Huso, and J. M. Szewczak, "Evaluating the effectiveness of an ultrasonic acoustic deterrent for reducing bat fatalities at wind turbines," *PloS one*, vol. 8, no. 6, p. e65794, 2013.

[9] M. Amano, M. Kusumoto, M. Abe, and T. Akamatsu, "Long-term effectiveness of pingers on a small population of finless porpoises in japan," *Endangered Species Research*, vol. 32, pp. 35–40, 2017.

[10] "Licado programme." [Online]. Available: https://www.observatoire-pelagis.cnrs.fr/pelagis/programmes/licado/?lang=en

[11] C. S. Clay and H. Medwin, "Acoustical oceanography: principles and applications," 1977.

[12] H. Medwin and C. S. Clay, "Chapter 2 - sound propagation," in *Fundamentals of Acoustical Oceanography*, ser. Applications of Modern Acoustics, H. Medwin and C. S. Clay, Eds. San Diego: Academic Press, 1998, pp. 17–69. [Online]. Available: https://www.sciencedirect.com/science/article/pii/B9780124875708500040

[13] H. P. Bucker, "A simple 3d gaussian beam sound propagation model for shallow water," *The Journal of the Acoustical Society of America*, vol. 95, no. 5, pp. 2437–2440, 1994. [Online]. Available: https://doi.org/10.1121/1.409853

[14] M. B. Porter and H. P. Bucker, "Gaussian beam tracing for computing ocean acoustic fields," *The Journal of the Acoustical Society of America*, vol. 82, no. 4, pp. 1349–1359, 1987.

[15] C. Tindle and Z. Zhang, "An adiabatic normal mode solution for the benchmark wedge," *The Journal of the Acoustical Society of America*, vol. 101, no. 1, pp. 606–609, 1997.

[16] K. D. Heaney, R. L. Campbell, and J. J. Murray, "Comparison of hybrid three-dimensional modeling with measurements on the continental shelf," *The Journal of the Acoustical Society of America*, vol. 131, no. 2, pp. 1680–1688, 2012.

[17] M. D. Collins, "The adiabatic mode parabolic equation," *The Journal of the Acoustical Society of America*, vol. 94, no. 4, pp. 2269–2278, 1993.

[18] D. Lee, A. D. Pierce, and E.-C. Shang, "Parabolic equation development in the twentieth century," *Journal of Computational Acoustics*, vol. 8, no. 04, pp. 527–637, 2000.

[19] H. Schmidt, "Virtual source approach to scattering from partially buried elastic targets," in *AIP Conference Proceedings*, vol. 728, no. 1. American Institute of Physics, 2004, pp. 456–463.

[20] M. B. Porter, "Acoustics toolbox, available," 2007. [Online]. Available: fromhttp://oalib.hlsresearch.com/FFP/ index.html

[21] D. Weston, "Sound focusing and beaming in the interference field due to several shallow-water modes," *The Journal of the Acoustical Society of America*, vol. 44, no. 6, pp. 1706–1712, 1968.

[22] C. H. Harrison, "Ray convergence in a flux-like propagation formulation," *The Journal of the Acoustical Society of America*, vol. 133, no. 6, pp. 3777–3789, 2013.

[23] L. Wang, K. Heaney, T. Pangerc, P. Theobald, S. Robinson, and M. Ainslie, "Review of underwater acoustic propagation models." 2014.

[24] M. C. Domingo, "Overview of channel models for underwater wireless communication networks," *Physical Communication*, vol. 1, no. 3, pp. 163–182, 2008.

[25] H. Medwin, C. S. Clay, and T. K. Stanton, "Fundamentals of acoustical oceanography," 1999.

[26] W. H. Thorp, "Analytic description of the low-frequency attenuation coefficient," *The Journal of the Acoustical Society of America*, vol. 42, no. 1, pp. 270–270, 1967.

[27] Y. Le Gall, "Problèmes inverses en acoustique sous-marine: prédiction de performances et localisation de source en environnement incertain," Ph.D. dissertation, Télécom Bretagne; Université de Bretagne Occidentale, 2015.

[28] A. APL-UW, "High-frequency ocean environmental acoustic models handbook," *Applied Physics Laboratory, University of Washington, US APL-UW*, vol. 9407, 1994.

[29] E. Pouliquen, "Identification des fonds marins superficiels à l'aide de signaux d'échosondeurs," Ph.D. dissertation, Université Denis Diderot, 1992.

[30] C. Augris and P. Clabaut, *Cartographie géologique des fonds marins côtiers: exemples le long du littoral français*. Editions Quae, 2001.

[31] F.-X. Socheleau, "Communications acoustiques sous-marines sur canal fortement dispersif en temps et en fréquence: point de vue de la théorie de l'information," Ph.D. dissertation, Université de Bretagne occidentale-Brest, 2011.

[32] J.-g. Huang, H. Wang, C.-b. He, Q.-f. Zhang, and L.-y. Jing, "Underwater acoustic communication and the general performance evaluation criteria," *Frontiers of Information Technology & Electronic Engineering*, vol. 19, no. 8, pp. 951–971, 2018.

[33] X. Cristol, J.-M. Passerieux, and J. Dassé, "Caractérisation expérimentale et modélisation physique des fluctuations temporelles du canal acoustique sous-marin," *Proc. Journées scientifiques 2009 dURSI-France*, 2009.

[34] P. Bello, "Measurement of random time-variant linear channels," *IEEE Transactions on Information Theory*, vol. 15, no. 4, pp. 469–475, 1969.

[35] P. A. Van Walree, T. Jenserud, and M. Smedsrud, "A discrete-time channel simulator driven by measured scattering functions," *IEEE journal on selected areas in communications*, vol. 26, no. 9, pp. 1628–1637, 2008.

[36] T. H. Eggen, A. B. Baggeroer, and J. C. Preisig, "Communication over doppler spread channels. part i: Channel and receiver presentation," *IEEE journal of oceanic engineering*, vol. 25, no. 1, pp. 62–71, 2000.

[37] B. Li, S. Zhou, M. Stojanovic, L. Freitag, and P. Willett, "Multicarrier communication over underwater acoustic channels with nonuniform doppler shifts," *IEEE Journal of Oceanic Engineering*, vol. 33, no. 2, pp. 198–209, 2008.

[38] M. Stojanovic and J. Preisig, "Underwater acoustic communication channels: Propagation models and statistical characterization," *IEEE communications magazine*, vol. 47, no. 1, pp. 84–89, 2009.

[39] S. Kullback and R. A. Leibler, "On information and sufficiency," *The annals of mathematical statistics*, vol. 22, no. 1, pp. 79–86, 1951.

[40] A. Bhattacharyya, "On a measure of divergence between two statistical populations defined by their probability distribution," *Bulletin of the Calcutta Mathematical Society*, vol. 35, pp. 99–110, 1943.

[41] J. Lin, "Divergence measures based on the shannon entropy," *IEEE Transactions on Information theory*, vol. 37, no. 1, pp. 145–151, 1991.

[42] A. Richardson, "Nonparametric statistics for non-statisticians: A step-by-step approach by gregory w. corder, dale i. foreman," 2010.

[43] P. Qarabaqi and M. Stojanovic, "Statistical modeling of a shallow water acoustic communication channel," in *Proc. Underwater Acoustic Measurements Conference, Nafplion, Greece*. Citeseer, 2009, pp. 1341–1350.

[44] A. Radosevic, J. G. Proakis, and M. Stojanovic, "Statistical characterization and capacity of shallow water acoustic channels," in *OCEANS 2009-EUROPE*. IEEE, 2009, pp. 1–8.

[45] B. Borowski, "Characterization of a very shallow water acoustic communication channel," in *OCEANS 2009*. IEEE, 2009, pp. 1–10.

[46] J. Zhang, J. Cross, and Y. R. Zheng, "Statistical channel modeling of wireless shallow water acoustic communications from experiment data," in *2010-MILCOM 2010 MILITARY COMMUNICATIONS CONFERENCE*. IEEE, 2010, pp. 2412–2416.

[47] H. Kulhandjian and T. Melodia, "Modeling underwater acoustic channels in short-range shallow water environments," in *Proceedings of the International Conference on Underwater Networks & Systems*, 2014, pp. 1–5.

[48] F. J. Cañete, J. López-Fernández, C. García-Corrales, A. Sánchez, E. Robles, F. J. Rodrigo, and J. F. Paris, "Measurement and modeling of narrowband channels for ultrasonic underwater communications," *Sensors*, vol. 16, no. 2, p. 256, 2016.

[49] W.-B. Yang and T. Yang, "High-frequency channel characterization for m-ary frequency-shift-keying underwater acoustic communications," *The Journal of the Acoustical Society of America*, vol. 120, no. 5, pp. 2615–2626, 2006.

[50] P. Qarabaqi and M. Stojanovic, "Statistical characterization and computationally efficient modeling of a class of underwater acoustic communication channels," *IEEE Journal of Oceanic Engineering*, vol. 38, no. 4, pp. 701–717, 2013.

[51] A. G. Zajić, "Statistical modeling of underwater wireless channels," in *2010 IEEE Global Telecommunications Conference GLOBECOM 2010*. IEEE, 2010, pp. 1–5.

[52] M. Naderi, A. G. Zajić, and M. Pätzold, "A nonisovelocity geometry-based underwater acoustic channel model," *IEEE Transactions on Vehicular Technology*, vol. 67, no. 4, pp. 2864–2879, 2017.

[53] J. Zhou, H. Jiang, P. Wu, and Q. Chen, "Study of propagation channel characteristics for underwater acoustic communication environments," *IEEE Access*, vol. 7, pp. 79 438–79 445, 2019.

[54] M. Pätzold, M. Patzold, and M. Paetzold, *Mobile fading channels*. Wiley Online Library, 2002.

[55] M. Patzold, C.-X. Wang, and B. O. Hogstad, "Two new sum-of-sinusoids-based methods for the efficient generation of multiple uncorrelated rayleigh fading waveforms," *IEEE Transactions on Wireless Communications*, vol. 8, no. 6, pp. 3122–3131, 2009.

[56] F.-X. Socheleau, C. Laot, and J.-M. Passerieux, "Stochastic replay of non-wssus underwater acoustic communication channels recorded at sea," *IEEE Transactions on Signal Processing*, vol. 59, no. 10, pp. 4838–4849, 2011.

[57] N. E. Huang, Z. Shen, S. R. Long, M. C. Wu, H. H. Shih, Q. Zheng, N.-C. Yen, C. C. Tung, and H. H. Liu, "The empirical mode decomposition and the hilbert spectrum for nonlinear and non-stationary time series analysis," *Proceedings of the Royal Society of London. Series A: mathematical, physical and engineering sciences*, vol. 454, no. 1971, pp. 903–995, 1998.

[58] M. B. Porter, "The kraken normal mode program (draft)," *Naval Research Laboratory, Washington DC*, 1992.

[59] ——, "The bellhop manual and users guide: Preliminary draft," *Heat, Light, and Sound Research, Inc., La Jolla, CA, USA, Tech. Rep*, vol. 260, 2011.

[60] J. Kim, H. Song, W. Hodgkiss, and M. Siderius, "Virtual time series experiment (virtex) simulation tool for underwater acoustic communications." *The Journal of the Acoustical Society of America*, vol. 126, no. 4, pp. 2174–2174, 2009.

[61] P. A. van Walree, F.-X. Socheleau, R. Otnes, and T. Jenserud, "The watermark benchmark for underwater acoustic modulation schemes," *IEEE journal of oceanic engineering*, vol. 42, no. 4, pp. 1007–1018, 2017.

[62] L. Bjørnø, "Underwater acoustic measurements and their applications," in *Applied Underwater Acoustics*. Elsevier, 2017, pp. 889–947.

[63] I. Kochańska, J. Schmidt, and M. Rudnicki, "Underwater acoustic communications in time-varying dispersive channels," in *2016 Federated Conference on Computer Science and Information Systems (FedCSIS)*. IEEE, 2016, pp. 467–474.

[64] A. N. Rice, J. T. Tielens, B. J. Estabrook, C. A. Muirhead, A. Rahaman, M. Guerra, and C. W. Clark, "Variation of ocean acoustic environments along the western north atlantic coast: A case study in context of the right whale migration route," *Ecological informatics*, vol. 21, pp. 89–99, 2014.

[65] R. Kastelein, W. Verboom, M. Muijsers, N. Jennings, and S. Van der Heul, "The influence of acoustic emissions for underwater data transmission on the behaviour of harbour porpoises (phocoena phocoena) in a floating pen," *Marine Environmental Research*, vol. 59, no. 4, pp. 287–307, 2005.

[66] M. F. McKenna, D. Ross, S. M. Wiggins, and J. A. Hildebrand, "Underwater radiated noise from modern commercial ships," *The Journal of the Acoustical Society of America*, vol. 131, no. 1, pp. 92–103, 2012.

[67] J. T. Hansen, "Link budget analysis for undersea acoustic signaling," NAVAL POSTGRADUATE SCHOOL MONTEREY CA, Tech. Rep., 2002.

[68] W. W. Clark, "Recent studies of temporary threshold shift (tts) and permanent threshold shift (pts) in animals," *The Journal of the Acoustical Society of America*, vol. 90, no. 1, pp. 155–163, 1991.

[69] R. Diamant and L. Lampe, "Low probability of detection for underwater acoustic communication: A review," *IEEE Access*, vol. 6, pp. 19 099–19 112, 2018.

[70] B. Sherlock, J. A. Neasham, and C. C. Tsimenidis, "Spread-spectrum techniques for bio-friendly underwater acoustic communications," *IEEE Access*, vol. 6, pp. 4506–4520, 2018.

[71] M. Stojanovic, "Ofdm for underwater acoustic communications: Adaptive synchronization and sparse channel estimation," in *2008 IEEE International Conference on Acoustics, Speech and Signal Processing*, 2008, pp. 5288–5291.

[72] *OFDM Basics*. John Wiley Sons, Ltd, 2014, ch. 2, pp. 23–38. [Online]. Available: https://onlinelibrary.wiley.com/doi/abs/10.1002/9781118693865.ch2

[73] G. Leus, P. van Walree, J. Boschma, C. Fanciullacci, H. Gerritsen, and P. Tusoni, *Covert underwater communications with multiband OFDM*. IEEE, 2008.

[74] Tiejun Wang, J. G. Proakis, E. Masry, and J. R. Zeidler, "Performance degradation of ofdm systems due to doppler spreading," *IEEE Transactions on Wireless Communications*, vol. 5, no. 6, pp. 1422–1432, 2006.

[75] P. Van Walree, E. Sangfelt, and G. Leus, *Multicarrier spread spectrum for covert acoustic communications*. IEEE, 2008.

[76] J. Ling, H. He, J. Li, W. Roberts, and P. Stoica, "Covert underwater acoustic communications," *The Journal of the Acoustical Society of America*, vol. 128, no. 5, pp. 2898–2909, 2010. [Online]. Available: https://doi.org/10.1121/1.3493454

[77] L.-j. Liu, J.-f. Li, L. Zhou, P. Zhai, H. Zhao, J.-c. Jin, and Z.-c. Lv, "An underwater acoustic direct sequence spread spectrum communication system using dual spread spectrum code," *Frontiers of Information Technology & Electronic Engineering*, vol. 19, no. 8, pp. 972–983, Aug 2018. [Online]. Available: https://doi.org/10.1631/FITEE.1700746

[78] E. Sangfelt, B. Nilsson, and J. Israelsson, "Covert underwater communication experiments using dsss and turbo equalization," *UDT Europe 2008*, 2008.

[79] Y. Yin, F. Zhou, G. Qiao, S. Liu, and Y. Yu, "Burst mode hybrid spread spectrum technology for covert acoustic communication," in *2013 OCEANS-San Diego*. IEEE, 2013, pp. 1–8.

[80] M. D. Green and J. A. Rice, "Channel-tolerant fh-mfsk acoustic signaling for undersea communications and networks," *IEEE Journal of Oceanic Engineering*, vol. 25, no. 1, pp. 28–39, 2000.

[81] G. Lee, W. Park, T. Kang, K. Kim, and W. Kim, "Chirp-based fhss receiver with recursive symbol synchronization for underwater acoustic communication," *Sensors*, vol. 18, no. 12, p. 4498, 2018.

[82] R. Diamant, A. Feuer, and L. Lampe, "Choosing the right signal: Doppler shift estimation for underwater acoustic signals," in *Proceedings of the 7th International Conference on Underwater Networks & Systems*, 2012, pp. 1–8.

[83] X. Wang, M. Fei, and X. Li, "Performance of chirp spread spectrum in wireless communication systems," in *2008 11th IEEE Singapore International Conference on Communication Systems*. IEEE, 2008, pp. 466–469.

[84] A. C. Pecci, C. Laot, and A. Bourre, "Quadratic chirp modulation for underwater acoustic digital communications," in *OCEANS 2015-Genova*. IEEE, 2015, pp. 1–7.

[85] J. An, H. Ra, C. Youn, and K. Kim, "Experimental results of underwater acoustic communication with nonlinear frequency modulation waveform," *Sensors*, vol. 21, no. 21, p. 7194, 2021.

[86] C. Li, X. Shen, Z. Jiang, and X. Wang, "Mobile underwater acoustic communication based on passive time reversal," in *2017 IEEE International Conference on Signal Processing, Communications and Computing (ICSPCC)*. IEEE, 2017, pp. 1–5.

[87] C. He, J. Huang, Q. Zhang, and K. Lei, "Reliable mobile underwater wireless communication using wideband chirp signal," in *2009 WRI International Conference on Communications and Mobile Computing*, vol. 1. IEEE, 2009, pp. 146–150.

[88] J. Lee, J. An, H.-i. Ra, and K. Kim, "Long-range acoustic communication using differential chirp spread spectrum," *Applied Sciences*, vol. 10, no. 24, p. 8835, 2020.

[89] X. Zhang, X. Han, J. Yin, and X.-l. Sheng, "Study on doppler effects estimate in underwater acoustic communication," in *Proceedings of Meetings on Acoustics ICA2013*, vol. 19, no. 1. Acoustical Society of America, 2013, p. 070062.

[90] M. A. Ben Temim, G. Ferré, and R. Tajan, "A novel approach to enhance the robustness of lora-like phy layer to synchronization errors," in *GLOBECOM 2020 - 2020 IEEE Global Communications Conference*, 2020, pp. 1–6.

[91] G. Ferré and M. A. Ben Temim, "A Dual Waveform Differential Chirp Spread Spectrum Transceiver for LEO Satellite Communications," in *IEEE International Conference on Communications (ICC 2021)*, Montréal, Canada, Jun. 2021. [Online]. Available: https://hal.archives-ouvertes.fr/hal-03134339

[92] Y. Zhao, H. Yu, G. Wei, F. Ji, and F. Chen, "Parameter estimation of wideband underwater acoustic multipath channels based on fractional fourier transform," *IEEE Transactions on Signal Processing*, vol. 64, no. 20, pp. 5396–5408, 2016.

[93] J. A. Sidorkina, R. Dyabirov, B. Shakhtarin, and A. Bychkov, "A proposed chirp synchronisation algorithm based on the fractional fourier transform for underwater acoustic communication," in *2019 Systems of Signal Synchronization, Generating and Processing in Telecommunications (SYNCHROINFO)*. IEEE, 2019, pp. 1–4.

[94] M. Xhonneux, D. Bol, and J. Louveaux, "A low-complexity synchronization scheme for lora end nodes," *ArXiv e-prints*, 2019.

[95] M. Xhonneux, O. Afisiadis, D. Bol, and J. Louveaux, "A low-complexity lora synchronization algorithm robust to sampling time offsets," *IEEE Internet of Things Journal*, vol. 9, no. 5, pp. 3756–3769, 2021.

[96] M. Stojanovic, J. A. Catipovic, and J. G. Proakis, "Phase-coherent digital communications for underwater acoustic channels," *IEEE journal of oceanic engineering*, vol. 19, no. 1, pp. 100–111, 1994.

[97] M. Stojanovic, "Recent advances in high-speed underwater acoustic communications," *IEEE Journal of Oceanic engineering*, vol. 21, no. 2, pp. 125–136, 1996.

[98] J. C. Preisig, "Performance analysis of adaptive equalization for coherent acoustic communications in the time-varying ocean environment," *The Journal of the Acoustical Society of America*, vol. 118, no. 1, pp. 263–278, 2005.

[99] A. Youcef, C. Laot, and K. Amis, "Adaptive frequency-domain equalization for underwater acoustic communications," in *OCEANS 2011 IEEE-Spain*. IEEE, 2011, pp. 1–6.

[100] Y. R. Zheng, C. Xiao, T. Yang, and W.-B. Yang, "Frequency-domain channel estimation and equalization for single carrier underwater acoustic communications," in *OCEANS 2007*. IEEE, 2007, pp. 1–6.

[101] B. Peng and H. Dong, "Dsp based real-time single carrier underwater acoustic communications using frequency domain turbo equalization," *Physical Communication*, vol. 18, pp. 40–48, 2016.

[102] G. Edelmann, H. Song, S. Kim, W. Hodgkiss, W. Kuperman, and T. Akal, "Underwater acoustic communications using time reversal," *IEEE Journal of Oceanic Engineering*, vol. 30, no. 4, pp. 852–864, 2005.

[103] H. C. Song, W. Hodgkiss, W. Kuperman, M. Stevenson, and T. Akal, "Improvement of time-reversal communications using adaptive channel equalizers," *IEEE Journal of Oceanic Engineering*, vol. 31, no. 2, pp. 487–496, 2006.

[104] V. M. Pinho, R. S. Chaves, and M. L. Campos, "On equalization performance in underwater acoustic communication," *XXXVI Simpósio Brasileiro de Telecomunicaçoes e Processamento de Sinais, SBrT, Campina Grande*, 2018.

[105] Y. R. Zheng, J. Wu, and C. Xiao, "Turbo equalization for single-carrier underwater acoustic communications," *IEEE Communications Magazine*, vol. 53, no. 11, pp. 79–87, 2015.

[106] X. Qin, F. Qu, and Y. R. Zheng, "Bayesian iterative channel estimation and turbo equalization for multiple-input–multiple-output underwater acoustic communications," *IEEE Journal of Oceanic Engineering*, vol. 46, no. 1, pp. 326–337, 2020.

[107] L. Sun, M. Wang, G. Zhang, H. Li, and L. Huang, "Filtered multitone modulation underwater acoustic communications using low-complexity channel-estimation-based mmse turbo equalization," *Sensors*, vol. 19, no. 12, p. 2714, 2019.

[108] I. B. F. De Almeida, M. Chafii, A. Nimr, and G. Fettweis, "Alternative chirp spread spectrum techniques for lpwans," *IEEE Transactions on Green Communications and Networking*, vol. 5, no. 4, pp. 1846–1855, 2021.

[109] K. Huang, R. Tao, and Y. Wang, "Study of frequency domain equalization for chirp spread spectrum systems," in *2010 IEEE International Conference on Wireless Communications, Networking and Information Security*. IEEE, 2010, pp. 132–136.

[110] V. Chandrasekhar, W. K. Seah, Y. S. Choo, and H. V. Ee, "Localization in underwater sensor networks: survey and challenges," in *Proceedings of the 1st International Workshop on Underwater Networks*, 2006, pp. 33–40.

[111] B. Zhang, H. Wang, T. Xu, L. Zheng, and Q. Yang, "Received signal strength-based underwater acoustic localization considering stratification effect," in *OCEANS 2016-Shanghai*. IEEE, 2016, pp. 1–8.

[112] Y. Sun, Y. Yuan, Q. Xu, C. Hua, and X. Guan, "A mobile anchor node assisted rssi localization scheme in underwater wireless sensor networks," *Sensors*, vol. 19, no. 20, p. 4369, 2019.

[113] G. Shen, R. Zetik, and R. S. Thoma, "Performance comparison of toa and tdoa based location estimation algorithms in los environment," in *2008 5th Workshop on Positioning, Navigation and Communication*. IEEE, 2008, pp. 71–78.

[114] O. Le Bot, J. I. Mars, C. Gervaise, and Y. Simard, "Cross recurrence plot analysis based method for tdoa estimation of underwater acoustic signals," in *2015 IEEE 6th International Workshop on Computational Advances in Multi-Sensor Adaptive Processing (CAMSAP)*. IEEE, 2015, pp. 1–4.

[115] K. Hao, Q. Xue, C. Li, and K. Yu, "A hybrid localization algorithm based on doppler shift and aoa for an underwater mobile node," *IEEE Access*, vol. 8, pp. 181 662–181 673, 2020.

[116] F. Beaubois, "Positionnement d'une balise sous-marine en environnement peu profond." Université du Littoral Côte d'Opale, 2016.

[117] T. Qiao, Y. Zhang, and H. Liu, "Nonlinear expectation maximization estimator for tdoa localization," *IEEE Wireless Communications Letters*, vol. 3, no. 6, pp. 637–640, 2014.

[118] J. Neering, "Optimization and estimation techniques for passive acoustic source localization," Ph.D. dissertation, École Nationale Supérieure des Mines de Paris, 2009.

[119] Y.-T. Chan, H. Y. C. Hang, and P.-c. Ching, "Exact and approximate maximum likelihood localization algorithms," *IEEE Transactions on Vehicular Technology*, vol. 55, no. 1, pp. 10–16, 2006.

[120] J. Wang and J. Guo, "Research on the base station calibration of multi-station and time-sharing measurement based on hybrid genetic algorithm," *Measurement*, vol. 94, pp. 139–148, 2016.

[121] L. Zhang, L. Liu, X.-S. Yang, and Y. Dai, "A novel hybrid firefly algorithm for global optimization," *PloS one*, vol. 11, no. 9, p. e0163230, 2016.

[122] H. C. So, "Source localization: Algorithms and analysis," *Handbook of Position Location: Theory, Practice, and Advances*, pp. 25–66, 2011.

[123] M. Rosić, M. Simić, and P. Pejović, "Hybrid genetic optimization algorithm for target localization using tdoa measurements," *Proceedings of the IcETRAN*, 2017.

[124] S. P. Ahmadi, A. Hansson, and S. K. Pakazad, "Distributed localization using levenberg-marquardt algorithm," *EURASIP Journal on Advances in Signal Processing*, vol. 2021, no. 1, pp. 1–26, 2021.

[125] M. Laaraiedh, S. Avrillon, and B. Uguen, "Cramer–rao lower bounds for nonhybrid and hybrid localisation techniques in wireless networks," *Transactions on Emerging Telecommunications Technologies*, vol. 23, no. 3, pp. 268–280, 2012.

[126] J. Smith and J. Abel, "Closed-form least-squares source location estimation from range-difference measurements," *IEEE Transactions on Acoustics, Speech, and Signal Processing*, vol. 35, no. 12, pp. 1661–1669, 1987.

[127] Y. T. Chan and K. Ho, "A simple and efficient estimator for hyperbolic location," *IEEE transactions on signal processing*, vol. 42, no. 8, pp. 1905–1915, 1994.

[128] B. Xu, W. Qi, L. Wei, and P. Liu, "Turbo-tswls: Enhanced two-step weighted least squares estimator for tdoa-based localisation," *Electronics letters*, vol. 48, no. 25, pp. 1597–1598, 2012.

[129] J. Chen, Y. Zhao, C. Zhao, and Y. Zhao, "Improved two-step weighted least squares algorithm for tdoa-based source localization," in *2018 19th International Radar Symposium (IRS)*. IEEE, 2018, pp. 1–6.

[130] L. Lin, H.-C. So, F. K. Chan, Y. T. Chan, and K. Ho, "A new constrained weighted least squares algorithm for tdoa-based localization," *Signal Processing*, vol. 93, no. 11, pp. 2872–2878, 2013.

[131] K. W. Cheung, H.-C. So, W.-K. Ma, and Y.-T. Chan, "A constrained least squares approach to mobile positioning: algorithms and optimality," *EURASIP Journal on Advances in Signal Processing*, vol. 2006, pp. 1–23, 2006.

[132] P. Wu, S. Su, Z. Zuo, X. Guo, B. Sun, and X. Wen, "Time difference of arrival (tdoa) localization combining weighted least squares and firefly algorithm," *Sensors*, vol. 19, no. 11, p. 2554, 2019.

[133] L. Zhang and Z. Tan, "A new tdoa algorithm based on taylor series expansion in cellular networks," *Frontiers of Electrical and Electronic Engineering in China*, vol. 3, pp. 40–43, 2008.

[134] D. Jose and S. Sebastian, "Taylor series method in tdoa approach for indoor positioning system." *International Journal of Electrical & Computer Engineering (2088-8708)*, vol. 9, no. 5, 2019.

[135] F. Liu, H. Chen, L. Zhang, and L. Xie, "Time-difference-of-arrival-based localization methods of underwater mobile nodes using multiple surface beacons," *IEEE Access*, vol. 9, pp. 31 712–31 725, 2021.

[136] H.-P. Tan, R. Diamant, W. K. Seah, and M. Waldmeyer, "A survey of techniques and challenges in underwater localization," *Ocean Engineering*, vol. 38, no. 14-15, pp. 1663–1676, 2011.

[137] R. Diamant and L. Chorev, "Emulation system for underwater acoustic channel," vol. 2, pp. 1043–1046, 2005.

[138] C. Bernier, F. Dehmas, and N. Deparis, "Low complexity lora frame synchronization for ultra-low power software-defined radios," *IEEE Transactions on Communications*, vol. 68, no. 5, pp. 3140–3152, 2020.

[139] O. B. A. Seller and N. Sornin, "Low complexity, low power and long range radio receiver," May 28 2019, uS Patent 10,305,535.

[140] J. Tapparel, O. Afisiadis, P. Mayoraz, A. Balatsoukas-Stimming, and A. Burg, "An open-source lora physical layer prototype on gnu radio," in *2020 IEEE 21st International Workshop on Signal Processing Advances in Wireless Communications (SPAWC)*. IEEE, 2020, pp. 1–5.

[141] S. Boumard and A. Mammela, "Robust and accurate frequency and timing synchronization using chirp signals," *IEEE Transactions on Broadcasting*, vol. 55, no. 1, pp. 115–123, 2009.

[142] N. Morozs, W. Gorma, B. T. Henson, L. Shen, P. D. Mitchell, and Y. V. Zakharov, "Channel modeling for underwater acoustic network simulation," *IEEE Access*, vol. 8, pp. 136 151–136 175, 2020.

[143] D. Medina, H. Li, J. Vilà-Valls, and P. Closas, "Robust statistics for gnss positioning under harsh conditions: A useful tool?" *Sensors*, vol. 19, no. 24, p. 5402, 2019.